



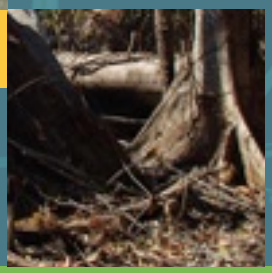

Appendix J

Density Current, Plume Dispersion and Hydrodynamic Modelling

DISCLAIMER

This disclaimer applies to and governs the disclosure and use of this Environmental Impact Statement ("EIS"), and by reading, using or relying on any part(s) of the EIS you accept this disclaimer in full.

This Environmental Impact Statement, including the Executive Summary, and all chapters of and attachments and appendices to it and all drawings, plans, models, designs, specifications, reports, photographs, surveys, calculations and other data and information in any format contained and/or referenced in it, is together with this disclaimer referred to as the "**EIS**".

Purpose of EIS

The EIS has been prepared by, for and on behalf of Wafi Mining Limited and Newcrest PNG 2 Limited (together the "**WGJV Participants**"), being the participants in the Wafi-Golpu Joint Venture ("**WGJV**") and the registered holders of exploration licences EL 440 and EL1105, for the sole purpose of an application (the "**Permit Application**") by them for environmental approval under the Environment Act 2000 (the "**Act**") for the proposed construction, operation and (ultimately) closure of an underground copper-gold mine and associated ore processing, concentrate transport and handling, power generation, water and tailings management, and related support facilities and services (the "**Project**") in Morobe Province, Independent State of Papua New Guinea. The EIS was prepared with input from consultants engaged by the WGJV Participants and/or their related bodies corporate ("**Consultants**").

The Permit Application is to be lodged with the Conservation and Environment Protection Authority ("**CEPA**"), Independent State of Papua New Guinea.

Ownership and Copyright

The EIS is the sole property of the WGJV Participants, who reserve and assert all proprietary and copyright ©2018 interests.

Reliance and Use

The EIS is intended and will be made available to CEPA, for review by CEPA and other applicable agencies of the Government of the Independent State of Papua New Guinea ("**Authorised Agencies**"), for the purpose of considering and assessing the Permit Application in accordance with the Act ("**Authorised Purpose**"), and for no other purpose whatsoever.

The EIS shall not be used or relied upon for any purpose other than the Authorised Purpose, unless express written approval is given in advance by the WGJV Participants.

Except for the Authorised Purpose, the EIS, in whole or in part, must not be reproduced, unless express written approval is given in advance by the WGJV Participants.

This disclaimer must accompany every copy of the EIS.

The EIS is meant to be read as a whole, and any part of it should not be read or relied upon out of context.

Limits on investigation and information

The EIS is based in part on information not within the control of either the WGJV Participants or the Consultants. While the WGJV Participants and Consultants believe that the information contained in the EIS should be reliable under the conditions and subject to the limitations set forth in the EIS, they do not guarantee the accuracy of that information.

No Representations or Warranties

While the WGJV Participants, their Related Bodies Corporate and Consultants believe that the information (including any opinions, forecasts or projections) contained in the EIS should be reliable under the conditions and subject to the limitations set out therein, and provide such information in good faith, they make no warranty, guarantee or promise, express or implied, that any of the information will be correct, accurate, complete or up to date, nor that such information will remain unchanged after the date of issue of the EIS to CEPA, nor that any forecasts or projections will be realised. Actual outcomes may vary materially and adversely from projected outcomes.

The use of the EIS shall be at the user's sole risk absolutely and in all respects. Without limitation to the foregoing, and to the maximum extent permitted by applicable law, the WGJV Participants, their Related Bodies Corporate and Consultants:

- do not accept any responsibility, and disclaim all liability whatsoever, for any loss, cost, expense or damage (howsoever arising, including in contract, tort (including negligence) and for breach of statutory duty) that any person or entity may suffer or incur caused by or resulting from any use of or reliance on the EIS or the information contained therein, or any inaccuracies, misstatements, misrepresentations, errors or omissions in its content, or on any other document or information supplied by the WGJV Participants to any Authorised Agency at any time in connection with the Authorised Agency's review of the EIS; and
- expressly disclaim any liability for any consequential, special, contingent or penal damages whatsoever.

The basis of the Consultants' engagement is that the Consultants' liability, whether under the law of contract, tort, statute, equity or otherwise, is limited as set out in the terms of their engagement with the WGJV Participants and/or their related bodies corporate.

Disclosure for Authorised Purpose

The WGJV Participants acknowledge and agree that, for the Authorised Purpose, the EIS may be:

- copied, reproduced and reprinted;
- published or disclosed in whole or in part, including being made available to the general public in accordance with section 55 of the Act. All publications and disclosures are subject to this disclaimer.

Development of Project subject to Approvals, Further Studies and Market and Operating Conditions

Any future development of the Project is subject to further studies, completion of statutory processes, receipt of all necessary or desirable Papua New Guinea Government and WGJV Participant approvals, and market and operating conditions.

Engineering design and other studies are continuing and aspects of the proposed Project design and timetable may change.

NEWCREST MINING LIMITED DISCLAIMER

Newcrest Mining Limited ("**Newcrest**") is the ultimate holding company of Newcrest PNG 2 Limited and any reference below to "Newcrest" or the "Company" includes both Newcrest Mining Limited and Newcrest PNG 2 Limited.

Forward Looking Statements

The EIS includes forward looking statements. Forward looking statements can generally be identified by the use of words such as "may", "will", "expect", "intend", "plan", "estimate", "anticipate", "continue", "outlook" and "guidance", or other similar words and may include, without limitation, statements regarding plans, strategies and objectives of management, anticipated production or construction commencement dates and expected costs or production outputs. The Company continues to distinguish between outlook and guidance. Guidance statements relate to the current financial year. Outlook statements relate to years subsequent to the current financial year.

Forward looking statements inherently involve known and unknown risks, uncertainties and other factors that may cause the Company's actual results, performance and achievements to differ materially from statements in this EIS. Relevant factors may include, but are not limited to, changes in commodity prices, foreign exchange fluctuations and general economic conditions, increased costs and demand for production inputs, the speculative nature of exploration and project development, including the risks of obtaining necessary licences and permits and diminishing quantities or grades of reserves, political and social risks, changes to the regulatory framework within which the Company operates or may in the future operate, environmental conditions including extreme weather conditions, recruitment and retention of personnel, industrial relations issues and litigation.

Forward looking statements are based on the Company's good faith assumptions as to the financial, market, regulatory and other relevant environments that will exist and affect the Company's business and operations in the future.

The Company does not give any assurance that the assumptions will prove to be correct. There may be other factors that could cause actual results or events not to be as anticipated, and many events are beyond the reasonable control of the Company. Readers are cautioned not to place undue reliance on forward looking statements. Forward looking statements in the EIS speak only at the date of issue. Except as required by applicable laws or regulations, the Company does not undertake any obligation to publicly update or revise any of the forward looking statements or to advise of any change in assumptions on which any such statement is based.

Non-IFRS Financial Information

Newcrest results are reported under International Financial Reporting Standards (IFRS) including EBIT and EBITDA. The EIS also includes non-IFRS information including Underlying profit (profit after tax before significant items attributable to owners of the parent company), All-In Sustaining Cost (determined in accordance with the World Gold Council Guidance Note on Non-GAAP Metrics released June 2013), AISC Margin (realised gold price less AISC per ounce sold (where expressed as USD), or realised gold price less AISC per ounce sold divided by realised gold price (where expressed as a %), Interest Coverage Ratio (EBITDA/Interest payable for the relevant period), Free cash flow (cash flow from operating activities less cash flow related to investing activities), EBITDA margin (EBITDA expressed as a percentage of revenue) and EBIT margin (EBIT expressed as a percentage of revenue). These measures are used internally by Management to assess the performance of the business and make decisions on the allocation of resources and are included in the EIS to provide greater understanding of the underlying performance of Newcrest's operations. The non-IFRS information has not been subject to audit or review by Newcrest's external auditor and should be used in addition to IFRS information.

Ore Reserves and Mineral Resources Reporting Requirements

As an Australian Company with securities listed on the Australian Securities Exchange (ASX), Newcrest is subject to Australian disclosure requirements and standards, including the requirements of the Corporations Act 2001 and the ASX. Investors should note that it is a requirement of the ASX listing rules that the reporting of Ore Reserves and Mineral Resources in Australia comply with the 2012 Edition of the Australasian Code for Reporting of Exploration Results, Mineral Resources and Ore Reserves (the JORC Code) and that Newcrest's Ore Reserve and Mineral Resource estimates comply with the JORC Code.

Competent Person's Statement

The information in the EIS that relates to Golpu Ore Reserves is based on information compiled by the Competent Person, Mr Pasqualino Manca, who is a member of The Australasian Institute of Mining and Metallurgy. Mr Pasqualino Manca, is a full-time employee of Newcrest Mining Limited or its relevant subsidiaries, holds options and/or shares in Newcrest Mining Limited and is entitled to participate in Newcrest's executive equity long term incentive plan, details of which are included in Newcrest's 2017 Remuneration Report. Ore Reserve growth is one of the performance measures under recent long term incentive plans. Mr Pasqualino Manca has sufficient experience which is relevant to the styles of mineralisation and type of deposit under consideration and to the activity which he is undertaking to qualify as a Competent Person as defined in the JORC Code 2012. Mr Pasqualino Manca consents to the inclusion of material of the matters based on his information in the form and context in which it appears.

HARMONY GOLD MINING COMPANY LIMITED DISCLAIMER

Harmony Gold Mining Company Limited ("**Harmony**") is the ultimate holding company of Wafi Mining Limited and any reference below to "Harmony" or the "Company" includes both Harmony Gold Mining Company Limited and Wafi Mining Limited.

Forward Looking Statements

These materials contain forward-looking statements within the meaning of the safe harbor provided by Section 21E of the Securities Exchange Act of 1934, as amended, and Section 27A of the Securities Act of 1933, as amended, with respect to our financial condition, results of operations, business strategies, operating efficiencies, competitive positions, growth opportunities for existing services, plans and objectives of management, markets for stock and other matters. These include all statements other than statements of historical fact, including, without limitation, any statements preceded by, followed by, or that include the words "targets", "believes", "expects", "aims", "intends", "will", "may", "anticipates", "would", "should", "could", "estimates", "forecast", "predict", "continue" or similar expressions or the negative thereof.

These forward-looking statements, including, among others, those relating to our future business prospects, revenues and income, wherever they may occur in this EIS and the exhibits to this EIS, are essentially estimates reflecting the best judgment of our senior management and involve a number of risks and uncertainties that could cause actual results to differ materially from those suggested by the forward-looking statements. As a consequence, these forward-looking statements should be considered in light of various important factors, including those set forth in these materials. Important factors that could cause actual results to differ materially from estimates or projections contained in the forward-looking statements include, without limitation: overall economic and business conditions in South Africa, Papua New Guinea, Australia and elsewhere, estimates of future earnings, and the sensitivity of earnings to the gold and other metals prices, estimates of future gold and other metals production and sales, estimates of future cash costs, estimates of future cash flows, and the sensitivity of cash flows to the gold and other metals prices, statements regarding future debt repayments, estimates of future capital expenditures, the success of our business strategy, development activities and other initiatives, estimates of reserves statements regarding future exploration results and the replacement of reserves, the ability to achieve anticipated efficiencies and other cost savings in connection with past and future acquisitions, fluctuations in the market price of gold, the occurrence of hazards associated with underground and surface gold mining, the occurrence of labour disruptions, power cost increases as well as power stoppages, fluctuations and usage constraints, supply chain shortages and increases in the prices of production imports, availability, terms and deployment of capital, changes in government regulation, particularly mining rights and environmental regulation, fluctuations in exchange rates, the adequacy of the Group's insurance coverage and socio-economic or political instability in South Africa and Papua New Guinea and other countries in which we operate.

For a more detailed discussion of such risks and other factors (such as availability of credit or other sources of financing), see the Company's latest Integrated Annual Report and Form 20-F which is on file with the Securities and Exchange Commission, as well as the Company's other Securities and Exchange Commission filings. The Company undertakes no obligation to update publicly or release any revisions to these forward-looking statements to reflect events or circumstances after the date of this EIS or to reflect the occurrence of unanticipated events, except as required by law.

Competent Person's Statement

The Wafi-Golpu Joint Venture is an unincorporated joint venture between a wholly-owned subsidiary of Harmony Gold Mining Company Limited and a wholly-owned subsidiary of Newcrest Mining Limited.

The information in the EIS that relates to Golpu Ore Reserves is based on information compiled by the Competent Person, Mr Pasqualino Manca, who is a member of The Australasian Institute of Mining and Metallurgy. Mr Pasqualino Manca, is a full-time employee of Newcrest Mining Limited or its relevant subsidiaries, holds options and/ or shares in Newcrest Mining Limited and is entitled to participate in Newcrest's executive equity long term incentive plan, details of which are included in Newcrest's 2017 Remuneration Report. Ore Reserve growth is one of the performance measures under recent long term incentive plans. Mr Pasqualino Manca has sufficient experience which is relevant to the styles of mineralisation and type of deposit under consideration and to the activity which he is undertaking to qualify as a Competent Person as defined in the JORC Code 2012. Mr Pasqualino Manca consents to the inclusion of material of the matters based on his information in the form and context in which it appears.

Wafi-Golpu DSTP Project

Density Current, Plume Dispersion, and Hydrodynamic Modelling

PRESENTED TO

Wafi-Golpu Joint Venture

APRIL 23, 2018
ISSUED FOR USE
FILE: 704-TRN.WTRM03002
532-1214-FS-REP-0014

Tetra Tech Canada Inc.
Suite 1000 – 10th Floor, 885 Dunsmuir Street
Vancouver, BC V6C 1N5 CANADA
Tel 604.685.0275 Fax 604.684.6241

This page intentionally left blank.

EXECUTIVE SUMMARY

This report describes the work completed on the density current, plume dispersion, and hydrodynamic modelling associated with the detailed design for the Deep Sea Tailings Placement (DSTP) system for the Wafi-Golpu Project, in Morobe Province, Papua New Guinea (PNG). The DSTP system consists of an overland pipeline of about 103km extent, delivering tailings slurry to the near-shore mix/de-aeration tank, where sea water is mixed with the tailings slurry, and discharged through an outfall pipe to a depth of 200m in the Huon Gulf. The DSTP modelling system described in this report simulates the transport and deposition/scour processes that govern the behaviour of the tailings in the receiving environment within a model grid domain that covers the Huon Gulf from the Markham River to an eastern boundary at about 147°42'E. The grid has a spatial resolution of 50m at its western boundary, increasing to 1,000m at its eastern boundary where the Huon Gulf connects to the flow passing through Vitiaz Strait. The modelled simulations were based on an annual tailings throughput of 16.5Mt.

Two models were used to simulate the transport and deposition/scour processes governing the movement of tailings in the marine environment: a density current model, and a 3D hydrodynamic model (H3D). Once coupled together, these models describe the behaviour of the tailings within the Huon Gulf, as well as the behaviour of the native sediments, both from direct river inputs and from episodic sediment plumes generated by seismic and slope stability events.

The density current model was successful in describing the transport, as well as deposition and scour processes related to the tailings while travelling as a bottom-attached density current with about 60% of the tailings initially being deposited within the Markham Canyon and almost 40% generating subsurface plumes at depths predominantly between 300m and 500m. Modelling conducted to date with regards to episodic mass movement events of natural sediments within the Markham Canyon agrees with oceanographic observations that tailings that are deposited within the Markham Canyon are likely to be conveyed down-canyon into the New Britain Trench over time as a result of persistent downslope turbidity currents as well as these episodic mass events of natural sediments through the canyon. Negligible amounts of material (0.8%) exit the modelled domain during the modelled period; therefore the numerical models obeyed all physical conservation laws and accounted for the transport, deposition, and scouring processes within the modelled period and domain that ultimately serve to describe the physical extent of the tailings within the Huon Gulf. No deposition occurs immediately in front of the outfall location and hence there is no concern of plugging up the pipe at its outlet during a shutdown. For the maximum through-put scenario of 16.5Mtpa, dilutions range from 20:1 at 20m downslope from the outfall location to greater than 200:1 at 150m downslope from the outfall.

The models simulate the discharge of mine tailings into a water body with its own significant and complex sedimentation characteristics. Numerous rivers, notably the Markham and Busu Rivers near the outfall site, contribute about 50 Mtpa of sediment to the Huon Gulf, augmented by ten other rivers along the north shore of the Huon Gulf which contribute another 10 Mtpa. The simulation of these natural sediment sources is based on a three-dimensional model, which enables evaluation of the depositional footprint as well as sediment plumes in the water column.

As observed through the oceanographic campaign, the presence of episodic natural sediment mass movement events in the Huon Gulf were taken into account and modelled on the basis of one large event per year, resulting in a re-suspension and subsequent transport of a considerable proportion of the tailings and natural sediment that were initially deposited at depths of 600m-1,000m to deeper depths, i.e. 1,600m to 2,400m. Several mass movement events have been observed over an approximately one-year period of oceanographic data collection, as described in the Oceanographic report (IHAconsult, 2018)". Modelling one such event per year was considered to be a conservative approach, given that the inter-annual variability for the interval of occurrence for these events is unknown over the life of the mine.

The combined modelling system (density current model and three-dimensional model) provides a realistic simulation of the sediment depositional processes in the Gulf:

- Coincident deposition of tailings and native sediment, but with different spatial distributions;
- Conveyance of re-suspended sediments in deeper depths of the Markham Canyon by the energetic episodic events;
- Burial by native sediment after mine closure.

The model was thoroughly and satisfactorily validated against observed data. In particular, the validation focused on ADCP current data, CTD water column properties and natural sediment footprint. Through this validation framework which incorporates a wide range of environmental forcing to the Huon Gulf, confidence has been developed in its ability to realistically simulate the transport, deposition, and scouring of the tailings. Taking into account the limitations of numerical modelling, i.e. the extrapolation of one year of deposition into 27 years, a conservative approach was undertaken with respect to simulating the transport, deposition, and scouring processes that dictate the extent of the tailings. That is, although several large mass movement events have been observed to occur in one year, the modelling only assumed one per year. This one event was able to sweep almost all the tailings deposited in the Markham Canyon to the deeper basin, indicating that there will be minimal build-up within the Canyon. Based on the current modelling work, as well as oceanographic data collected during 2016 – 2017, and past literature review (i.e. Buleka et al., 1999) that describe the persistent nature of the down-canyon turbidity current within the Huon Gulf, it is expected that the majority of the tailings that is initially deposited within the Markham Canyon will be conveyed to greater depths thereafter by way of these natural episodic events and down-canyon turbidity currents. However, there will be significant build-up on the slopes leading away from the outfall pipe, at depths of 300 to 500m. Two processes serve to mitigate this tailings deposition. First, this side-slope area is also an area of significant natural deposition, so that the tailings footprint will be covered over with natural sediments in a relatively short time after mine cessation, thereby inhibiting release of metals from the deposited tailings. Second, morphological analysis of the sloping sea bottom from the outfall terminus to the Markham Canyon (Tetra Tech Updated Slope Stability Assessment, 2018) indicates that there are a number of down-slope channels, both active and abandoned, that serve to enable the down-slope migration of natural sediments. These channels would similarly serve to allow deposited tailings to move downslope to the Markham Canyon, on an episodic basis. It is shown in this report that any material that arrives at the Markham Canyon is ultimately transported down-canyon towards the New Britain Trench.

TABLE OF CONTENTS

LIST OF TABLES IN TEXT

LIST OF FIGURES IN TEXT

APPENDIX SECTIONS

APPENDICES

LIMITATIONS OF REPORT

This report and its contents are intended for the sole use of WGJV and their agents. Tetra Tech Canada Inc. (Tetra Tech) does not accept any responsibility for the accuracy of any of the data, the analysis, or the recommendations contained or referenced in the report when the report is used or relied upon by any Party other than WGJV, or for any Project other than the proposed development at the subject site. Any such unauthorized use of this report is at the sole risk of the user.

1.0 INTRODUCTION

Wafi-Golpu Joint Venture (WGJV) engaged Tetra Tech to conduct the engineering investigations for a Deep Sea Tailings Placement (DSTP) system for the Wafi-Golpu Project in Morobe Province, Papua New Guinea. In December 2017, Tetra Tech completed a Feasibility Study for a DSTP system capable of placing 16.5Mtpa of tailings into the deep waters of the Huon Gulf. This report is concerned with an additional item, the numerical modelling of the physical impacts of the project on the marine environment, specifically, a description of the transport, deposition and scouring processes of the mine tailings slurry containing tailings solids and liquor that will be released by the DSTP system.

The purpose of this report is to provide details on the available datasets, the numerical modelling tools, the validation of the model inputs and outputs, and to present the modelled results related to the behaviour and physical description of the transport, deposition, and scouring processes as they relate to the tailings within the marine environment.

1.0 Project Location

The study area is located near Lae, the capital city of Morobe Province on the eastern coast of Papua New Guinea. Lae experiences a tropical climate with high temperatures and relative humidity and high precipitation. The average daily temperature is 29°C with a relative humidity of 93% in the morning and 72% in the evening (Weatherbase, 2017). The Busu River, located near Lae is the fastest flowing river in Papua New Guinea, and brings a high sediment load into the Huon Gulf (Betasolo et al., 2014). The Markham River also brings in even larger amounts of sediment to the Huon Gulf. The estimated suspended sediment load in the Markham River is approximately 42Mtpa (IHAconsult & GDA Consult, 2018). The outer Huon Gulf (i.e. east of approximately 147°12'E (IHAconsult, 2018)) predominantly experiences southeasterly trade winds between May and October and northwesterly winds during the monsoon season between October and April. Squalls develop occasionally during monsoon season resulting in strong localized winds from the south. These strong localized winds do not appear to generate large waves in the vicinity of the project site. The inner Huon Gulf, based on WaveWatch III winds, is seeing two distinct wind seasons: May to October when the persistent southeast trade winds occur, and October to April when the northwesterly monsoon winds dominate. Figure 1.1 shows the geographical setting of the site location: Huon Gulf in Papua New Guinea.

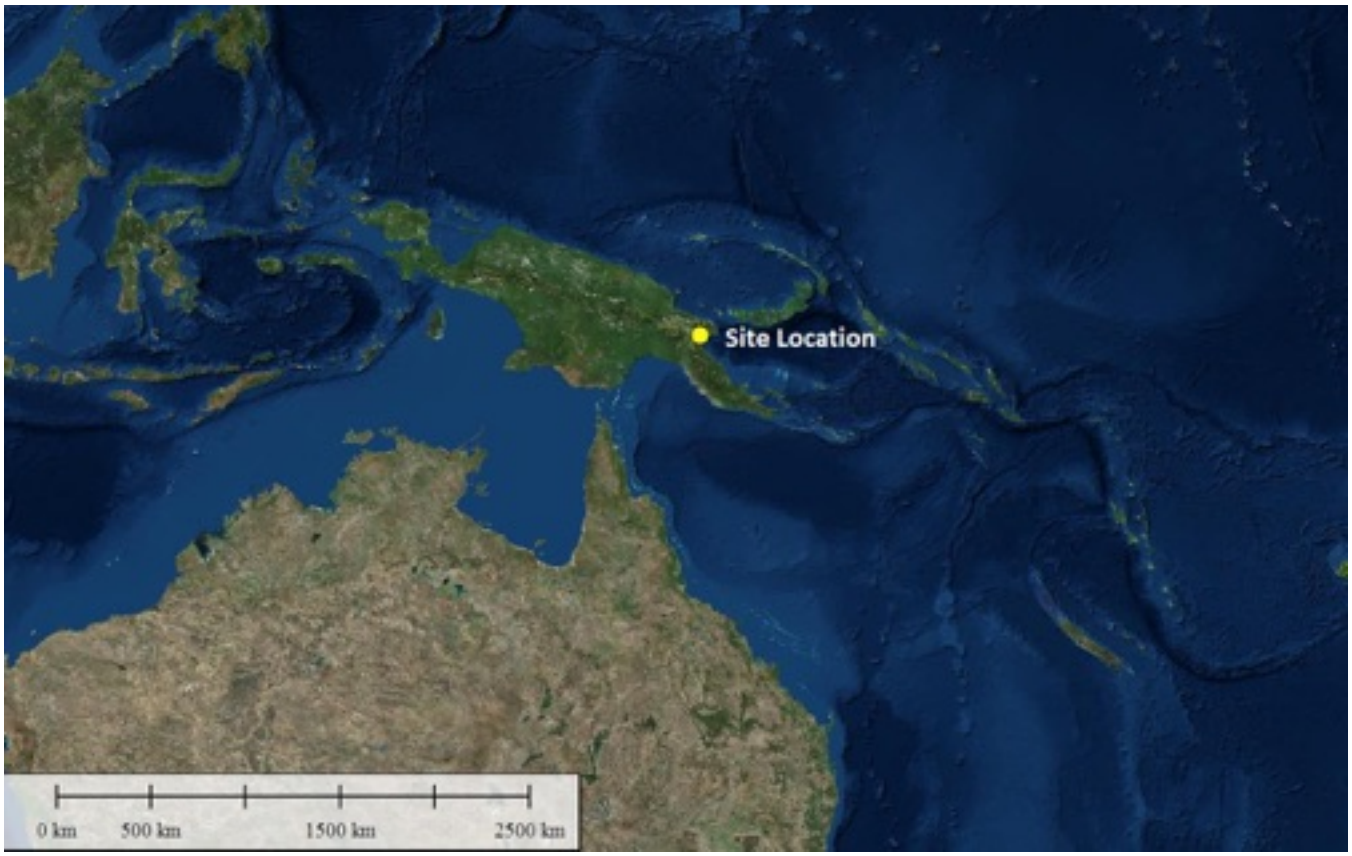

Figure 1.1 Geographical Setting of Site Location

It is proposed that the tailings slurry will be brought from the mine processing plant, about 100 km inland, to a mix/de-aeration tank located near the shore, where the tailings will be pre-diluted with sea water, in this case in the ratio of four parts seawater to one part tailings slurry (by volume). The mix/de-aeration tank will allow any air bubbles that occur in the slurry/seawater mixture to escape before the diluted tailings are discharged to the ocean. The mix/de-aeration tank will be located at UTM Zone 55M, 504,703 m E and 9,255,925 m S. The outfall pipe will descend to 200m depth, where it will terminate, discharging tailings slurry to the deep ocean. Several simulations were conducted using the near-field density current model in order to determine the optimal discharge location. The plan view for the final optimal route is shown in Figure 1.2, as well as the mix/de-aeration tank location. The proposed DSTP system is located between Wagang Village and the Busu River.

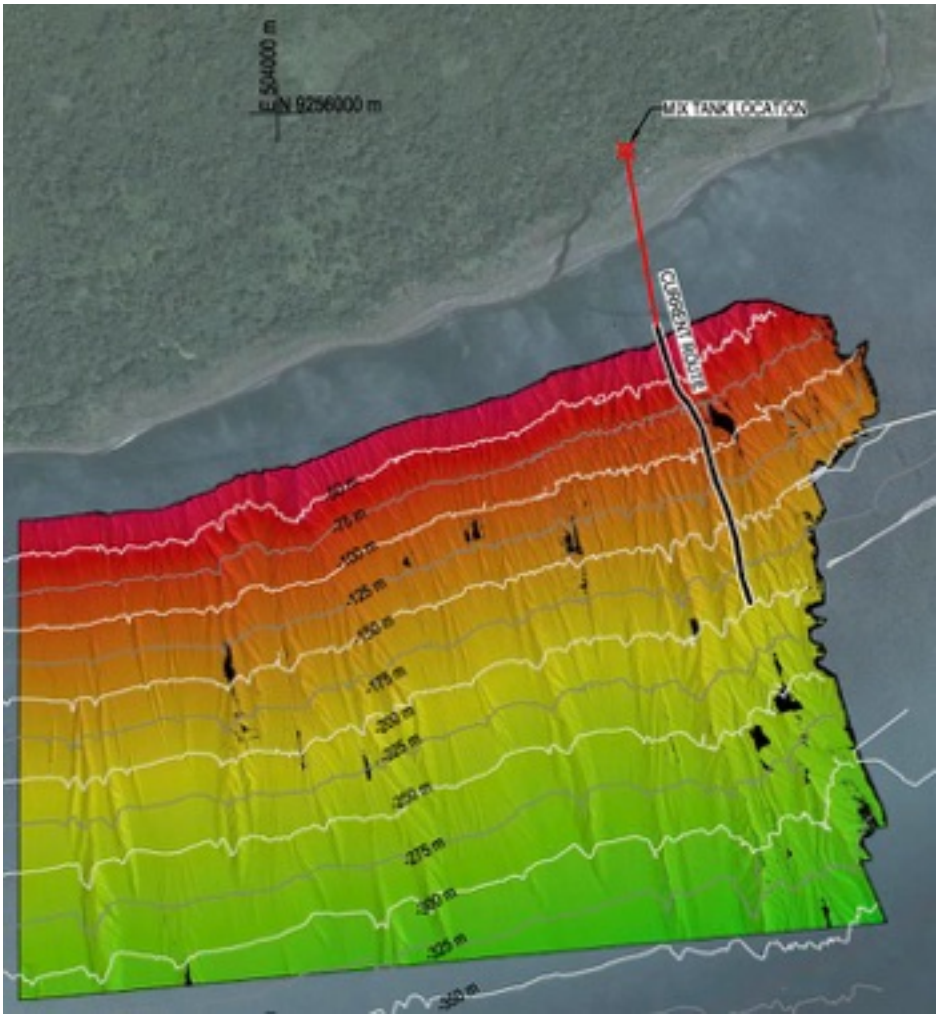

Figure 1.2 Mix Tank Location, Pipe Route, and Outfall Location

1.1 Tailings Behaviour in the Marine Environment

Simulating the transport, deposition, and scour of the Wafi-Golpu tailings requires two types of models, corresponding to the two predominant physical transport mechanisms for tailings after discharge into the Huon Gulf. As the diluted tailings leave the outfall pipe, being negatively buoyant, they will form a density current that travels downslope close to the seabed. As the density current proceeds downslope, it will progressively entrain more seawater which will reduce the density contrast with the surrounding seawater and result in subsurface tailings plumes shearing off from the descending density current. These subsurface tailings plumes will be neutrally buoyant within the stratified layer within which they shear off and will disperse horizontally as they are transported by ocean currents.

The initial phase of the tailings transport, deposition, and scouring is modelled using a two-dimensional Density Current Model. The subsurface plumes are modelled as part of the overall three-dimensional circulation model, H3D, implemented for the Huon Gulf. Meanwhile, the various rivers entering the Huon Gulf introduce considerably more sediment (about 60Mtpa) than the tailings discharge (about 16.5Mtpa), and this sediment deposits in the Huon Gulf, mixing with, and ultimately burying, the tailings sediment. These naturally-occurring sedimentary processes are also simulated by the H3D and Density Current models. A detailed technical description of both models is given in Appendix A.

2.0 THREE-DIMENSIONAL HYDRODYNAMIC MODEL: H3D

2.0 Background Information

H3D is a three-dimensional time-stepping numerical model which computes the three components of velocity (u,v,w) on a regular grid in three dimensions (x,y,z), as well as scalar fields such as temperature and contaminant concentrations. The model uses the Arakawa C-grid (Arakawa and Lamb, 1977) in space, and uses a two level semi-implicit scheme in the time domain. H3D bears many similarities to the well-known Princeton Ocean Model (POM) (Blumberg and Mellor, 1987), and other similar models (Delft 3D, Mike 3) in terms of the equations it solves, but differs in how the time-domain aspects are implemented. H3D uses a semi-implicit scheme, allowing relatively large timesteps, and does not separately solve the internal and external modes as POM does. It also uses a considerably simpler grid in the vertical, allowing for faster and more accurate simulations.

H3D is an implementation of the numerical model developed by Backhaus (1983; 1985) which has had numerous applications to the European continental shelf, (Duwe et al., 1983; Backhaus and Maier-Reimer, 1983), Arctic waters (Kampf and Backhaus, 1999; Backhaus and Kampf, 1999) and deep estuarine waters (Stronach et al., 1993). In western Canada, H3D has been used to model the temperature structure of Okanagan Lake (Stronach et al., 2002), the transport of scalar contaminants in Okanagan Lake (Wang and Stronach, 2005), sediment movement and scour/deposition in the Fraser River, circulation and wave propagation in Seymour and Capilano dams, and salinity movement in the lower Fraser River. H3D has had extensive application to sediment management issues in the Fraser River, as a consultant to the Port of Vancouver. Tetra Tech has developed a comprehensive high-resolution model of the navigable portion of the river, and use H3D for almost all proposed works in the river that could change sedimentation patterns and dredging requirements. H3D forms the basis of the model developed by Saucier and co-workers for the Gulf of St. Lawrence (Saucier et al., 2003), and has been applied to the Gulf of Mexico (Rego et al., 2010). H3D and its hydrocarbon transport and weathering module have been used in three recent environmental assessment applications concerning marine transportation of hydrocarbons by tanker vessels. H3D was used to simulate an existing and a proposed reservoir for BC Hydro's Site C Clean Energy Project. Temperature, ice cover and sedimentation characteristics of the proposed reservoir were predicted, supported by model validation in the existing Dinosaur Reservoir.

H3D has also been used on other DSTP projects, in a similar manner to the way it is used here: the Lihir and Ramu Projects in Papua New Guinea and Moa in Cuba are three other DSTP projects of similar size.

In order to test the model, a simulation of the 2016 and 2017 calendar years was conducted, using meteorological and oceanographic data that was available starting from January 2016. The 2016 run is viewed as a ‘spinup’ or test run, aimed at identifying any input data gaps and confirming appropriate model settings, as well as testing the coupling between the two models, H3D and Density Current. The next set of simulations, starting in October 2016 and extending into 2017, underwent a more comprehensive validation, and project-specific data presentations have been developed from that run, and are described in this report.

Section 2.1 below describes the inputs that H3D requires, and Section 2.1 presents the observed data used for the validation of H3D, as well as the validations themselves.

2.1 Numerical Modelling Inputs

H3D depends strongly on the data that is provided to it, both as initial conditions to start a simulation, and forcing inputs, required over the course of the simulation. The following is a summary of the main data requirements:

Initial Conditions

1. Bathymetry, interpolated onto H3D’s curvilinear computational grid. The grid has a horizontal resolution of 50m in the vicinity of the Markham River. The grid size increases in the easterly direction, in the same way

that the Huon Gulf opens out, reaching a resolution of 1,000m at the eastern boundary of the model. The model grid has a total of 67,000 cells in plan view, 65 layers in the vertical and in three dimensions, a total of 2,849,896 cells. Vertical resolution varies from 2m near the surface to 250m at depths greater than 1000m.

2. Temperature, salinity and sediment distributions. For the simulations reported here, the sediment concentration in the water column is assumed to be zero initially, and allowed to grow as the various rivers provide sediment to the Huon Gulf. Salinity and temperature throughout the model domain are initialized from archived gridded data produced by the global HYCOM model, as confirmed by the oceanographic observed data (IHAconsult, 2018).

Time-Varying Forcing Conditions

1. Tide levels at the open boundaries of the model (in this case, the east boundary), simulated by time-varying water levels calculated from tidal harmonic constants;

2. Winds velocities, which provide momentum to drive surface currents, and are correlated with heat and mass transfers at the air-water interface, typically provided on an hourly basis over the model domain;

3. River inputs: flow, sediment and temperature; and

4. Meteorological forcing for temperature simulation: incident short-wave radiation, long-wave back radiation, sensible heat flux (due to air/water temperature differences) and sensible heat flux (due to the difference between humidity in the air over Huon Gulf and the saturated humidity value). Section 2.1.5 summarizes these heating and cooling processes.

More details on these forcing requirements are provided below.

2.1.1 Bathymetry

The bathymetric data used is a compilation of data sourced from studies conducted by IHAconsult on behalf of Wafi-Golpu, and the General Bathymetric Chart of the Oceans (GEBCO) for the most eastern and southern areas of the Gulf. Figure 2.1 illustrates the bathymetry used within the numerical modelling studies. The area shown is the domain of the three-dimensional model, covering the entire Huon Gulf.

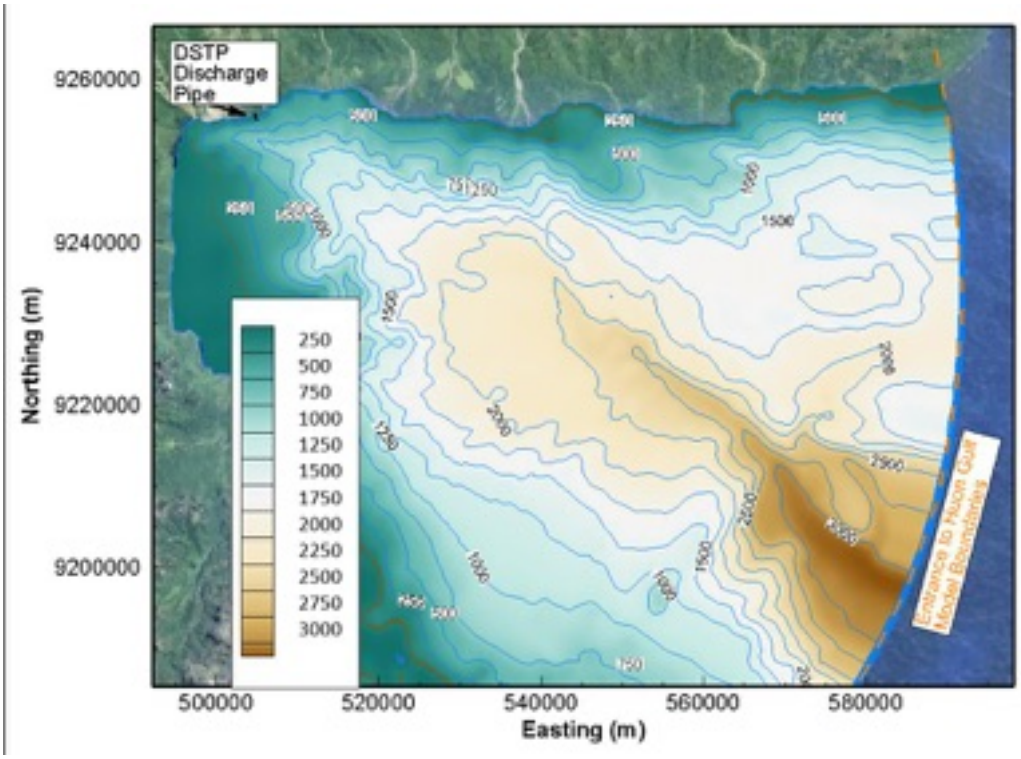

Figure 2.1 Bathymetry of the Huon Gulf

2.1.2 Water Temperature and Salinity Initialization

Water temperature and salinity were derived from data products produced by HYCOM (Hybrid Coordinate Ocean Model, (Wallcraft et al., 2009). HYCOM is a general circulation ocean model developed by the Consortium for Data Assimilative Modeling as a multi-institution partnership. Output datasets from the HYCOM model are available for download with a spatial resolution of 1/12° which is approximately 8 km. Temperature and salinity parameters were downloaded for the Huon Gulf region with a temporal resolution of 30 days (approximately monthly) to be used for initialization of H3D in any particular month. Data from a particular day is used for initialization, whereas all the downloaded data is used to create time-varying boundary conditions for salinity and temperature at the open boundary of the model.

CTD data has been collected by Ian Hargreaves & Associates (IHAconsult, 2018) since August 2016 and this is an ongoing program. There are 15 sampling locations in total: A1-A5, B1-B5, CTD5, CTD6, MCA, MCB, and MCC. Figure 2.2 displays the locations of the CTD data collection points. Profile locations A1-A5 and B1-B5 have been sampled at two to four week intervals starting October 2016 and are illustrated in white, the remaining profile locations were sampled over single voyages in August 2016 and February 2017 (illustrated in orange). The location of the outfall pipeline is also indicated in Figure 2.2. Most of the data is collected at approximately biweekly intervals along the A and B transects. Transects A and B are in close proximity to the anticipated tailings flow path. Table 2.1 presents the temporal availability of the different profile data.

Salinity and density can be calculated from the measured parameters of conductivity, temperature, and depth (pressure). In addition to conductivity, temperature, and depth (pressure), the CTD instrument also measures light within a certain wavelength band transmitted from the surface through the water column.

The CTD profiles were used as the basis for ocean density inputs to the density current model and to validate the temperature, salinity, and density outputs of the H3D model.

Table 2.1: Temporal Availability of Collected CTD Data

	2016					2017										
	Aug	Sep	Oct	Nov	Dec	Jan	Feb	Mar	Apr	May	Jun	Jul	Aug	Sep	Oct	Nov
A1					●	●	●	●	●	●	●	●	●	●	●	●
A2					●	●	●	●	●	●	●	●	●	●	●	●
A3			●	●	●	●	●	●	●	●	●	●	●	●	●	●
A4					●	●	●	●	●	●	●	●	●	●	●	●
A5					●	●	●	●	●	●	●	●	●	●	●	●
B1			●	●	●	●	●	●	●	●	●	●	●	●	●	●
B2			●	●	●	●	●	●	●	●	●	●	●	●	●	●
B3			●	●	●	●	●	●	●	●	●	●	●	●	●	●
B4			●	●	●	●	●	●	●	●	●	●	●	●	●	●
B5			●	●	●	●	●	●	●	●	●	●	●	●	●	●
CTD5							●									
CTD6							●									
MCA	●															
MCB	●															
MCC	●															

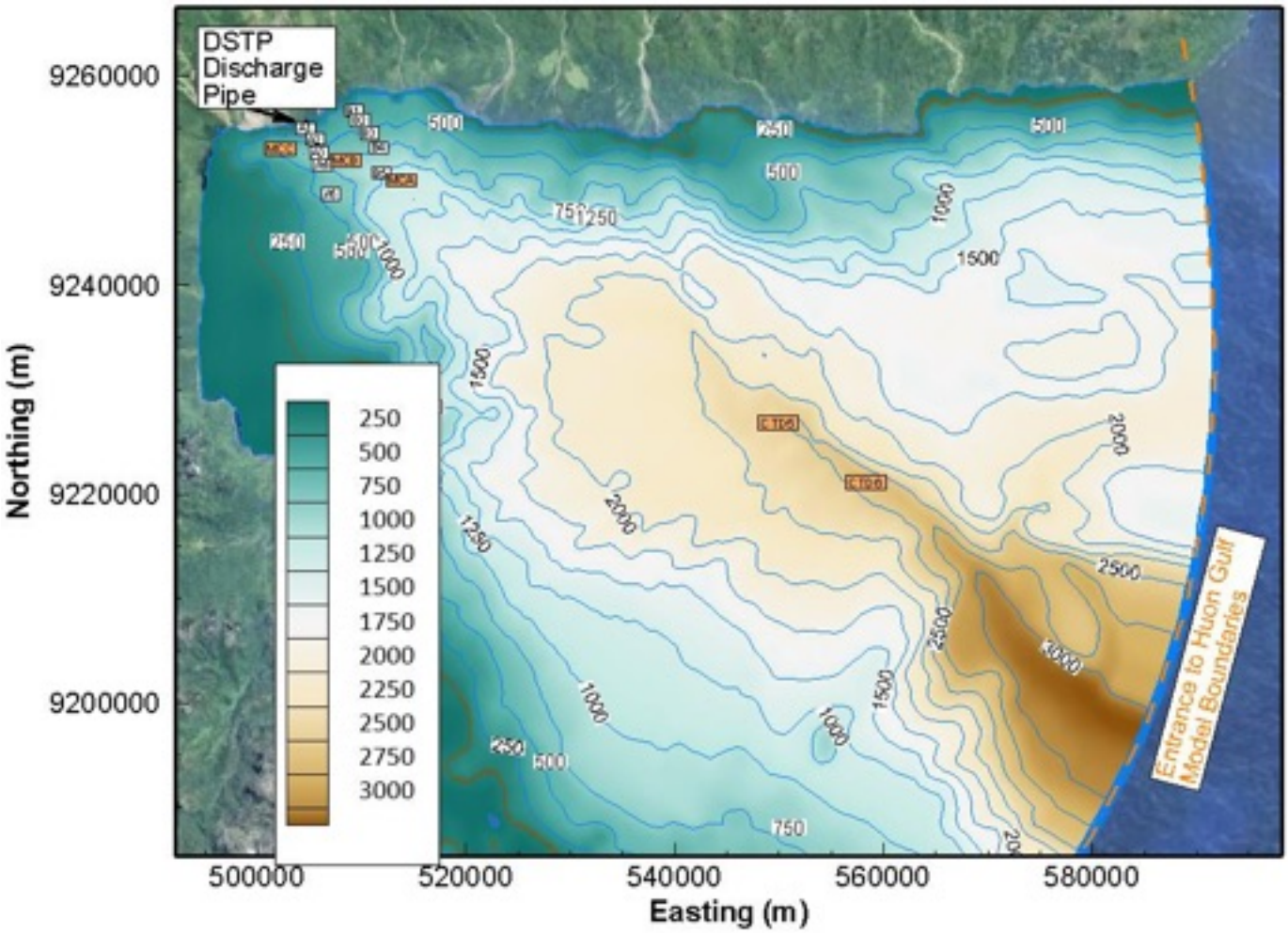

Figure 2.2 Location of CTD Profiles A1-A5, B1-B5, MCA, MCB, MCC, CTD5, and CTD6 (Including Model Bathymetry for Huon Gulf)

2.1.3 River Flows and Suspended Sediment Loads

All of the available river flow and suspended sediment concentration data were compiled for the Busu River and the Markham River in order to formulate the best estimate of a two-year record for 2016 – 2017 for each of these two rivers respectively. River flow and suspended sediment concentrations were originally compiled by ALS Hydrographics Australia. The additional data source was the project report: Physical, Chemical and Biological Sedimentology of the Huon Gulf (IHAconsult & GDA Consult, 2018). From 2016-2017, the gauging stations on the Busu and Markham Rivers each consisted of a pressure recorder to measure water level, which was then converted to river discharge, and a Sequoia Lisst ABS (acoustic backscatter sensor) to measure acoustic backscatter, which can be converted to concentration of suspended solids in mg/L. This conversion was calibrated using laboratory measurements of samples of know sediment concentration, as reported in IHAconsult & GDA Consult, (2018).

Markham River flow and sediment concentration data have historically been monitored at three different locations over the period of record 2011 to 2017.

From December 2011 to April 2015, a discontinuous data set of flow and suspended solids (TSS) was recorded at station MH3KMMAR (452184mE, 9266684mS), just below the confluence of the Watut River. This station derived

suspended solids concentration from a direct measurement of turbidity using an optical turbidity sensor (IHAconsult & GDA Consult, 2018). Year 2013 had the most consistent record (i.e. about 8 months) of both flow and TSS during this time period.

In September 2016, a gauging station on the Markham was implemented at MWMARKHAM (462432m E, 9268146mS), on the only lowland section where the flow was confined to a single channel. The sensor malfunctioned shortly after installation and data was lost from mid-October 2016 to mid-December 2016. Data collection then recommenced at the same location in mid-December until about mid-January, when the station was vandalised. The gauging station and Lisst ABS sensor were then moved slightly upstream to MWMARKHAM (461848mE, 9267575mS) in March 2017, and data collection commenced at this location in May 2017. Therefore, for the period of 2016 – 2017, data was unavailable from January to mid-September 2016, mid-October to mid-December 2016, and mid-January to mid-May 2017.

In order to generate a complete data series of flow and suspended sediment concentration to be implemented into H3D, these missing time periods were estimated from the 2011 to 2015 data sets (measured at MH3KMMAR) as follows. All data at both stations was measured in 10-minute intervals, and averaged into hourly intervals. The sediment concentration values derived from continuous measurements of turbidity at MH3KMMAR were notably consistently lower than those measured from station MWMARKHAM further downstream between years 2016 – 2017, as seen in Figure 2.3 below. The scattered data shown in Figure 2.3 is the hourly-averaged flow and sediment concentration data received from ALS Hydrographics Australia. In fact, IHA (2017) reports that the mean daily suspended sediment load derived from the available months of flow and sediment concentration data at MH3KMMAR is about 50,800 – 66,180 t/day or a mean annual suspended sediment load of 18 - 24Mtpa. However, suspended sediment load estimates for the Markham based on station MWMARKHAM (2016 – 2017) with the Lisst ABS sensor (calibrated based on suspended sediment sampling conducted in September 2017) are over 40Mtpa (i.e. the product of the mean flow multiplied by the mean TSS (mg/L) and multiplied by 365 days, yields as estimated annual suspended sediment load of 43.1Mt) as seen in Table 3-1 of IHAconsult (2018).

This rough estimate for the annual suspended sediment load somewhat underestimates the annual suspended sediment load, since multiplying mean daily flow and mean daily TSS does not account for the peak concentrations that tend to coincide with peak flows in the Markham River. Therefore, a better estimate is made by calculating the daily suspended sediment load (daily flow and daily suspended sediment concentration) and then summing the product of these values over a one-year period. Unfortunately, due to the incompleteness of the dataset for 2016 – 2017, this method is not possible for these years without filling in the gaps of missing data with the best estimate from 2011 – 2015.

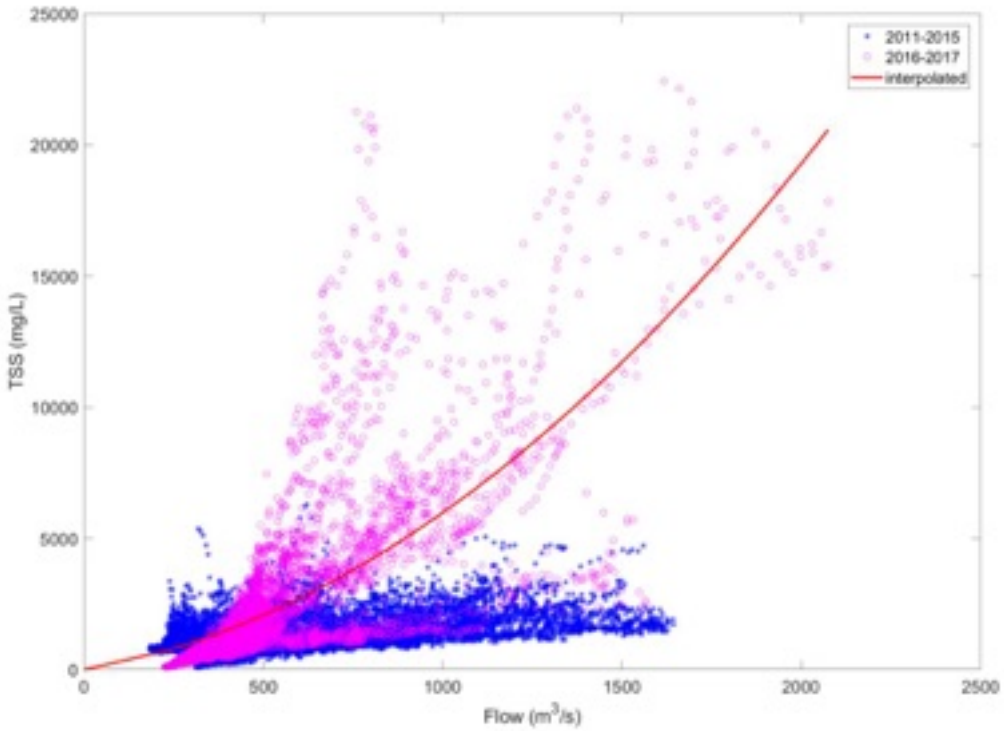

Figure 2.3 TSS (mg/L) and Flow (m^3/s) Measured at Station MH3KMMAR (2011 – 2015) and MWMARKHAM (2016 – 2017)

Given that the suspended sediment concentration data from 2011 – 2015 for a given flow rate was lower on average for a given measured flow rate when compared to the 2016 – 2017 data, then a second order polynomial linear regression of the 2016 – 2017 data for suspended sediment concentration vs flow was generated (Figure 2.3) in order to adjust the TSS measurements for 2011 – 2015, based on the hourly averaged measured flow rate from 2011 - 2015. Flow data from 2011 – 2015 was compiled into a single year record of hourly averaged values, and corresponding hourly averaged TSS values were computed based on this second order linear regression. The resulting data was used to fill in the gaps in the 2016 – 2017 time series. All flow and suspended sediment concentration input data for H3D for the Markham River was reported to H3D as hourly averages; 2016 – 2017 data was utilized where it was available, and all other periods were derived from the 2011 – 2015 field data.

The resulting annual suspended sediment load calculated for 2016 was 49.2Mt for 2016 and 50.1Mt for 2017. Figure 2.4 and Figure 2.5 shows available data record from 2011 – 2015 from station MH3KMMAR (adjusted TSS data as described above), and from 2016 – 2017 from station MWMARKHAM respectively.

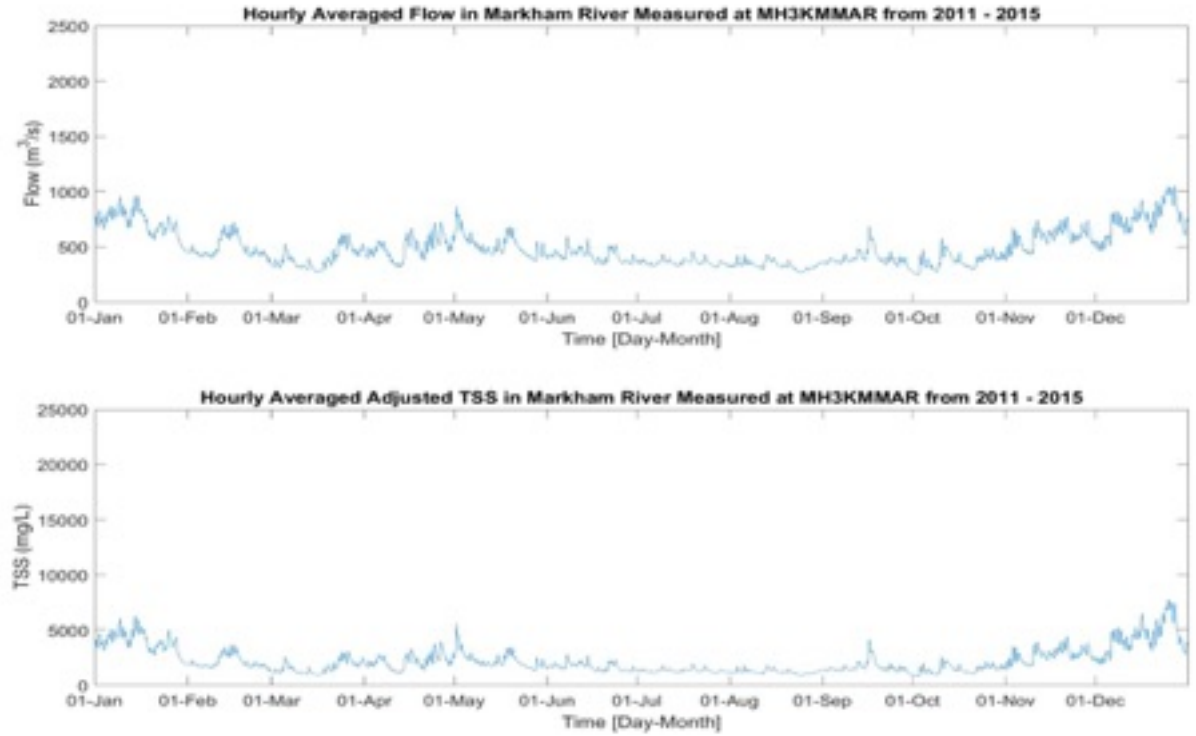

Figure 2.4 Hourly average flow and adjusted TSS in Markham River, measured at station MH3KMMAR (2011 – 2015)

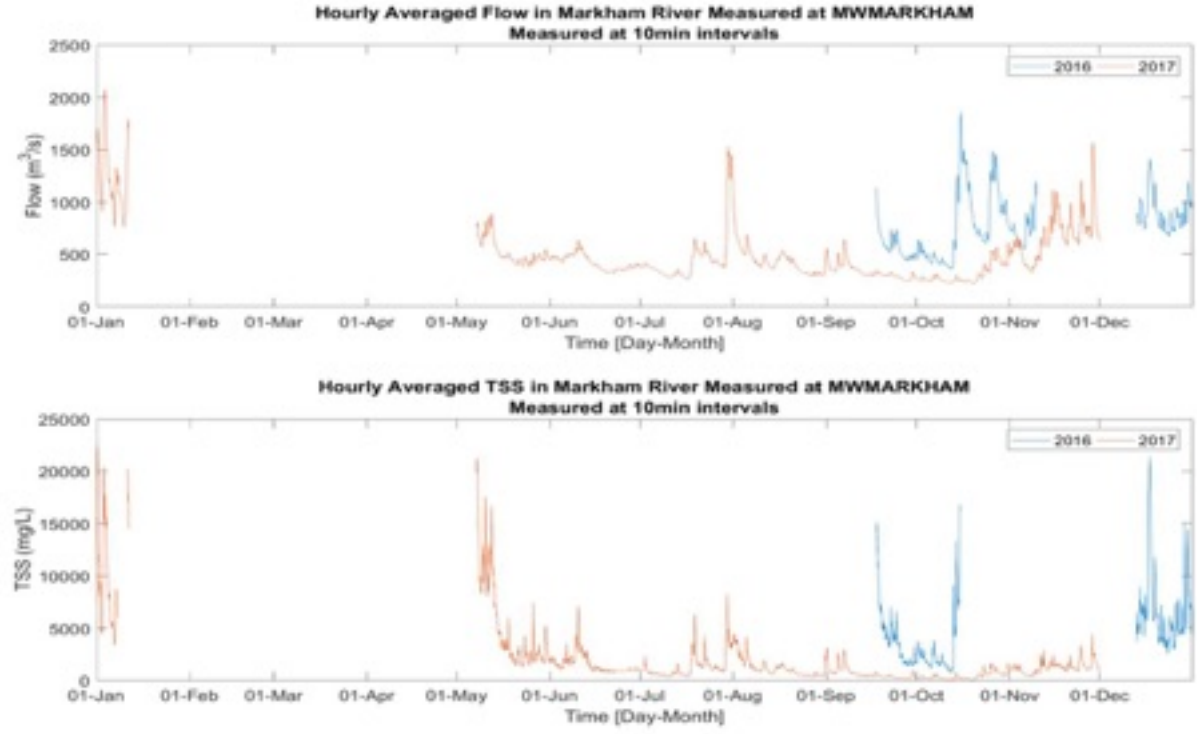

Figure 2.5 Hourly average flow and TSS in Markham River, measured at station MWMARKHAM (2016 – 2017)

Measured daily Busu River flow and suspended sediment concentration data was available from September 2016 to December 2017. For the period of record from January 2016 to September 2016, where no measured data was available, the measured daily values from 2017 were used to complete the time series. Likewise, where data was missing from December 2 – 31, 2017, data was copied from December 2 – 31, 2016 for flow and suspended sediment concentrations. Data was compiled into daily average values for input into H3D. As seen in Figure 2.6, this provided a more complete record of flow and suspended sediment concentration for the Busu for the time period of interest (2016 – 2017), than was available for the Markham River (described above).

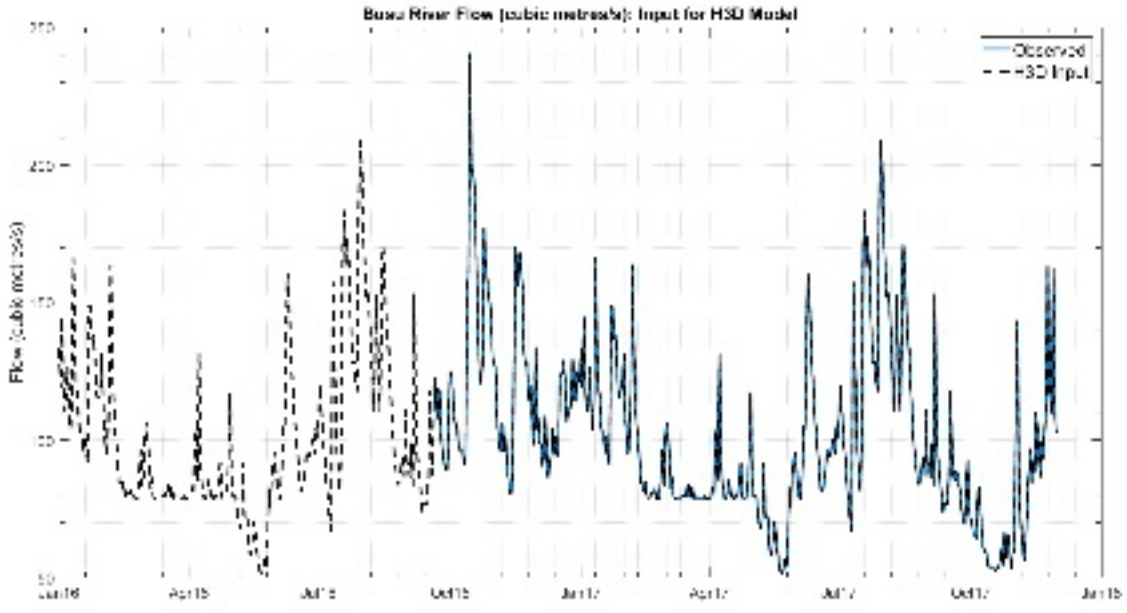

Figure 2.6 Busu River Flow (2016 – 2017)

Given that flow and suspended sediment concentration data are not available from the other rivers along the northern coast of the Huon Gulf, these have been inferred from the Busu River flow and suspended sediment concentration data described above. The Busu River data described above was used as the basis to establish an estimate of the flow and suspended sediment concentration of the other 10 rivers listed in Table 2.2 below because of the geographic proximity of these rivers, which suggests more similar catchment topology and geology than compared to the Markham River catchment. The size of the catchment for each river was taken from IHAconsult & GDA Consult (2018), as shown in Table 2.2, and these quantities were then used to linearly scale the Busu River daily average flow according to the ratio of their respective catchment sizes, to form a time series of flow for each river for 2016 and 2017. The daily average suspended sediment concentration time series for 2016 – 2017 was assumed to be equal to that of the Busu River, given that the geographic proximity of these watersheds and assumed similarity in suspended sediment origin and characteristics.

Table 2.2 shows the assumed catchment area, and calculated average flow (m^3/s), average TSS (mg/L), daily average suspended sediment load, and mean annual suspended sediment load for 2016 – 2017 for all of the rivers described above, including the Markham and the Busu Rivers. The total computed annualized average suspended sediment load from all 12 of these rivers into the Huon Gulf is 60.5 Mt per year, as displayed in Table 2.2 below.

Table 2.2: Characterization of River Flow into the Huon Gulf

River	Catchment Elevation Category	Catchment Area (km^2)	Mean Flow (m^3/s)	Mean TSS (mg/L)	Estimated Daily Average Suspended Sediment Load (t/day)	Estimated Annual Suspended Sediment Load (Mt/a)
Markham			528.2	2344	135, 814	49.6
Busu	High Mountain	1,400	101.4	1025	10, 317	3.8
Bumbu	Upland	60	4.4	1025	442	0.2
Bupu	Mountain	75	5.4	1025	553	0.2
Bunga	Mountain	60	4.4	1025	442	0.2
Buiem	Mountain	50	3.6	1025	368	0.1
Buso	High Mountain	275	19.9	1025	2027	0.7
Bulu	Mountain	90	6.5	1025	663	0.2
Buhem	High Mountain	250	18.1	1025	1842	0.7
Busa	Mountain	75	5.4	1025	553	0.2
Bukang	Mountain	125	9.1	1025	921	0.3
Mongi	High Mountain	1,650	119.5	1025	12,159	4.4
	Total	**4,100**				**60.5**

2.1.4 Wind Data

IHAconsult (2018) indicated that "*the wind regime of the southern hemisphere tropical Pacific Basin, west of 170˚E, is dominated by two distinct wind seasons. The effect of the atmospheric low-pressure system over northern Australia, Papua New Guinea, and the Coral Sea during summer, and its reduction during winter, produces a monsoonal wind pattern in the southwest Pacific Basin. From May to October the persistent southeast trade winds occur, while from October to April the northwesterly monsoon winds dominate the wind regime*".

Two sources of hourly or three-hourly wind data were available. First, the National Oceanic and Atmospheric Administration (NOAA, USA) National Center for Environmental Prediction (NCEP) provides operational wind and wave predictions using the WAVEWATCHIII model. WAVEWATCHIII only provides output over bodies of water. Modelled datasets are available for the geographic region of interest at a spatial resolution of 0.5° (roughly 56 km) in three hour time steps. Second, a meteorological station was installed at the Wagang Village. The data available at Wagang Village covers, at the time of this report, May to November 2017 and is representative of wind conditions that one would see near the shore. However, since it is a land station, located away from the Markham valley – hence possibly missing northwesterly winds – the Wagang Village station may not be representative of winds over the entire Huon Gulf.

As a result, WAVEWATCHIII wind data was used as input for the 3D hydrodynamic model H3D due to its availability over the timeframe required for simulation and due to its representativeness of the Huon Gulf conditions. Model grid points and the location of the Wagang meteorological station are shown in Figure 2.7.

Figure 2.8 shows a wind rose from WAVEWATCHIII modelled data. The direction on the wind rose is defined as where the wind is *coming from*. Note that the Wave Watch III modelled winds in this figure spans over an entire year January-December 2016. Table 2.3 summarizes the wind speed and direction frequency distribution data for the WAVEWATCHIII data. One can observe that winds are from the W-NW about 39% of the time and from the E-SE about 27% of the time, in agreement with the typical observed wind climate: "*From May to October the persistent southeast trade winds occur, while from October to April the northwesterly monsoon winds dominate the wind regime*" (IHAconsult, 2018).

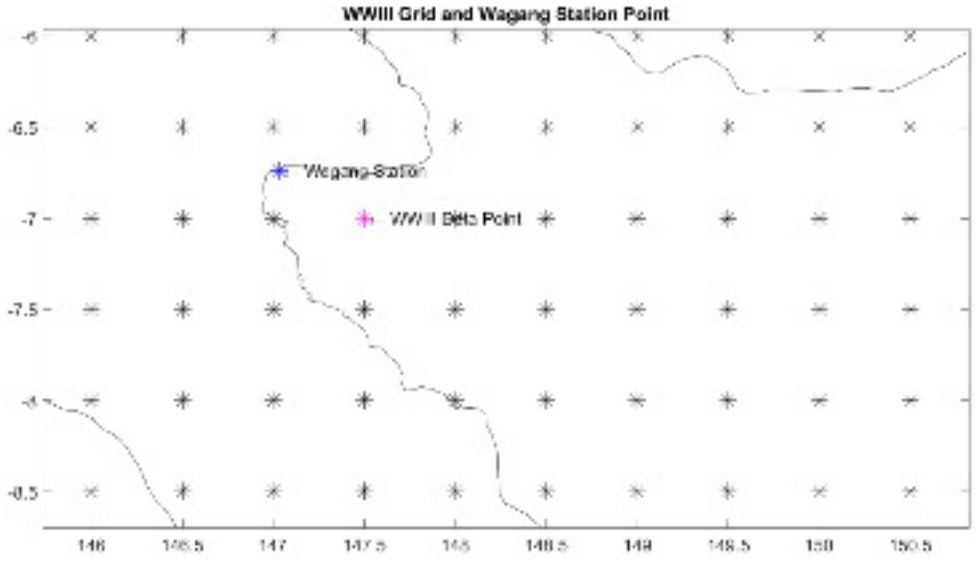

Figure 2.7 WAVEWATCHIII Data Points in Relation to Wagang Village

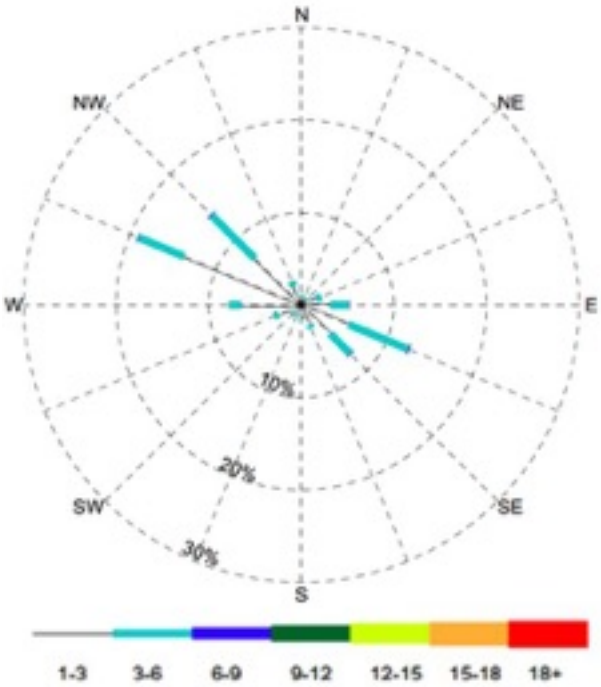

Figure 2.8 Wind Rose Presenting Modelled Winds (WAVEWATCHIII at 7S and 147.5E)

Table 2.3: Wind Speed and Direction Frequency Distribution Table: WAVEWATCH III

	Percent Occurrence (%)					
Direction	0-1 m/s	1-3 m/s	3-6 m/s	6-9 m/s	9-12 m/s	Total (%)
ENE	-	1.75	0.57	-	-	2.32
NE	-	0.82	0.11	-	-	0.93
NNE	-	0.80	0.09	-	-	0.89
N	-	1.01	0.08	-	-	1.09
NNW	-	2.21	0.05	-	-	2.76
NW	-	7.13	6.61	0.08	-	13.82
WNW	-	13.69	5.35	0.06	-	19.10
W	-	6.52	1.31	-	-	7.83
WSW	-	2.66	0.52	-	-	3.19
SW	-	1.37	0.14	-	-	1.50
SSW	-	1.06	0.12	-	-	1.18
S	-	1.55	0.06	-	-	1.61
SSE	-	2.30	0.40	-	-	2.70
SE	-	4.41	3.07	0.05	-	7.53
ESE	-	5.49	7.02	0.10	-	12.61
E	-	3.12	2.02	0.03	-	5.17
Calm	15.77	-	-	-	-	15.77
Total (%)	15.77	55.89	28.03	0.32	-	100.00

As indicated above, another set of data was available: the Wagang Village meteorological station, covering May to November 2017. This station is representative of land conditions, hence may not be representative of winds over the entire Huon Gulf. Figure 2.9 shows a wind rose from the Wagang data. The direction on the wind rose is defined as where the wind is *coming from*.

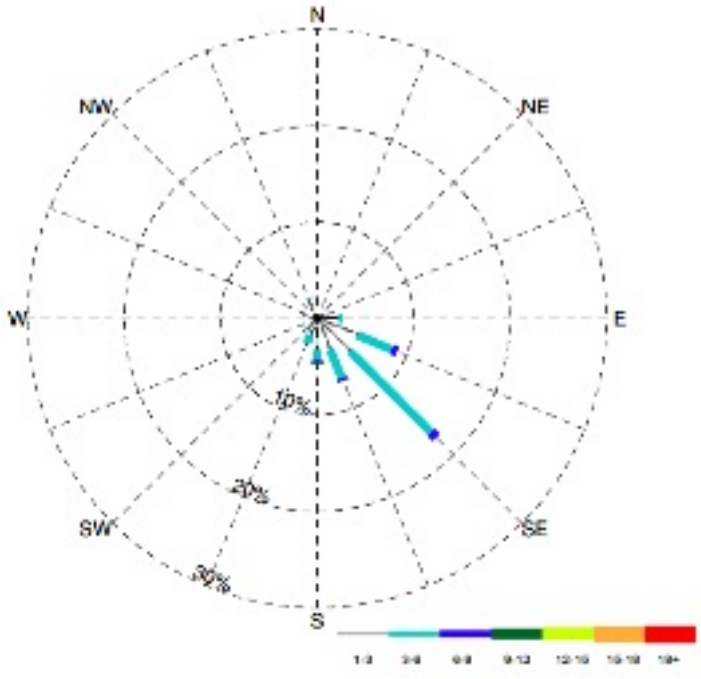

Figure 2.9 Wind Rose Presenting Observed Winds (Wagang Station)

Since the Wavewatch III wind data is based on global scale modelling and observations, and is generated so as to represent over-the-water winds, it was selected over the Wagang Village for the Huon Gulf modelling reported here**.**

2.1.5 Meteorological Fluxes

There are several important fluxes of heating energy at the air water interface which play a large role in determining the thermal structure of the surface waters, and hence determining the density structure of these waters:

- Incident solar radiation
- Long-wave back radiation
- Sensible heat flux
- Latent heat flux.

These are described in more detail in the following sections and illustrated in Figure 2.10.

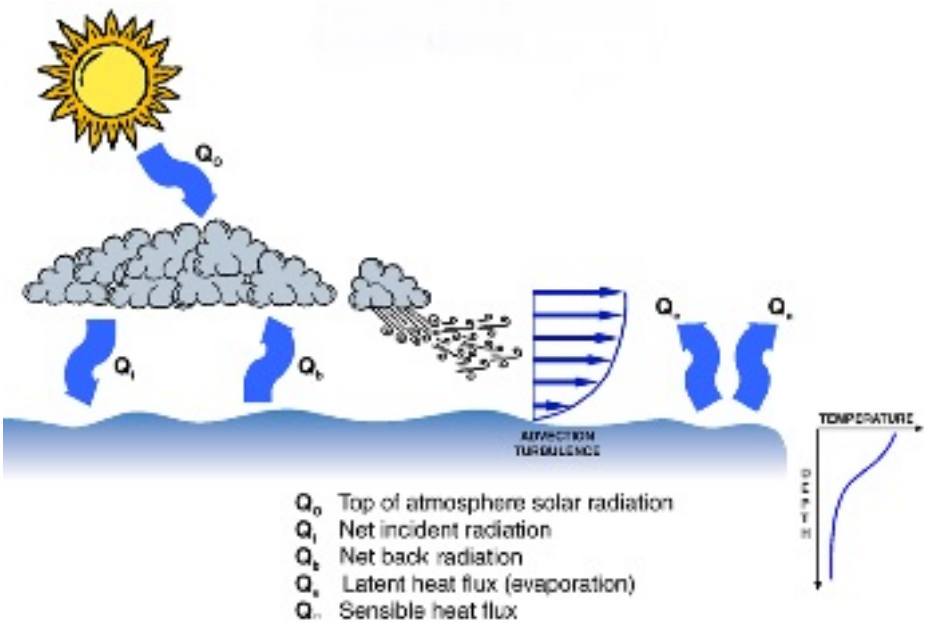

Figure 2.10 Meteorological Heat Exchanges

2.1.5.1 Solar Radiation, Latent Heat Flux, and Sensible Heat Flux

Solar radiation is the most important meteorological forcing input into H3D. Solar radiation data is recorded in 10-minute intervals at the Wagang Village, however observations do not cover the entire modelled period. Ahmad (1983) provides a theoretical estimate of the annual mean hourly solar radiation (W/m^2) at ground level at Lae, assuming no cloud cover, based on an analysis of observed solar radiation data between 1975 and 1977. In principal, one could estimate the incident solar radiation at any other date and time, based solely on cloud cover at that time. A comparison between Ahmad's (1983) theoretical annual solar radiation values and the observed solar radiation at Wagang for a one week period in May (2017) is shown in Figure 2.11, as an example to illustrate the discrepancy between observed incident solar radiation at Wagang Village compared to the relatively steady daily periodic theoretical incident radiation for Lae predicted by Ahmad (1983).

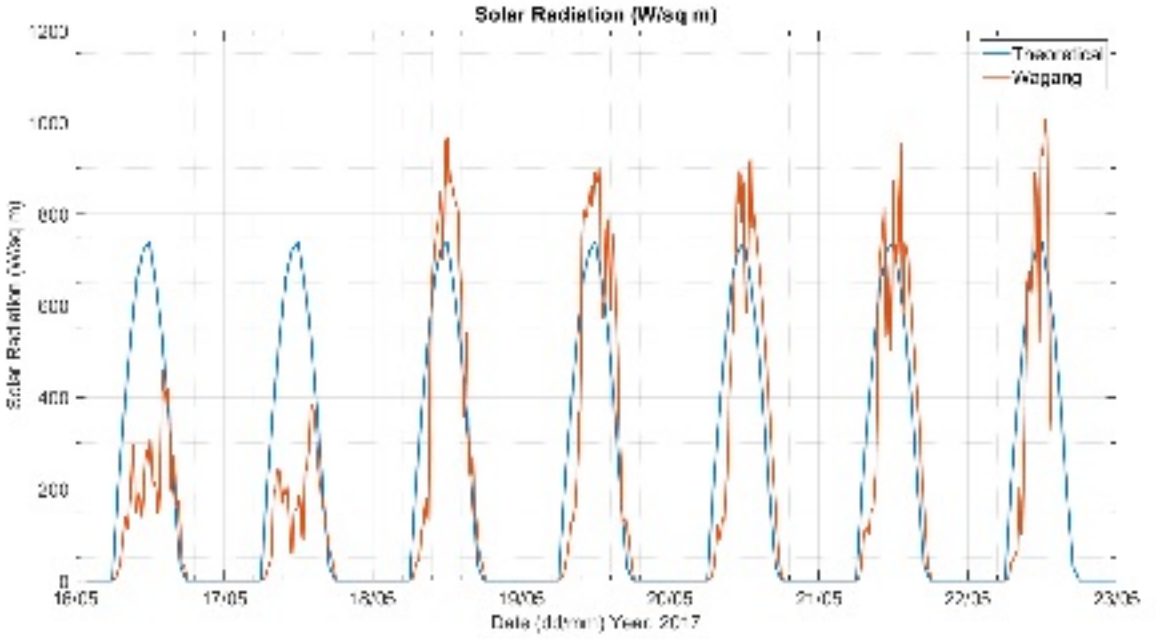

Figure 2.11 Theoretical Solar Radiation (W/m^2) as described in Ahmad (1983) and Observed at Wagang

Ahmad's (1983) solar radiation values do not take cloud cover into consideration. After trying several alternatives, it was found that an assumption of 80% cloud cover, corresponding to 48% energy transfer to the water surface, in conjunction with Ahmad(1983)'s cloud-free values, gave the best reproduction of the observed air-water temperature differences over the Huon Gulf.

The top panel of Figure 2.12 shows the incident solar radiation (green line) used in the H3D simulations reported. Peak values in Figure 2.12 (almost 400 W/m^2) are about half the peak values in Figure 2.11, reflecting the current understanding that cloud cover is relatively frequent in Huon Gulf. The long wave back radiation (red line) is also shown in the top panel of Figure 2.12, which is always negative, and represents the heat loss through long-wave back radiation.

The bottom panel of Figure 2.12 shows the latent and sensible heat flux, the latent heat flux in green, the sensible heat flux in red. Latent heat flux, generally a cooling effect on the ocean, is due to the heat carried off by evaporating water. Sensible heat flux is the heat flux associated with the air-water temperature difference, and is often negative, reflecting the fact that the air is frequently cooler than the water.

Latent heat flux is computed according to:

$$Latent\ Heat\ Flux\ (W/m^2) = C_e * L * speed * (q_{obs}-q_{sat})$$

Where:

- C_e is a bulk transfer coefficient, 1.32×10^{-3} in simulations reported here
- L = latent heat of evaporation, 2.499×10^6 joule/kg
- speed = wind speed, m/s
- q_{obs} = observed specific humidity (kg water /kg moist air), computed as relative humidity * q_{sat}
- q_{sat} = saturated humidity, a function of air temperature

Sensible heat flux is computed according to:

$$Sensible\ heat\ flux\ (W/m^2) = C_h * \rho_{air} * c_p\ * speed\ *(\ T_{air} - T_{water}\ )$$

- C_h is a bulk transfer coefficient, 1.46x10-3 in simulations reported here
- ρ_{air} is density of air, Kg/m3
- c_p = heat capacity of water, 4,186 joule/Kg deg C
- *speed* = wind speed, m/s
- T_{air} = air temperature, from an external source such as the GFS model
- T_{water} = water temperature, from each H3D surface cell.

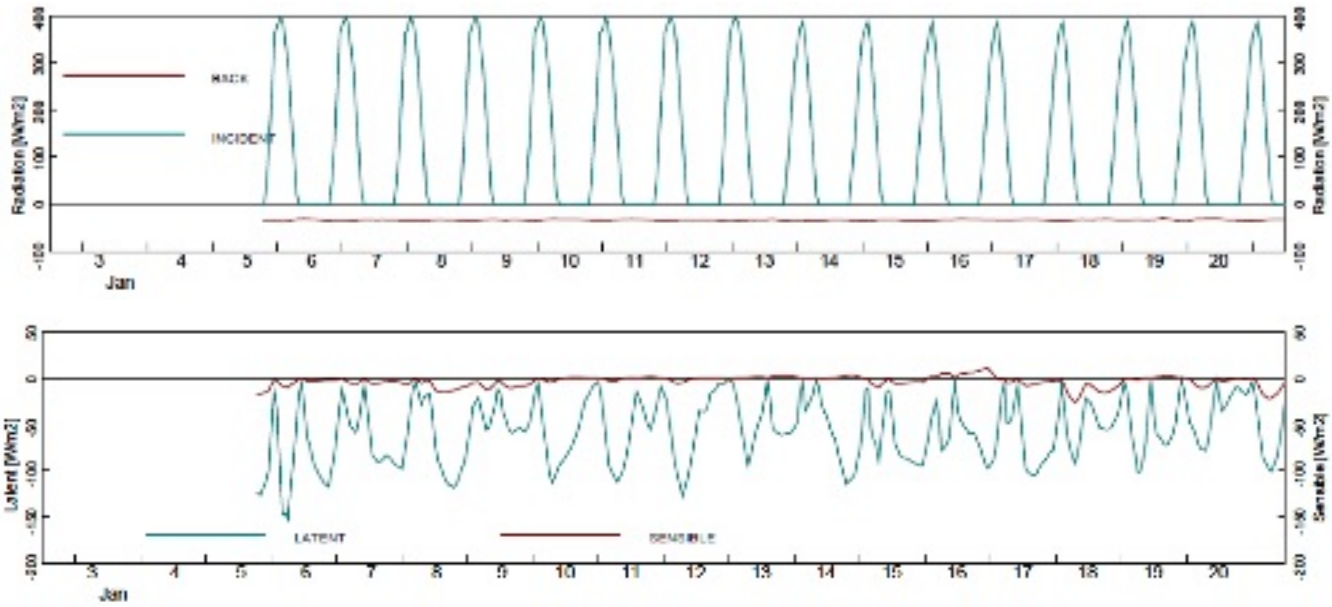

Figure 2.12 Incident Solar Radiation (Top Panel) and Latent and Sensible Heat Fluxes (Bottom Panel) Used as H3D Input

2.1.6 Air Temperature & Relative Humidity

Air temperature and relative humidity observations are recorded at Wagang at 10-minute intervals. Air temperature and relative humidity over the Huon Gulf are also available from the National Oceanic and Atmospheric Administration (NOAA)'s Global Forecast System (GFS). The GFS model is comprised of atmospheric, oceanic, land/soil and sea ice models, which are coupled together to produce a global simulation of weather conditions at a spatial resolution of 0.5º and a three-hour archival interval. A map is provided in Figure 2.13 showing the location of Wagang Village in relation to the closest 3 GFS data points that were taken into consideration.

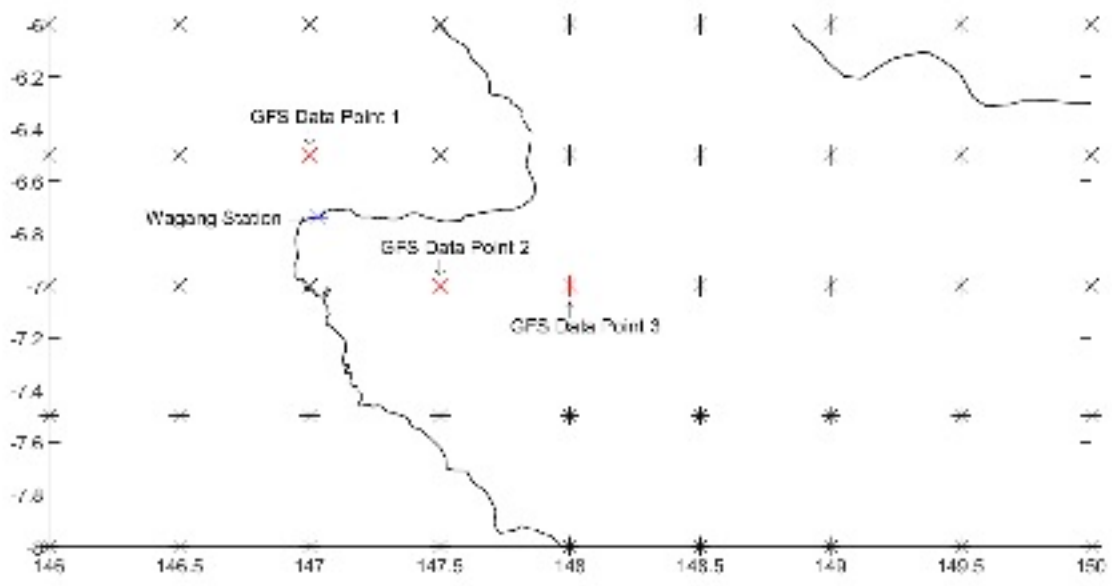

Figure 2.13 Map of GFS Data Points in relation to Wagang Village

GFS Data Point 1 is the closest over-land GFS grid point to Wagang station, whereas GFS Data Points 2 and 3, also in close proximity, are representative of meteorological conditions over the ocean in the Huon Gulf. Figure 2.14 below displays the comparison of GFS air temperature with the observed data at Wagang Village. The GFS model's air temperature is lower than that observed at Wagang station for GFS Data Point 1. However, the air temperature at GFS Data Points 2 and 3 are higher and represent the high air temperatures of the Huon Gulf. An average of the values at GFS Data Points 2 and 3 were used as a temperature forcing over the Huon Gulf.

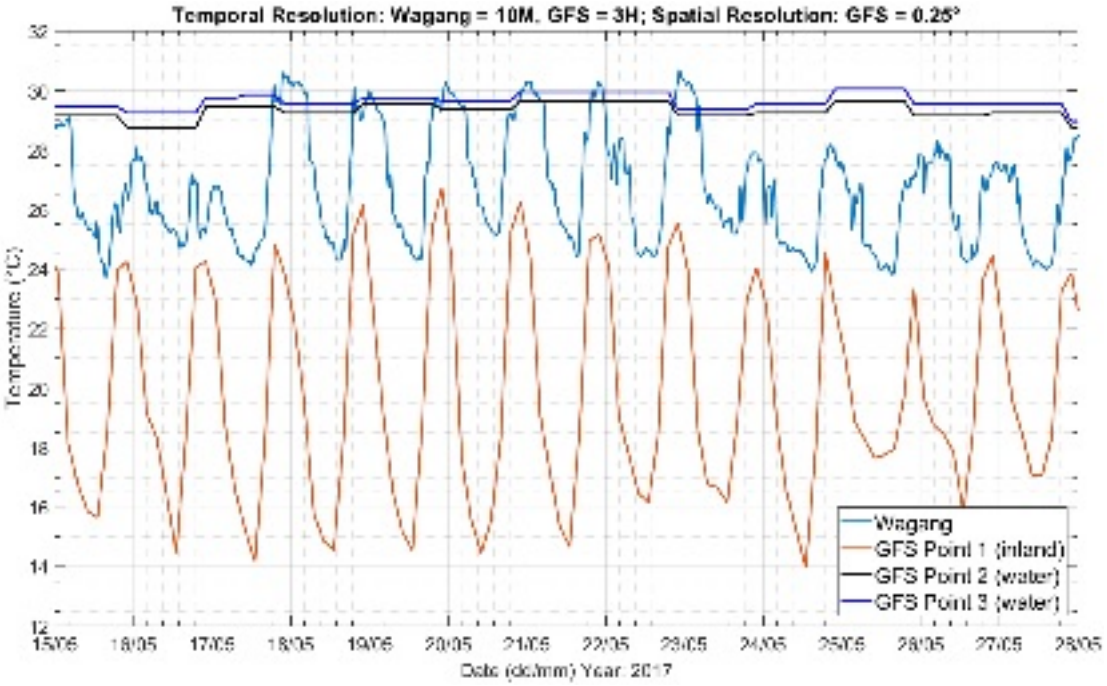

Figure 2.14 Air Temperature (°C) Observations at Wagang, and Modelled GFS Output at Three GFS Data Points

Relative humidity is recorded at the Wagang observation station in 10-minute intervals. Relative humidity data to cover the entire period required for modelling was obtained from the GFS model datasets. Figure 2.15 shows relative humidity data extracted from outputs at 3 GFS Data Points compared to observed relative humidity. The GFS Data Points in relation to Wagang observation station are the same as the ones shown in Figure 2.13 above. The relative humidity used as input to H3D should represent the relative humidity over the Huon Gulf. GFS data extracted from GFS Data Point 1 is closer in value to what is observed at Wagang station, however GFS Data Point 2 and 3 represent the relative humidity over the Huon Gulf. The average relative humidity of GFS Data Point 2 and 3 was used as input into the H3D model (i.e. same two GFS Data Points used for temperature forcing).

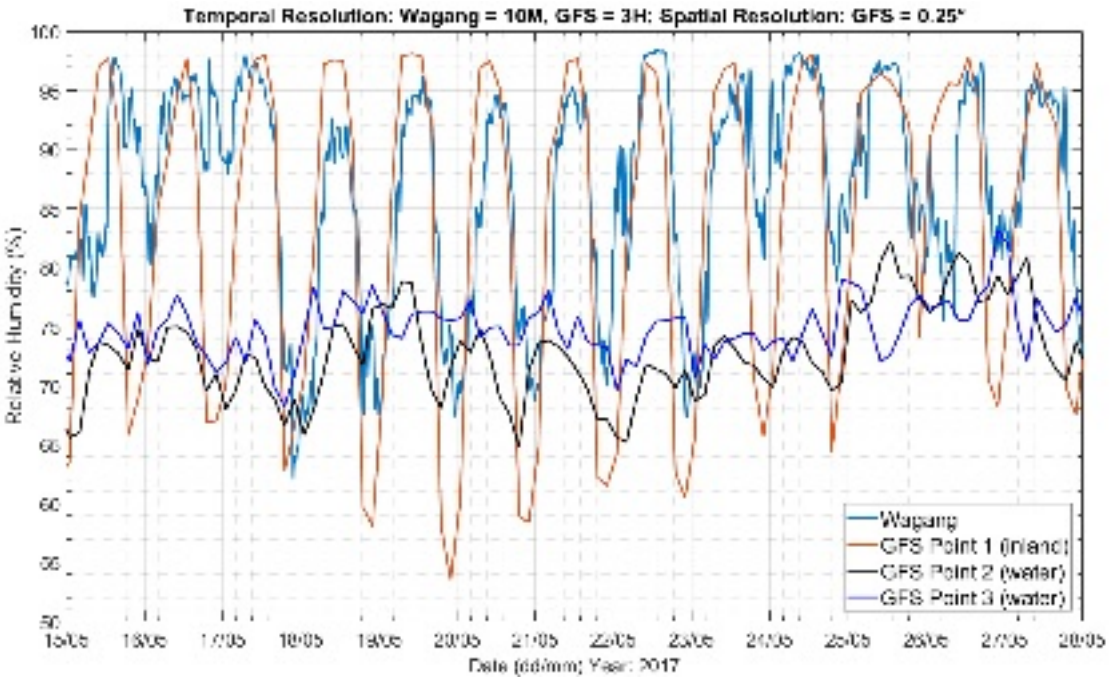

Figure 2.15 Relative Humidity (%) Validation between Three GFS Data Points and Observations at Wagang

2.2 H3D Model Validation

2.2.1 Water Level

The H3D model outputs were validated against metocean observations. Water level is recorded at Lae Yacht Club every 2 minutes with data available through 2017. Good agreement between observed and modelled water levels has been observed and is shown in Figure 2.16, focusing on December 2016 period (for comparison purposes).

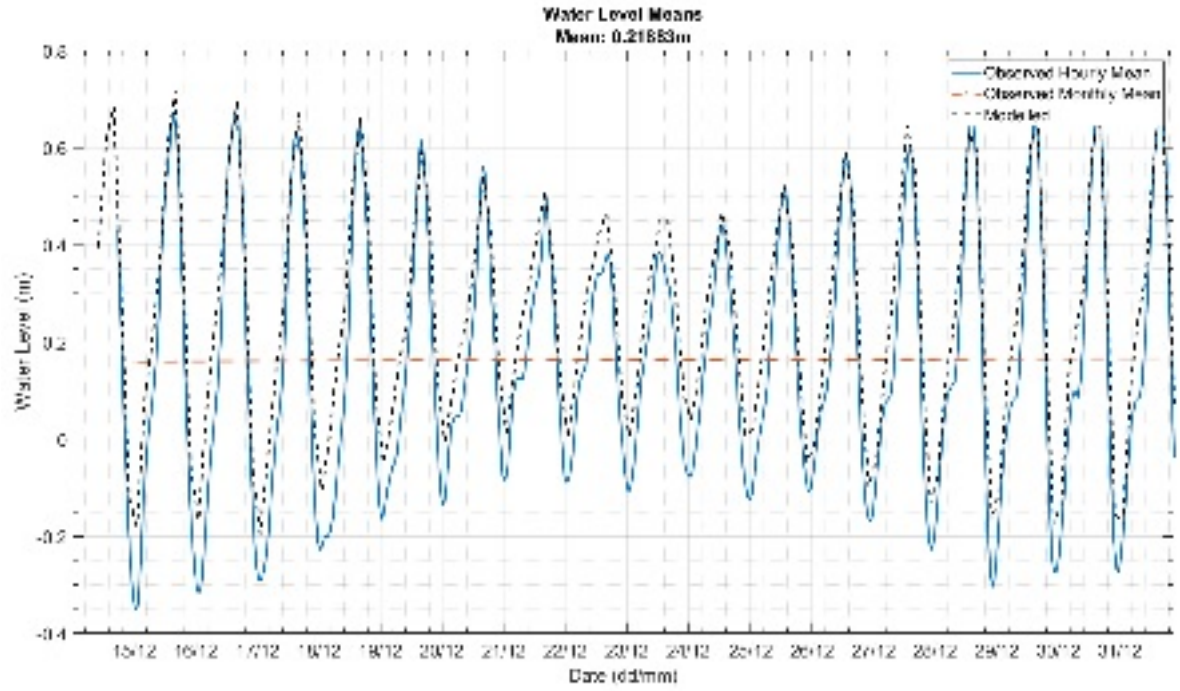

Figure 2.16 Validation of H3D Model Water Level

2.2.2 Temperature and Salinity CTD Profiles

H3D temperature and salinity output validation is shown for the set of profiles taken on the A and B transects (temperature) and from CTD profile locations CTD5 (temperature and salinity), CTD6, MCA, MCB, and MCC (salinity). The profiles occurred on an approximate monthly basis between October 2016 and November 2017. The H3D simulated profiles were extracted for the same dates within 2016. It is acknowledged that the model and data years are different, but the comparison is informative given that little inter-annual variability is expected in this region of the world.

Figure 2.17 illustrates the temperature profiles simulated by H3D (H3D output) over a one year period, together with observed CTD profiles measured at station A3 over the course of February – November 2017. H3D simulations are represented in colored solid lines with circular markers to identify the model layers whilst the CTD deployments are represented in black dashed lines. There is a systematic disagreement between the modelled and observed temperature profiles in the top 80m of the water column, with the modelled values being too cold and developing a relatively well mixed upper layer, not seen in the observed data. There are two reasons for this difference in behaviour: the model underestimates the atmospheric warming and likely over estimates wind velocities. As noted in Sections 2.1.4 and 2.1.5, assumptions were required with regard to some of these atmospheric forcing parameters. There is an excellent level of agreement between modelled and observed temperature, particularly in the upper thermocline and in deep waters below 400m depth. Intermediate layers between 100m and 400m depth show a slight deviation between and observed temperature profiles (i.e. modelled temperature is somewhat lower than observed for a portion of the year). However the overall shape of the profiles, as well as the depth and extent of the thermocline, are well represented throughout the year. Note the high resolution of model layers in the upper 400m of the water column (as represented by the circular markers on the modelled profiles) used to resolve the background parameters (temperature, salinity, density) in the water column, as well as the subsurface plumes generated by the density current..

Figure 2.18 shows a similar comparison between modelled and measured temperature profiles at location B5 (location at 1000m depth). The comparison at Station B5 is equally as strong as that for station A3 throughout the year. Figure 2.19 shows a comparison between the modelled and measured temperature profile at location CTD5 (location where depth is about 2400m) near the middle of the Huon Gulf on February 19, 2017. Note that this is the only day in which CTD data was collected at this station; however, excellent agreement throughout the water column between the modelled and observed temperature is noted at this location as well on this particular day (5 months following model initialization).

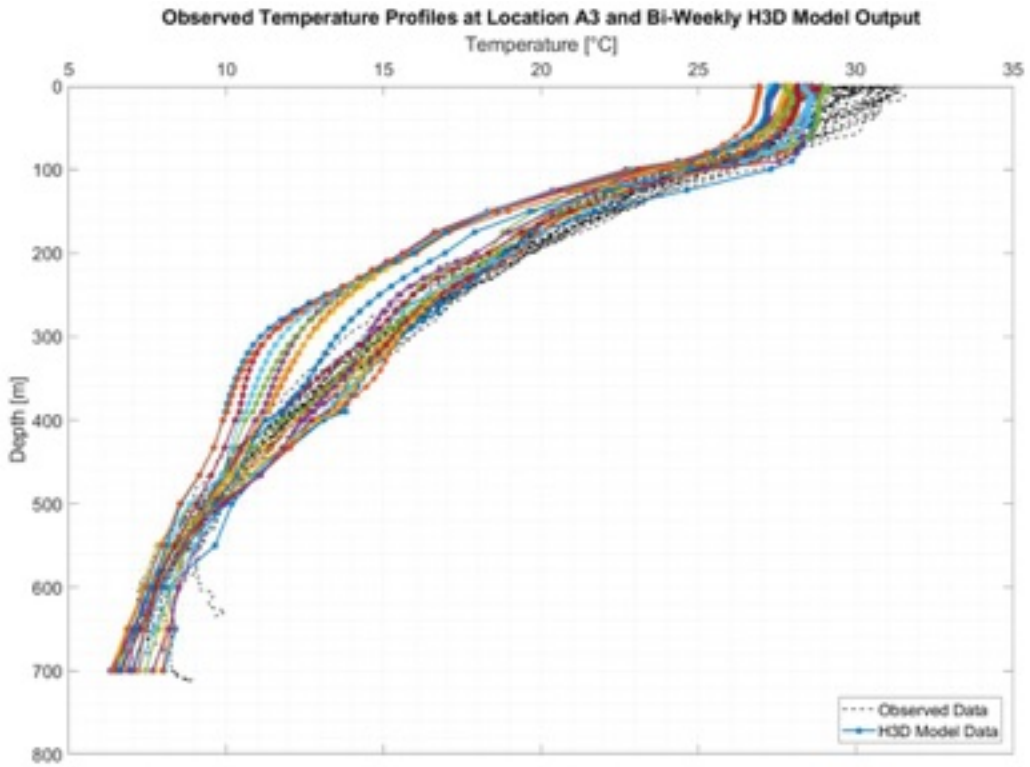

Figure 2.17 Temperature Validation - CTD A3 Deployments (Black dashed Lines) from February to November 2017 and H3D Output (Solid Colored Lines with Markers)

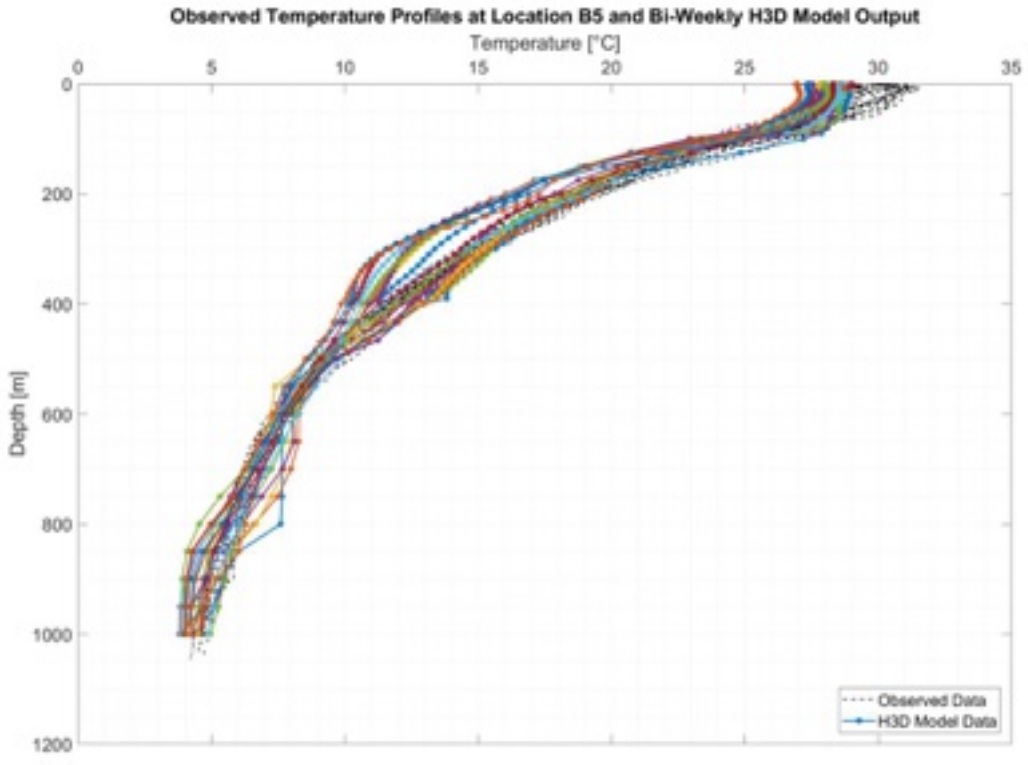

Figure 2.18 Temperature Validation - CTD B5 Deployments (Black dashed Lines) from February to November 2017 and H3D Output (Solid Colored Lines with Markers)

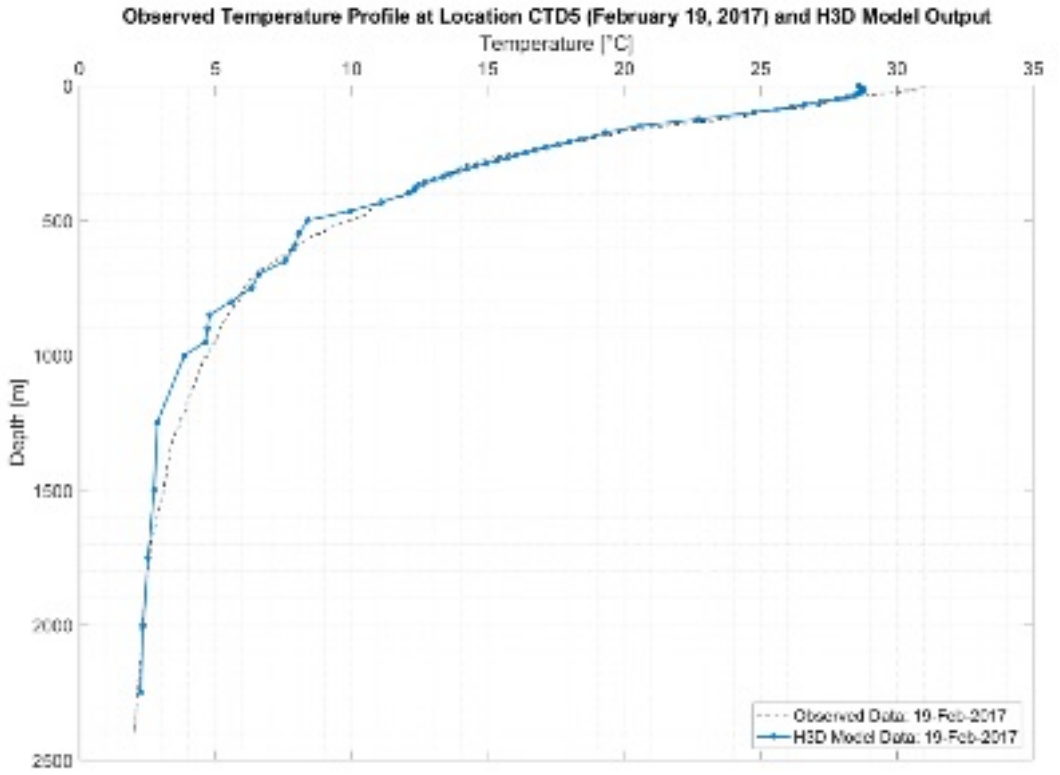

Figure 2.19 Temperature Validation – CTD5 Deployment (Black dashed Lines) on February 19, 2017 and H3D Output (Solid Blue Line with Markers)

Figures 2.20 to Figure 2.24 illustrate the validation for salinity at five different locations. Note that CTD profiles were conducted at locations CTD5 and CTD6 on 19 February 2017, and field profiles were taken at MCA, MCB, and MCC in mid-August 2016. A reasonably good agreement with the modelled output is observed.

The H3D model was initialized on 20 September 2016; therefore, a direct comparison was made between the profiles taken at locations CTD5 and CTD6 on 19 February 2017 with modelled data on the same day (5 months after model initialization). A very strong agreement between the measured and modelled salinity profiles is noted at both locations; the only notable discrepancy lies within the upper 25-30m where the model overestimates the salinity.

At locations MCA, MCB, and MCC the model was initialized (20 September 2016) after these locations were sampled (13-15 August 2016). Therefore, in order to provide comparable profiles, the field salinity profiles at MCA, MCB, and MCC (Figures 2.20 – Figure 2.22) are overlaid with the model data from 20 September 2016 (initial profile from HYCOM for the given location), as well 4 additional profiles from the subsequent three months (1 October to 1 December 2016) to show the evolution of these salinity profiles over time in relation to the measured profiles from mid-August 2016. It is observed that the initial HYCOM salinity profile for this day slightly overestimated the subsurface maximum salinity values around 125-200m depth. However, as the model advances from this initial condition, the subsurface maximum decreases to more closely resemble that which was measured during the field observations at these locations in md-August. The salinity between 20 – 100m depth also decreases slightly as time advances between October and November at these locations, which may be a result of the spike in Markham river freshwater flows around this time in 2016 (Figure 2.6). The salinity values below 300-400m appear to be slightly greater than those measured at MCA, MCB, and MCC in mid-August 2016; however, this is expected given that the initial HYCOM profile in September also had slightly higher salinity than the three profiles taken in mid-August at

these locations and depths. The slightly higher salinity values at these locations for depths below 300m are considered reasonable considering the variation observed salinity values below 300m depth for CTD5, CTD6, MCA, MCB, and MCC range between 34.5 and 35.3PSU.

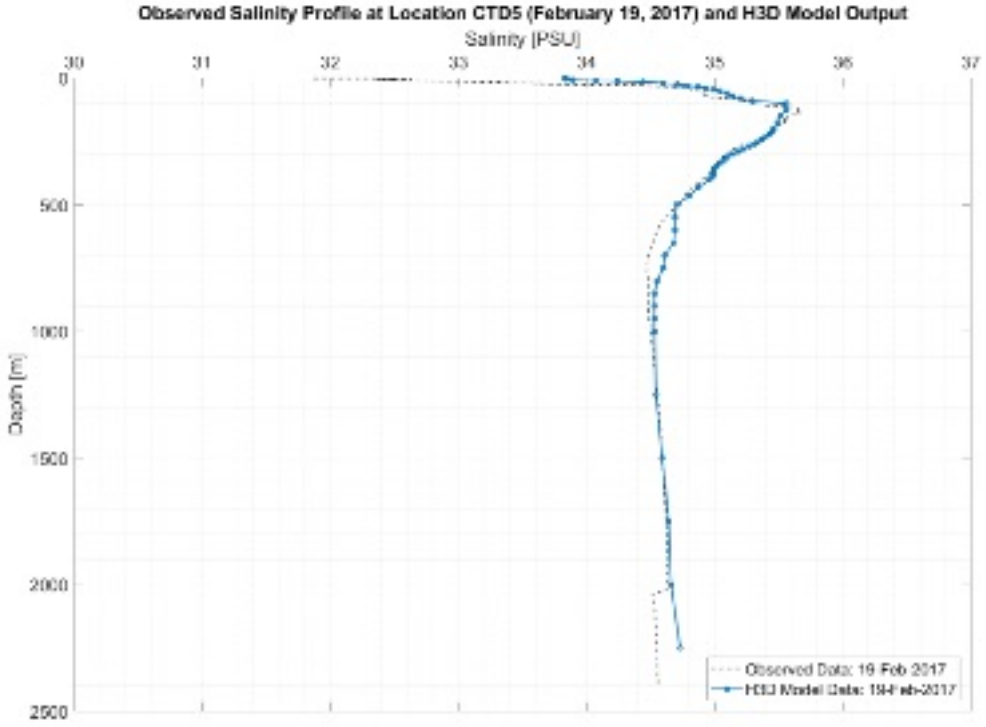

Figure 2.20 Salinity Validation – CTD5 (Black Line) and H3D Output (Blue Line)

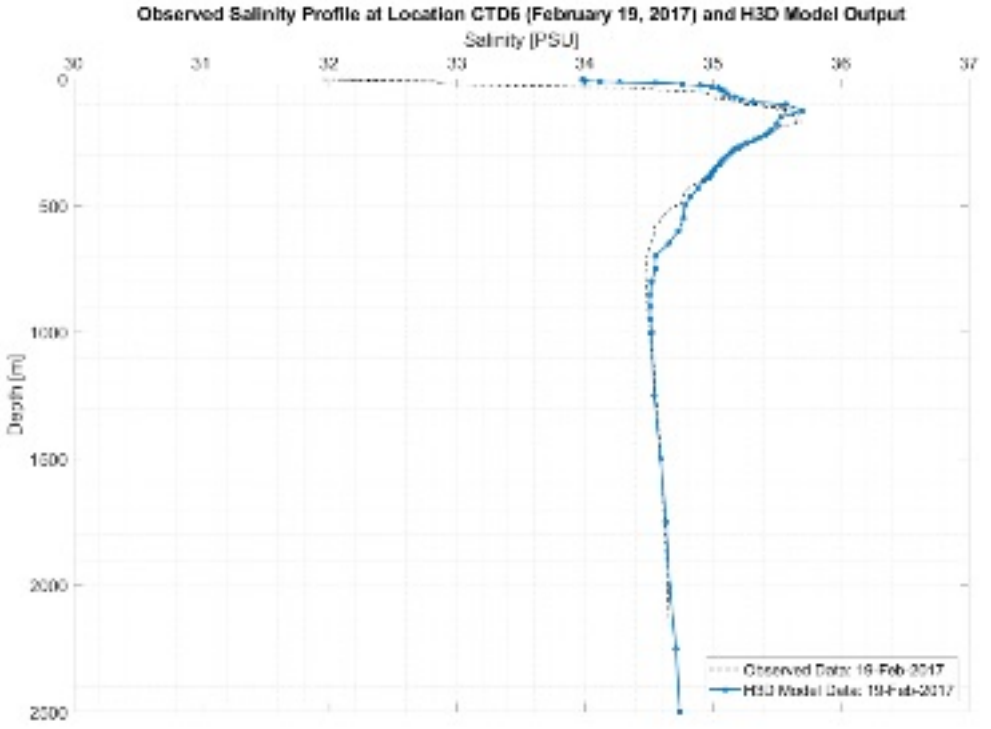

Figure 2.21 Salinity Validation – CTD6 (Black Line) and H3D Output (Blue Line)

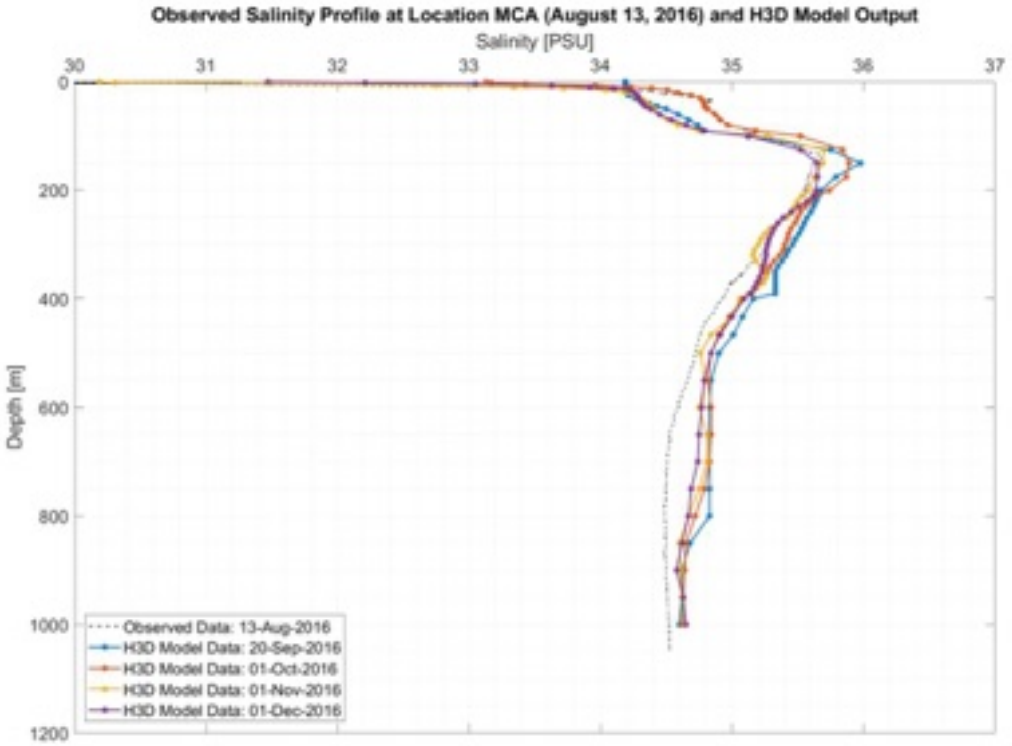

Figure 2.22 Salinity Validation – MCA (Black Line) and H3D Output (Blue Line)

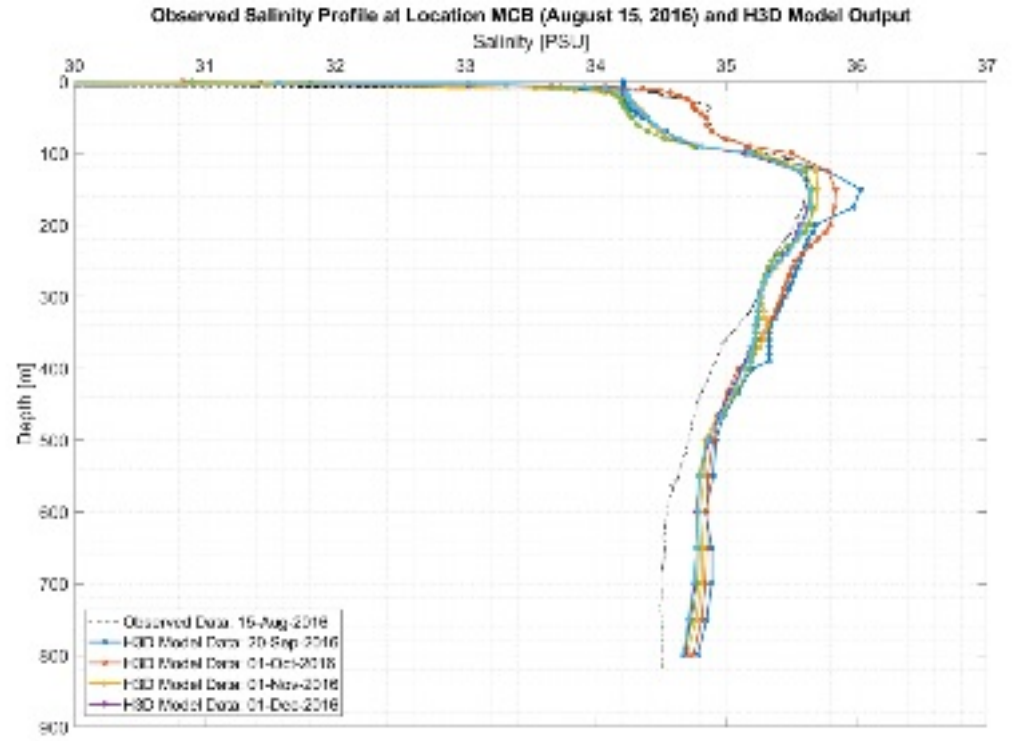

Figure 2.23 Salinity Validation – MCB (Black Line) and H3D Output (Blue Line)

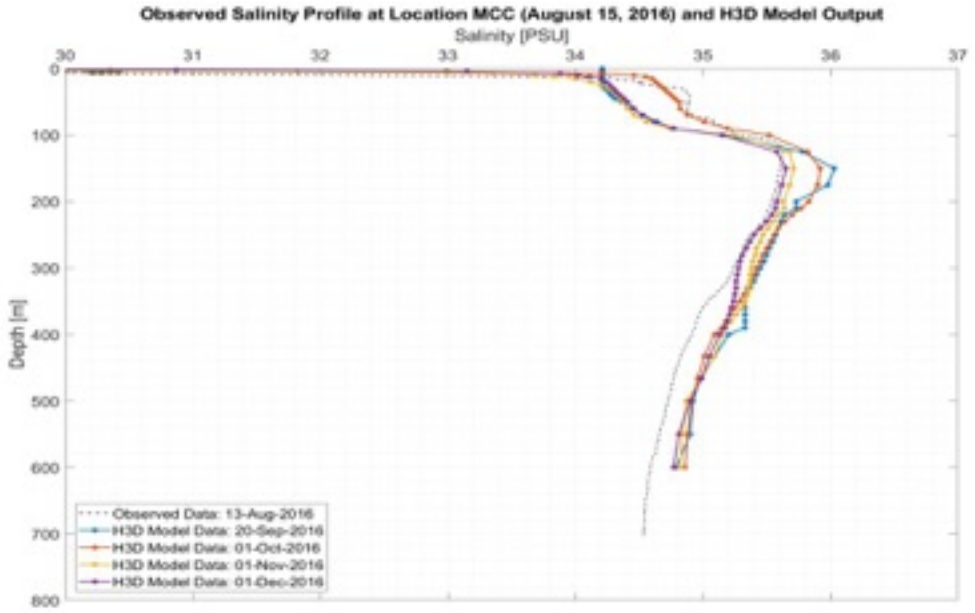

Figure 2.24 Salinity Validation – MCC (Black Line) and H3D Output (Blue Line)

Figures 2.25 and 2.26 illustrate the modelled temperature and salinity fields in the Huon Gulf. Figure 2.25 illustrates surface water temperatures and velocities (vectors) in the top panel, and a section of water temperature along the Markham Canyon thalweg in the bottom panel. Similarly, Figure 2.26 shows the surface salinity (top panel) and a section along the canyon thalweg (bottom panel). The CTD monitoring stations A3, B5, MCA, MCB, and MCC are also shown on Figures 2.25 and 2.26. Stations CTD5 and CTD6 are outside of the domain of these two figures (i.e. to the southeast).

Due to surface meteorological forcing (long wave and short wave energy), the model is able to maintain a surface temperature approximately equal to (and even slightly warmer than) the air temperature, which is characteristic of this area. As noted in Figure 2.17 to Figure 2.19, a strong agreement between modelled and observed temperatures is observed; particularly in the upper thermocline and below 400m depth. The modelled water temperatures tend to be slightly cooler than those observed in the immediate surface layer and also between 100m-400m depth at stations A3 (Figure 2.17) and B5 (Station 2.17). At station CTD5 (Figure 2.19), an excellent agreement was also noted throughout the water column, with a similarly slightly cooler trend in the immediate surface layer as well as between 500-1500m depth.

Freshwater provided by the Markham and Busu Rivers significantly influences the temperature and salinity within the northwest area of the Huon Gulf, as is particularly evident in the modelled surface layer salinity (and section view) in Figure 2.26. Note the relatively low salinity values (<30 PSU) in the upper panel in Figure 2.25 corresponding to the influx of the relatively lower density (buoyant) freshwater from the Markham and Busu Rivers that enters the uppermost layer in the water column. This interpretation is corroborated by satellite imagery from this area (not shown) where one can observe a remarkable comparison between these temperature and salinity plan views with the spatial extent of the freshwater plume (evidenced by suspended sediment) from each of these rivers. The section view along the thalweg in the lower panel (Figure 2.26) shows that this inflowing freshwater quickly becomes mixed with the ambient water in the Huon Gulf. The background stratification in salinity is also observed in this lower panel as well. Recall in the modelled and observed profile comparisons shown in Figures 2.20 to 2.24 at various locations throughout the Huon Gulf (CTD5, CTD6, MCA, MCB, and MCC) the modelled salinity values in the immediate surface were slightly lower than those observed at these locations; however,

excellent agreement was shown throughout the water column. Values in the upper 100m tend to range between 30 – 35 PSU, subsurface peak values between 35.5 – 36 PSU were observed between 100-200m depth, and values below 300m depth are typically between 34.5 – 35.3 PSU.

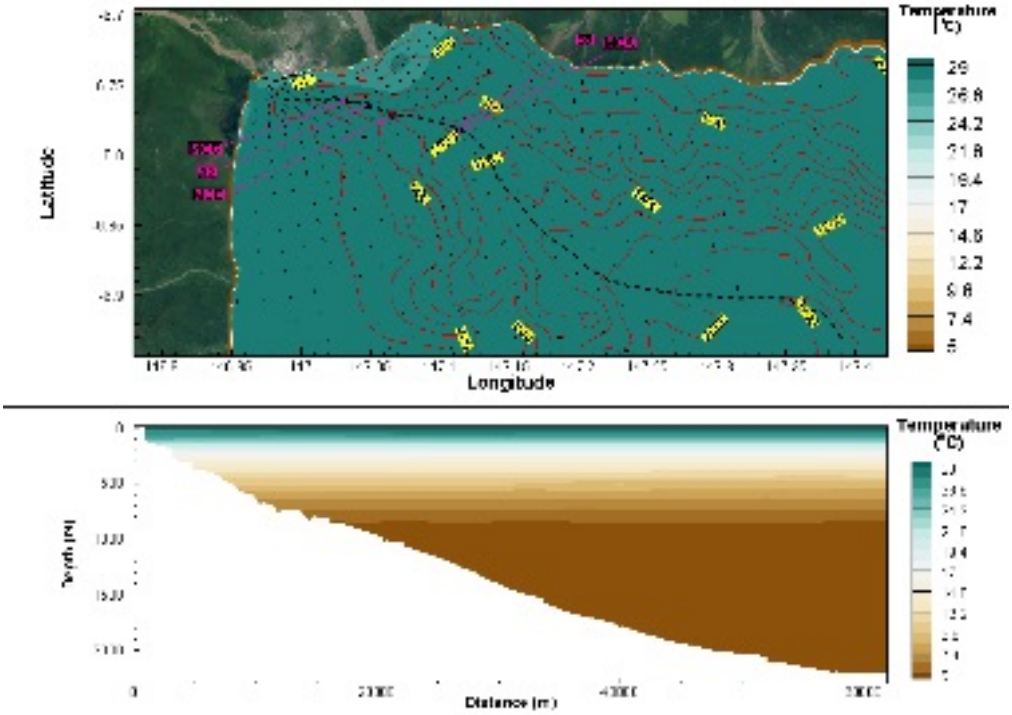

Figure 2.25 Modelled H3D Water Temperature on February 19, 2017

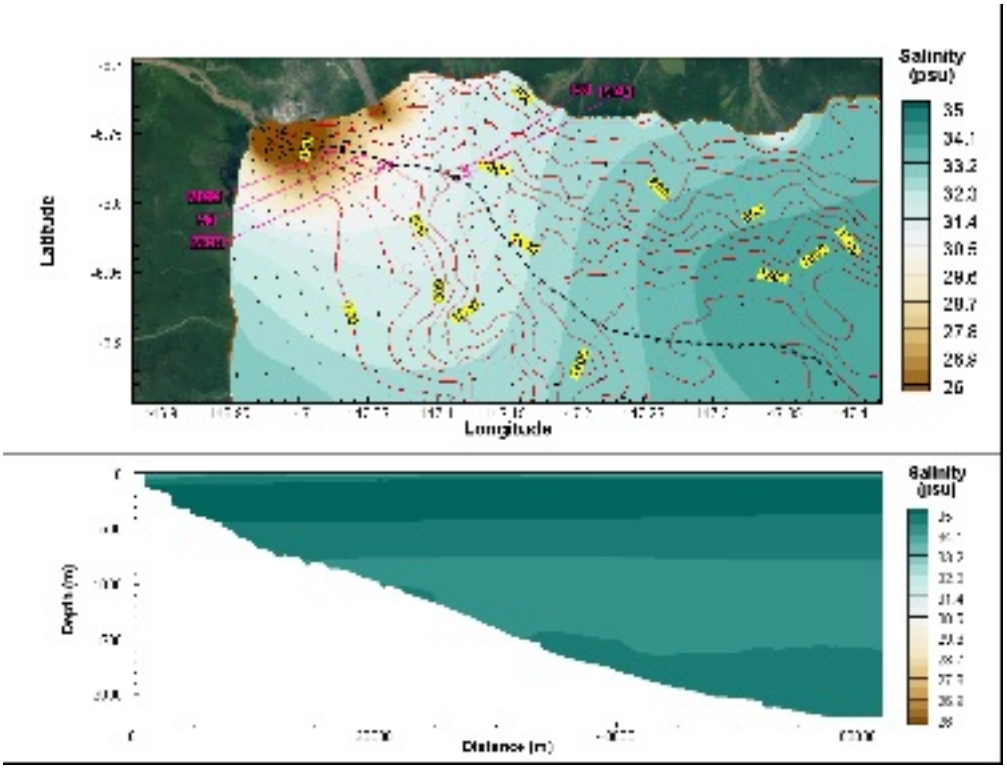

Figure 2.26 Modelled H3D Salinity on February 19, 2017

2.2.3 ADCP Currents

Appendix B presents the ADCP data that has been collected by IHAconsult. ADCP data has been collected throughout 2016-2017 at the Outfall Location, Canyon (A, B, C) Locations, Basin B Location, Far Field Location, and Trench Location (Figure 2.27). Given the footprint of the tailings (Section 3.0), the focus for modelled current validation described herein is at the Outfall and Canyon Locations. From the bar graph plots shown in Appendix B, current roses were produced at various levels throughout the water column in order to compare the model versus the observed current data.

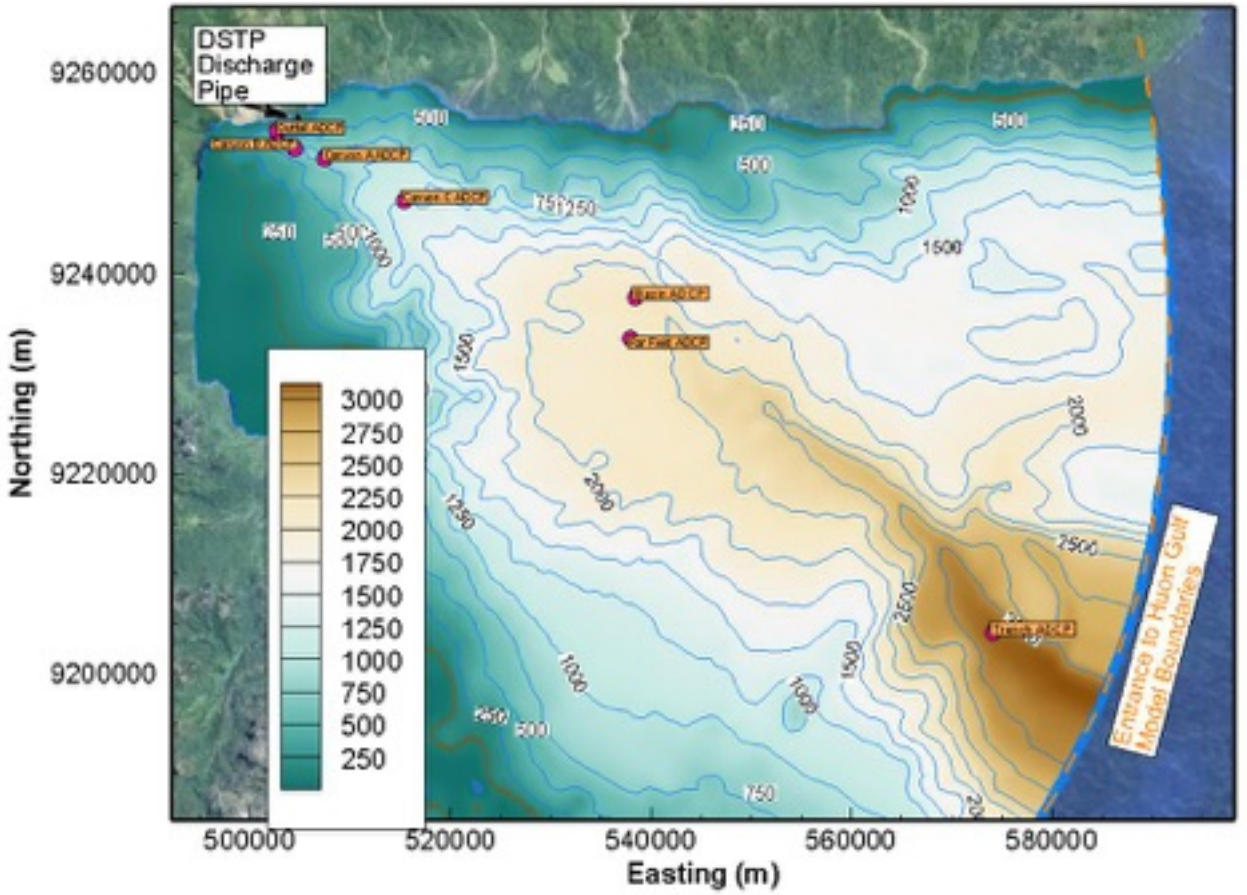

Figure 2.27: ADCP stations in the Huon Gulf (Refer to IHAconsult, 2018)

Figure 2.28 illustrates the current rose for the ADCP observations (left panel) versus modelled by H3D (right panel) at the Canyon A ADCP location. To simplify the comparison process, a representative sample from the ADCP observed dataset (121m to 177m depth range, from 24 October 2016 to 11 December 2016) over which current conditions were relatively similar was selected for comparison between modelled and observed currents. Vertically averaged currents were computed and compared to currents from a similar depth range from the H3D dataset. Figure 2.28 shows the resulting comparison as current roses.

Note that the direction on the current roses is defined as *flowing towards* in accordance with oceanographic convention. Note that this is opposite to the standard meteorological convention employed for the wind roses presented in Section 2.1.4.

Tables 2.4 and 2.5 represent the speed and direction frequency distribution corresponding to Figure 2.28, with the observed hourly-averaged ADCP data and the simulated hourly H3D current data respectively. The agreement between modelled and observed currents is reasonable. Both model and observations agree that the fastest currents flow towards the west and southwest directions, and both agree that current speeds are quite low: more than 90% of the time, currents are below 10 cm/s in speed. Although not perfect, the modelling results were deemed satisfactory for simulation of tailings behaviour, since the tailings will form a density current, which, as will be seen, has sufficient density contrast with the overlaying oceanic waters that it can self-direct itself to follow the downslope direction, with minor modification from the oceanic currents.

Table 2.4: Observed Current Speed and Direction Frequency Distribution at Canyon A ADCP Location

	Percent Occurrence (%)								
Direction	**0.0-0.01 m/s**	**0.01-0.03 m/s**	**0.03-0.05 m/s**	**0.05-0.07 m/s**	**0.07-0.09 m/s**	**0.09-0.11 m/s**	**0.11-0.13 m/s**	**0.13+ m/s**	**Total (%)**
ENE	-	1.64	1.60	1.23	0.43	0.06	0.01	0.01	4.98
NE	-	1.88	1.98	0.85	0.20	0.06	0.03	0.03	5.03
NNE	-	1.86	1.66	0.75	0.20	0.04	0.07	0.04	4.63
N	-	1.73	1.57	0.57	0.15	0.01	0.01	0.01	4.06
NNW	-	1.79	1.72	0.85	0.12	0.03	0.01	-	4.51
NW	-	2.02	2.52	0.87	0.31	-	0.03	0.01	5.76
WNW	-	2.20	3.09	1.36	0.34	0.12	0.04	-	7.15
W	-	2.35	3.18	2.35	1.04	0.47	0.15	0.04	9.57
WSW	-	2.74	4.06	4.15	1.98	0.82	0.16	0.06	13.97
SW	-	2.46	3.19	2.55	1.13	0.23	0.06	0.07	9.70
SSW	-	1.99	2.26	1.22	0.40	0.09	-	-	5.95
S	-	2.21	1.55	0.45	0.19	0.01	-	-	4.43
SSE	-	2.18	1.07	0.40	0.04	-	0.01	-	3.71
SE	-	1.42	0.91	0.34	0.01	-	-	-	2.68
ESE	-	1.66	1.32	0.50	0.10	0.03	0.03	-	3.63
E	-	1.42	1.92	1.08	0.18	0.03	0.04	-	4.68
Calm	5.57	-	-	-	-	-	-	-	5.57
Total (%)	5.57	31.55	33.59	19.50	6.81	2.01	0.67	0.29	100.00

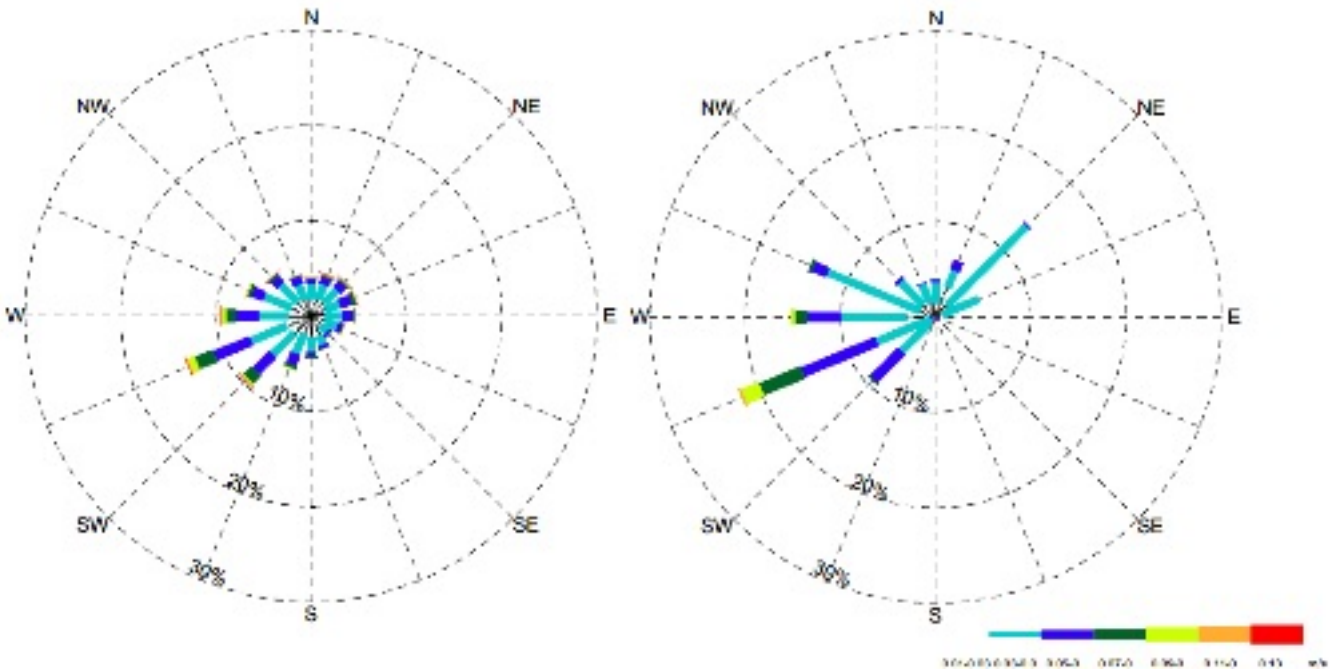

Figure 2.28 Observed ADCP (left panel) and H3D Model Output (right panel): Currents at Canyon A Location: 121m to 177m depth range, 24 October 2016 to 11 December 2016

Table 2.5: Modelled Current Speed and Direction Frequency Distribution at Canyon A Location

	Percent Occurrence (%)								
Direction	**0.0-0.01 m/s**	**0.01-0.03 m/s**	**0.03-0.05 m/s**	**0.05-0.07 m/s**	**0.07-0.09 m/s**	**0.09-0.11 m/s**	**0.11-0.13 m/s**	**0.13+ m/s**	**Total (%)**
ENE	-	0.69	4.25	-	-	-	-	-	4.95
NE	-	1.74	11.81	0.17	-	-	-	-	13.72
NNE	-	3.30	2.00	1.04	-	-	-	-	6.34
N	-	1.39	2.26	0.35	-	-	-	-	3.99
NNW	-	1.65	2.08	0.09	-	-	-	-	3.82
NW	-	1.82	3.38	0.35	-	-	-	-	5.56
WNW	-	1.74	10.5	1.65	0.35	-	-	-	14.24
W	-	2.95	7.03	3.47	1.30	0.43	0.09	-	15.28
WSW	-	0.69	5.99	8.42	4.69	2.00	0.26	-	22.05
SW	-	-	5.03	4.17	0.17	-	-	-	9.38
SSW	-	0.09	-	0.17	-	-	-	-	0.26
S	-	-	-	-	-	-	-	-	-
SSE	-	-	-	-	-	-	-	-	-
SE	-	-	-	-	-	-	-	-	-
ESE	-	-	-	-	-	-	-	0.09	0.09
E	-	-	-	-	-	-	-	-	-
Calm	0.35	-	-	-	-	-	-	-	0.35
Total (%)	0.35	16.06	54.34	19.88	6.51	2.43	0.35	0.09	100.00

Figures 2.29 and 2.30 illustrate the current speed and direction distribution, respectively, over the water column per layer of ADCP measurement or vertical model layer at the Outfall A location (Figure 2.29). Figure 2.29 shows that, while the modelled currents (bottom panel) are a bit weaker than the observed currents, both present average values ranging between 0.02 to 0.05m/s through the water column. Figure 2.30 shows the direction and a very good agreement between the directions of currents observed with ADCP and modelled currents: two predominant directions heading either westward or eastward.

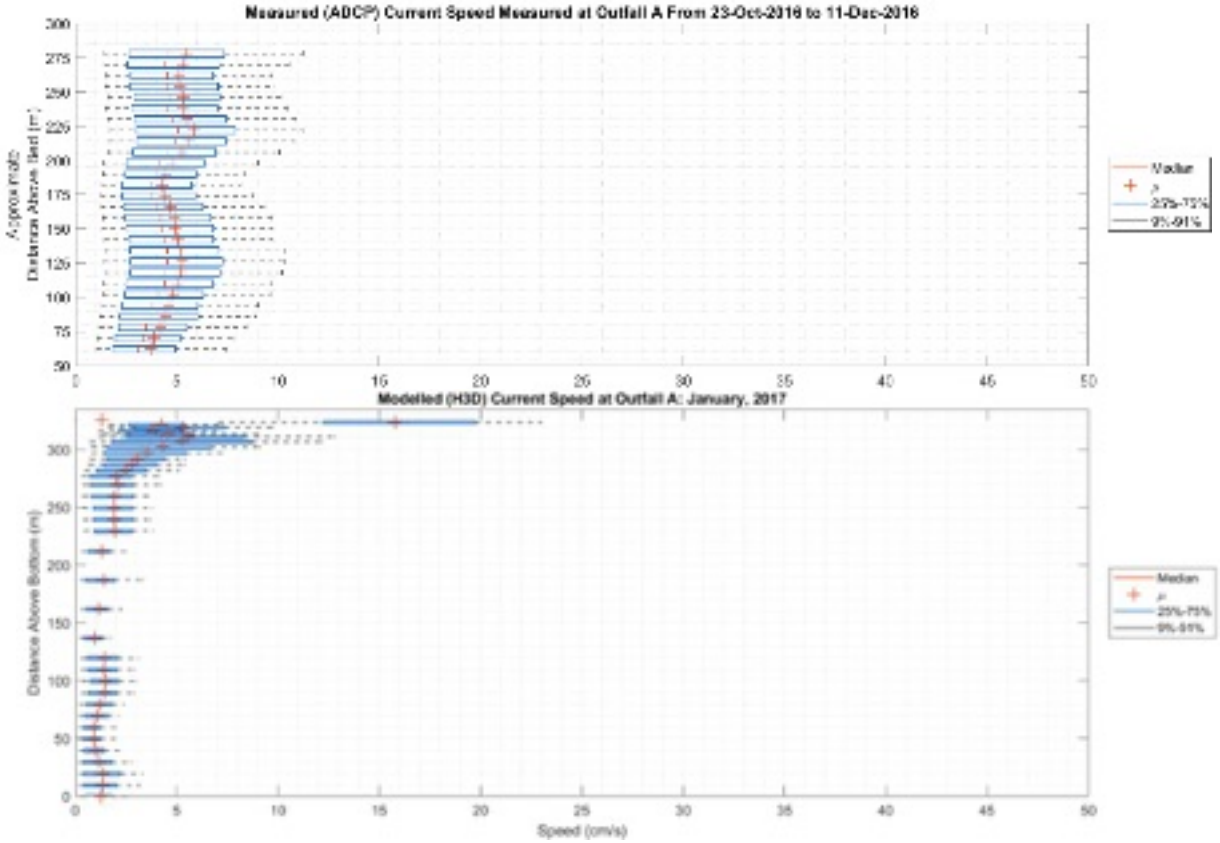

Figure 2.29 ADCP Observed Current Speed (top) and H3D Modelled Current Speed (bottom) at Outfall A

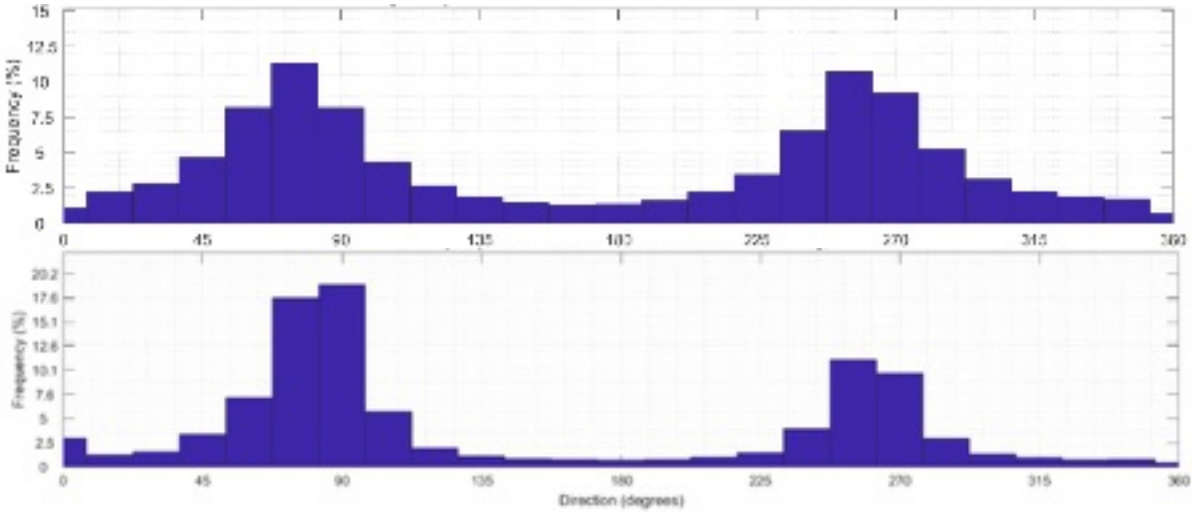

Figure 2.30 ADCP Observed Current Direction (top) and H3D Modelled Current Direction (bottom) at Outfall A

2.2.4 Predicted Natural Sedimentation within the Huon Gulf

A one-year simulation was conducted, looking at the transport, deposition and scouring of natural suspended sediment from all rivers on the north shore of the Huon Gulf, including the Markham and Busu Rivers. The river flow and sediment time-series were shown in Figures 2.4 to 2.6. Understanding the depositional footprint of settled suspended sediment on the floor of the Huon Gulf is important when considering the potential interaction between natural sediments and tailings as they deposit on the seabed. Section 4 will present this comparison.

Figure 2.31 shows the predicted depositional pattern after one year of simulation, representing about 60Mt of natural suspended sediment discharged into the Huon Gulf by rivers. Note that a cut-off at 5mm was applied to the deposition map.

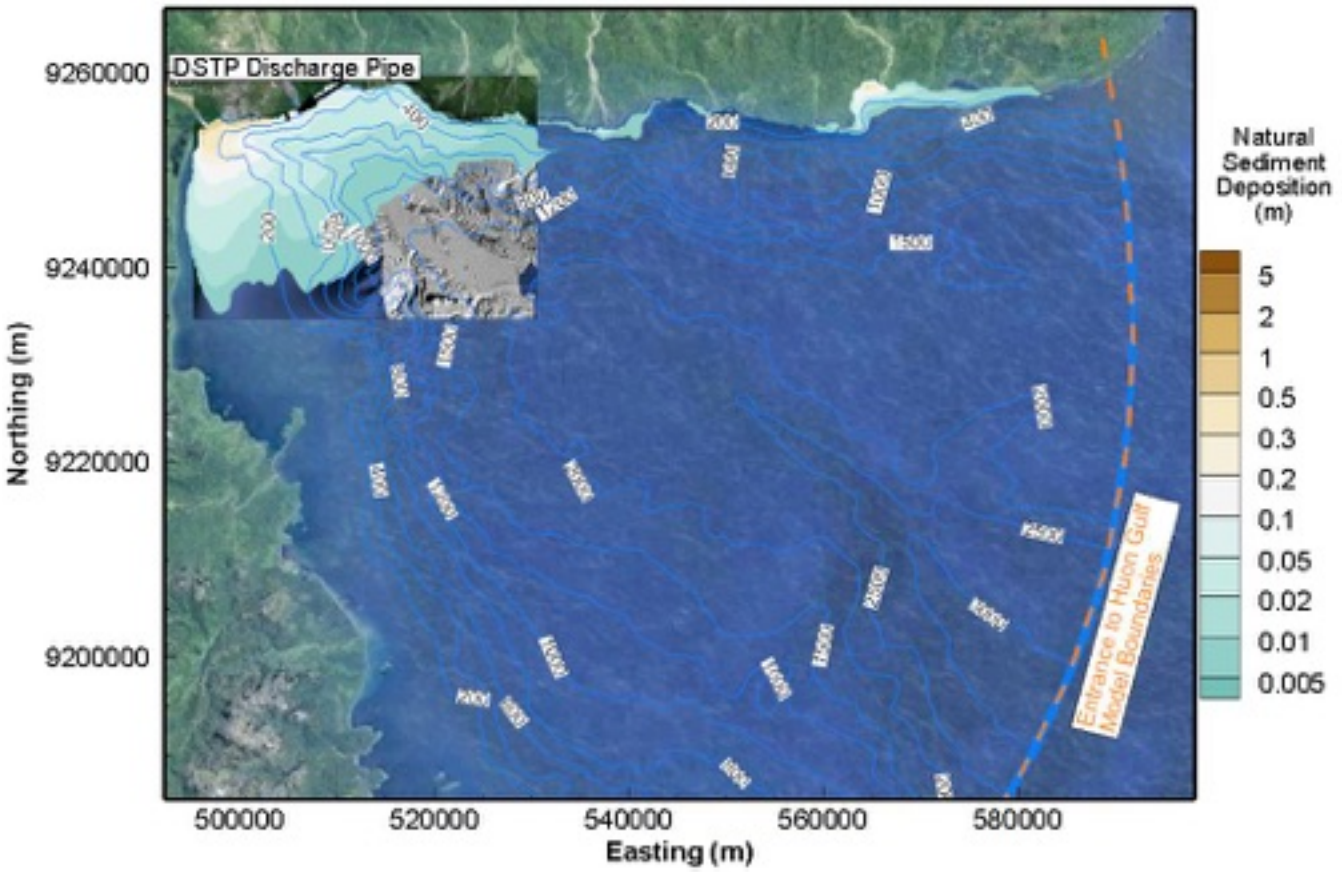

Figure 2.31 Natural Sediment Deposition Footprint

This distribution accords well with the known high rate of sedimentation south of the Markham River, an area where the high level of unconsolidated (i.e., freshly deposited) sediment led to difficulties for the AUV in obtaining high resolution definition of the seabed using acoustic techniques (reported in the Preliminary Slope Stability Assessment Report, Tetra Tech, 2016).

2.2.5 Comparison with Observed Sediment Trap Data

IHAconsult & GDA Consult (2018) installed sediment traps at various locations shown on Figure 2.27 (outfall, canyon, basin, far-field and trench). Figure 2.32 summarized the observed sediment traps results (annualized mass

of deposited sediment per unit area of seabed) at various locations (Outfall, Canyon, Basin, Far-Field and Trench). This statistical bar diagram shows minimum, maximum and median values (line within the red box), as well as 25th and 75th percentile defining the upper and lower limits of the red box. The unit is in tonnes of natural sediment per square metre per year. One can appreciate the spatial variability of the system, in particular at the outfall, canyon and basin areas. Details on observed sediment traps are available in IHAconsult & GDA Consult (2018).

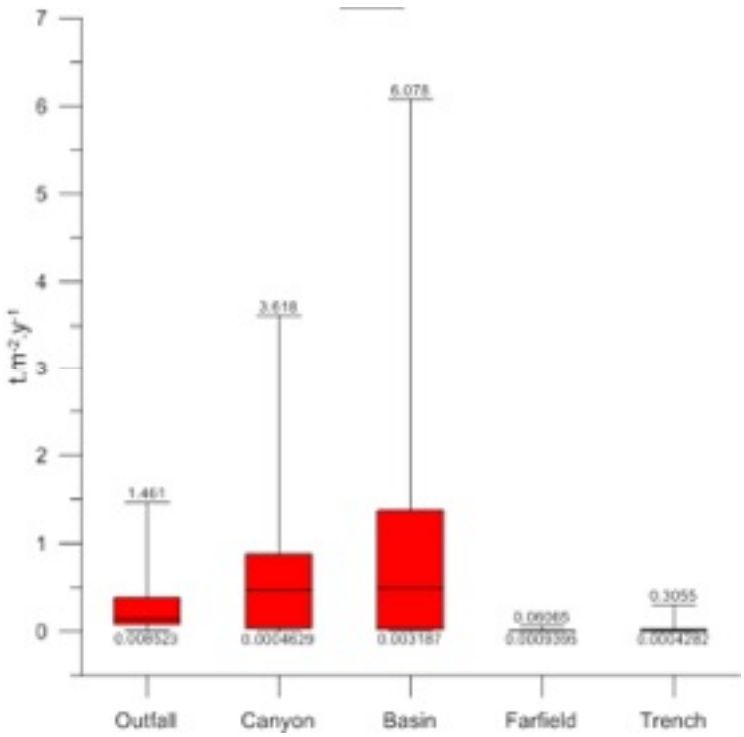

Figure 2.32 Deposition Corresponding to Currently-Occurring Settling (IHAconsult & GDA Consult, 2018)

At the same locations, natural sedimentation simulated by the 3D hydrodynamic model was extracted for comparison purpose and annualized mean modelled values are presented in Table 2.6 along with the annualized observed mean values, and additional statistics. Note that the annualized observed values are derived from bottle collection intervals that range from 1 – 7 days, with total sample durations between about 157 days and 354 days at the various sites: Outfall Location, Canyon Location, Basin Location, Far-Field Location, and Trench Location. The annualized model values are extrapolated form a one-month run without consideration of mass movement events.

At all locations, the modelled natural sedimentation fits within the range of observed sedimentation values, although with some apparent underestimation, particularly at the Canyon and Basin locations. At all but the Outfall site, there are various levels of re-suspension occurring, including as a result of the episodic mass movement events and the persistent down-canyon turbidity current, such that the sediment traps positioned within the bottom attached turbidity plume collected both the sediment settling through the water column and the additional remobilized material. Where the modelled average deposition differs most significantly from the observed values (i.e. the Canyon and Basin locations), the standard deviation in observed deposition rates is greater than the observed mean value, illustrating the high variability resulting from mass movement events and turbidity currents at these locations. The modelled natural sedimentation within the 3D hydrodynamic model described in Table 2.6 accounts for river sediments and the scouring and resuspension of deposited natural sediment by currents, but does not account for the remobilized sediment strictly from the turbidity plumes and mass movement events. Nevertheless, the modelled mean is within one standard deviation of the observed mean, an acceptable result. At the Outfall, Far-

Field, and Trench locations, where the effects of the mass movement events and turbidity currents are less significant, the model mean/median values are comparable to the observed mean/median values.

Further discussion of the settling rate data is provided in IHAconsult & GDA Consult (2018), wherefrom the following text is extracted: *"The sediment trap settling rate data show the dominance of processes within the Markham Canyon in the transport of sediment through the Huon Gulf, with settling rate and particle size being higher at the canyon mooring locations compared to off-canyon locations. The highest sediment deposition rate occurred at the Canyon Mooring site; the lowest was at the Far Field location. The data also likely reflects two different mechanisms of sediment transport. Data from the Markham Canyon moorings likely represents a greater contribution from mass movement events through the systems, while the Outfall site likely represents settling from the extensive nearshore surface plumes of suspended sediment originating from the Markham and Busu rivers in particular. The occasional but less frequent elevated concentrations of sediment collected in the Far Field sediment trap demonstrates the ability of larger, less frequent mass movement events to extend beyond the normal confines of the Markham Canyon." (IHAconsult & GDA Consult, 2018).* Suffice it to say, that both model and observations agree that there is a dramatic drop in deposition of suspended sediment at the Far-Field and Trench sites compared to the other three sites.

Table 2.6: Comparison with Observed Sediment Traps

	Locations[1]				
	Outfall	**Canyon**	**Basin**	**Far-Field**	**Trench**
	t/m^2/year	t/m^2/year	t/m^2/year	t/m^2/year	t/m^2/year
Minimum Observed Annualized Deposition	0.009	0.0004	0.003	0.0009	0.0004
Maximum Observed Annualized Deposition	1.46	3.6	6.1	0.06	0.31
Observed Standard Deviation in Annualized Deposition	0.35	1.08	1.23	0.013	0.061
Observed Median Annualized Deposition	0.18	0.61	0.49	0.004	0.002
Observed Average Annualized Deposition	0.33	0.98	0.92	0.008	0.034
Modelled Average Annualized Deposition	0.98	0.05	0.019	0.003	0.002
[1]Corresponding to Figure 2.32 (IHAconsult & GDA Consult, 2018)					

3.0 TRANSPORT, DEPOSITION AND SCOUR OF DISCHARGED TAILINGS

The tailings behaviour numerical model is a two-dimensional reduced-gravity model of the density current created by the tailings discharge (density current model, DC). That is, it considers the two-layer flow consisting of the density current flowing under, and distinct from, the overlying oceanic waters. The model has been validated against laboratory data (Stronach et al., 1999, Stronach et al., 2000). A technical description of the model is available in Appendix A.

Three implementations of the density current model were used for this study: near-field, intermediate-field, and far-field, differing in coverage area and in spatial resolution: the near-field model has the highest spatial resolution and the smallest coverage area, and the far-field model has the largest spatial coverage and the lowest resolution. As discussed earlier, the three resolutions are used so as to provide good spatial resolution of the key features of the density current as it transforms from a near-pipe flow to a slowing moving broad stream in the Markham Canyon.

The model grids for the different versions are shown in Figure 3.1. The near-field, or fine-grid model has a spatial resolution of 20cm and a spatial coverage of 300m x 140m. The intermediate-field model has a spatial resolution of 10m and a spatial coverage of 10,000m x 10,000m. The far-field, or coarse grid model has a resolution of 50m covering 21,000m x 65,000m. The intermediate-field model has been used to assess the transport, deposition, and scouring of the tailings discharge, subsurface tailings plume generation and tailings solids deposition on the ocean floor. The far-field model was used to assess episodic mass movement events.

All simulations presented in this report incorporate oceanic currents, provided by the 3D hydrodynamic model H3D.

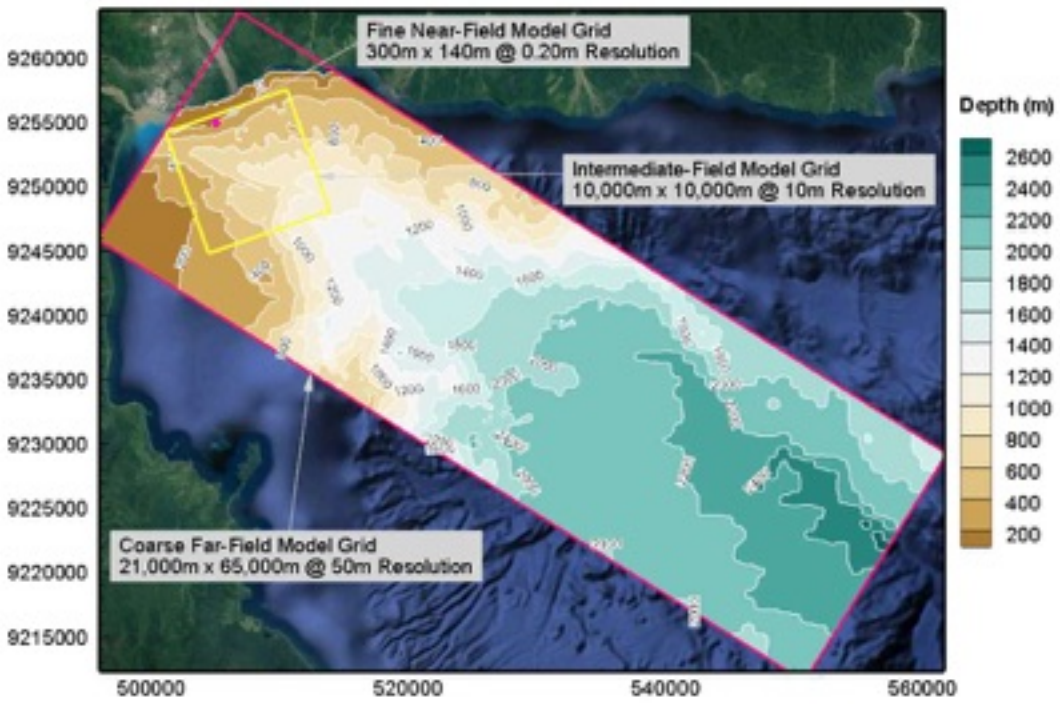

Figure 3.1 Density Current Model Grids and Spatial Resolutions

3.0 Inputs to the Density Current Model

3.0.1 Tailings Particle Size

Solid tailings were divided in two categories for the density current modelling. A cut-off at 38µm was selected to separate the fine from the coarse material.

- Fine fraction with grain size less than 38µm representing 45% of the tailings solids
  - d_{50} = 13.5µm
  - d_{90} = 30.4µm
  - sinking velocity: 0.17mm/s
- Coarse fraction with grain size greater than 38µm representing 55% of the tailings solids
  - d_{50} = 83.0µm

- d_{90} = 148.0µm
- sinking velocity: 6.47mm/s

The particle size distribution was determined by Slurry Systems (Slurry Systems, 2017a, 2017b). Sinking velocities were calculated based on Van Rijn's terminal fall velocity for non-spherical particles (Van Rijn, 1993). Slurry Systems' glass graduated cylinder settling test confirmed the minimum fall velocity for fine particles.

The bathymetry data that was used was provided by the AUV survey conducted in September 2016. The density profile used in the modelling was provided by a combination of IHA's CTD profiles.

A 4:1 dilution prior to discharge into the fine grid model was simulated, replicating the pre-dilution in the mix-de-aeration tank. The scenario investigated in this modelling report is the following:

Table 3.1: Modelled Scenario

Entering Mix Tank					Discharged from Outfall Pipe				
Throughput (tph)	**Solids Content (%)**	**Feed Pipe Flow Rate (m3/s)**	**Initial Slurry Density (kg/m3)**	**Sea Water Intake Flow Rate (m3/s)**	**Outfall Flow Rate (m3/s)**	**Dilution**	**Outfall Slurry Density (kg/m3)**	**Outfall Solids Content (%)**	**Outfall Velocity (m/s)**
1,891.4	30% (v/v) 55% (w/w)	0.617	1,547.05	2.673	3.29	4.33:1	1,120.53	14.2% (Cw) 5.6% (Cv)	3.9

3.0.2 Above-Bed Bottom Currents

Through the 2017 ADCP's campaign, IHAconsult (2017) identified that a localized strong and persistent current was present close to the seabed within the Markham Canyon: "*occurrence of both up and down-canyon flow, with a dominance of down-canyon flow just above the bed*" (Section 4.2.2.4 of IHAconsult (2017)). As an illustration of these localized strong near bed currents, Figure 3.2 shows current speed profiles at five different selected times (selected to clarify the range of current profiles at this site), at depths ranging from the seabed to 15 m above the seabed, at the Canyon B location (Figure 2.27). One can clearly appreciate the variability in these currents, ranging from less than 0.10m/s up to almost 1.5m/s between two samplings, but also ranging between 0.05m/s and 1.5m/s within a single 15m water profile. The two high velocity events, on May 10 and May 24, are presumably associated with the passage of naturally occurring intermittent turbidity currents flowing down the Markham Canyon.

While the comparison between the 3D model H3D and observed data was satisfactory (Section 2), the relative thickness of this persistent current (sometimes less than 5m) made it a challenge to simulate and reproduce numerically in areas where the 3D model would be characterized by 50m layer thicknesses at depths of 500m and deeper. As a result, a linear scaling process of bottom currents generated by H3D was conducted, so that the density current would experience velocities characteristic of the Markham Canyon. Note that this scaling process did not affect the H3D model, but only the inputs used by the density current model, i.e. the near-bed bottom current layer. Through this process, it was ensured that near-bed velocities were representative of this localized and persistent down-canyon current feature, while velocities through the rest of the water column were satisfactorily compared with the observed currents.

Following this scaling process, a comparison was conducted for the near-bed bottom layer currents between observed ADCP data and scale-up modelled currents. Figure 3.3 shows the results of this comparison. Acceptable agreement was observed at Canyon B and Canyon C locations. No ADCP data was available at Canyon A; however the modelled velocity is presented in Figure 3.3 in order to indicate the average velocity that the density current would experience, when entering the canyon, typically near Canyon A. In addition, the outfall location was kept on this graph in order to show typical velocities in the vicinity of the discharge location, as well as the good agreement between observed and modelled.

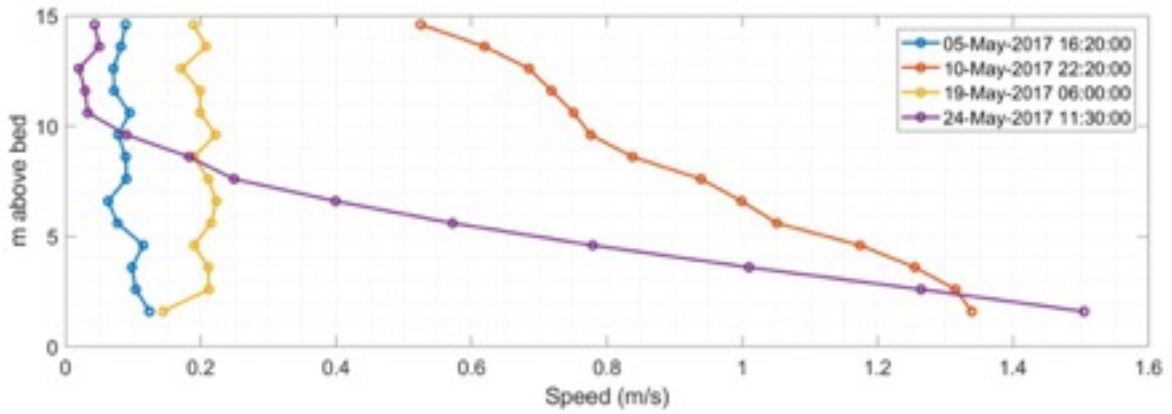

Figure 3.2 Selected ADCP Observed Current Speed Profiles at Canyon B (5 May 2017 at 16:20, 10 May 2017 at 22:20, 19 May 2017 at 6:00, and 24 May 2017 at 11:30)

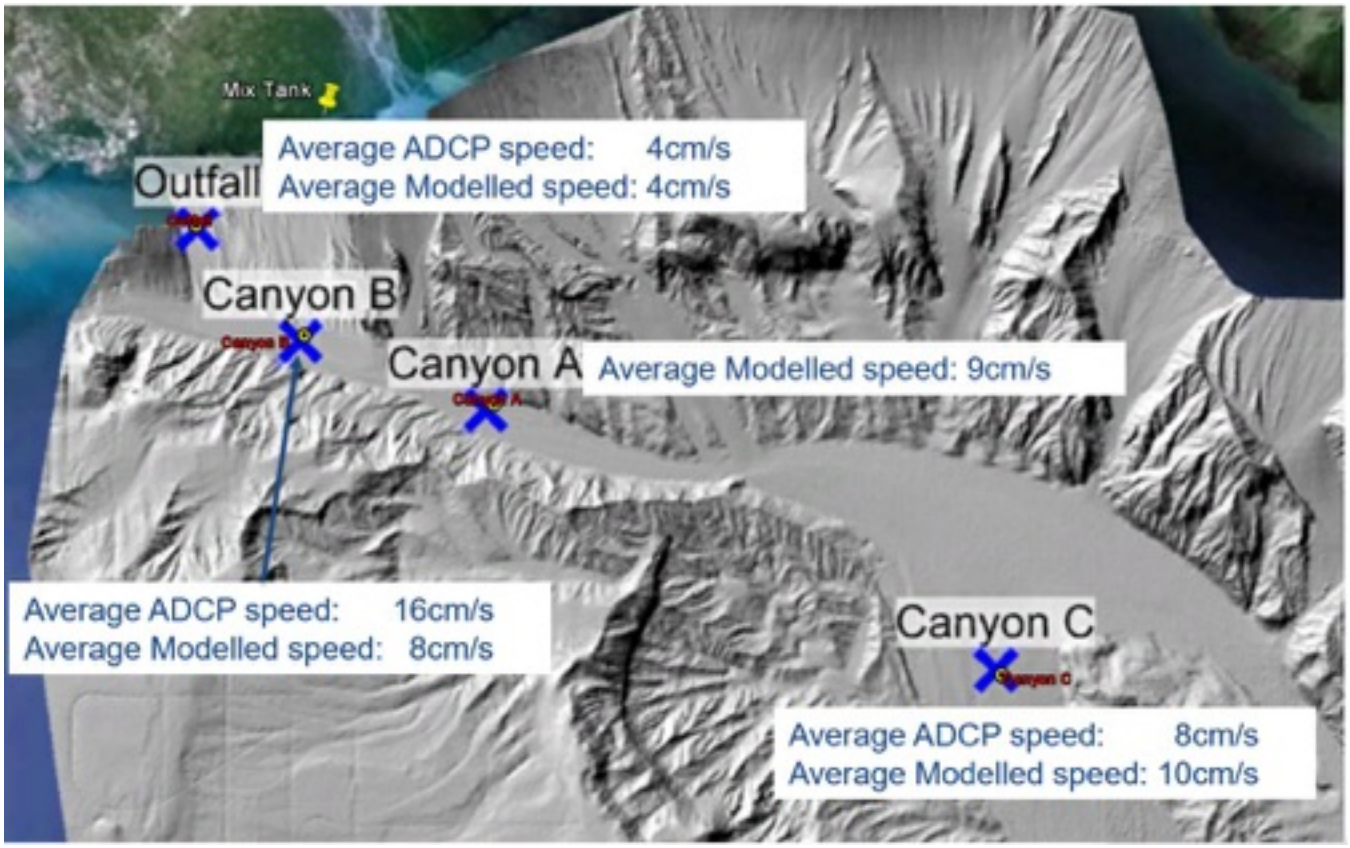

Figure 3.3 Comparison of Near-Bed Bottom Velocities for the Upper Portion of the Canyon

3.1 Near-Field Density Current Model

The results of the near-field density current model simulation are based on the final proposed outfall configuration comprising two outfall pipes descending to a depth of 200m. Results are presented for the time after the model reaches a steady-state. As Figure 3.4 shows, a short amount of time, about 300s, is necessary for the system in the near-field to establish itself and reach a steady-state. Steady-state is characterized by negligible temporal variations in the system. During steady-state, the tailings mass balance is as summarized in Table 3.2. Most of the discharged tailings – almost 99% - is predicted to exit the boundaries of the fine grid domain located about 120m downstream of the pipe terminus. The remainder is predicted to settle on the side of the main axis of the density current (<0.1%) or exit in the form of sub-surface tailings plumes (1.2%).

Table 3.2: Predicted Mass Balance for the Near-Field Density Current Model

Item	Percent
Discharged Tailings	100%
Tailings exiting the boundaries of the near-field domain	98.8%
Tailings depositing within the boundaries of the near-field domain	< 0.1%
Tailings exiting through sub-surface plumes within the near-field domain	1.2%

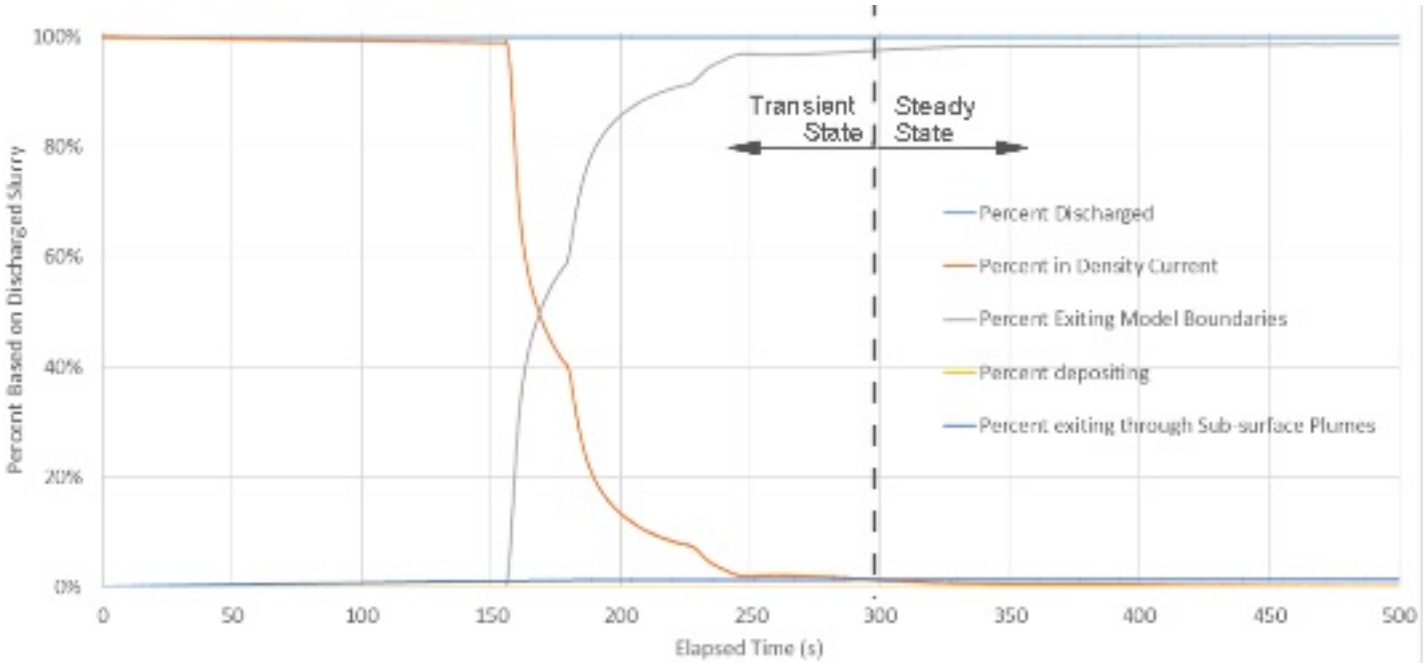

Figure 3.4 Distribution of Discharged Tailings in Near-Field Density Current Model

Predicted total dilutions in the near-field are shown in Figure 3.5. The model shows that total dilutions, i.e. including pre-discharge dilutions in the mix-tank, of 10:1 are achieved at about 10m downstream the outfall terminus. At 100m downstream of the terminus, total dilutions of 120:1 are achieved. Finally, at the boundaries of the fine-grid model, total dilutions of 180:1 are observed. Vectors enable the pathway of the density current to be observed, in particular two main arms of the tailings density current that formed in order to follow the shallow submarine valleys that run down the northern wall of the Markham Canyon below the proposed outfall terminus.

The predicted thickness of the density current (Figure 3.6) reaches an average of 5m at the boundaries of the model domain about 120m downslope of the outfall terminus, in those sections along this boundary where the density current is flowing most strongly.

The predicted near-field depositional footprint can be seen in Figure 3.7. This footprint corresponds to the steady state reached by the system, i.e. negligible temporal variations in the system are observed, and levees grow and collapse with their slumped material being carried to deeper depths. The steady-state condition was reached within one hour of simulated time from the start of tailings released. As the density current exits the pipe, the central core maintains a high velocity. The flow along the two outer boundaries, to either side of the main core, is slower. This results in the formation of small levees along the lateral boundaries. The height of the levees is limited because once they are tall enough to exceed a critical slope, the model predicts that they collapse into the main core of the flow where the high turbulence and velocity carry the remobilised sediment away from the pipe. The levee growth and failure cycle is simulated in the model - levees grow until the slope exceeds the angle of repose, at which point they then collapse and begin to grow again. The angle of repose is considerably less than the angle of repose in stationary water due to the velocity of the flow and the associated shear stress.

Deposition of tailings solids immediately below the outfall terminus has caused problems at some DSTP sites elsewhere in the world, but not in PNG. If tailings deposition is severe, it can cause plugging of the outfall pipe. However, this has only occurred where the bottom slopes are gentle which encourages deposition immediately below the outfall terminus. The PNG Government's draft general guidelines for DSTP require a minimum bottom slope of 12° at the outfall. The bottom slope at the proposed DSTP outfall is about 20° and well in excess of the guidelines. The predicted tailings depositional footprint in Figure 3.7 shows no deposition occurring near the outfall terminus which supports the suitability of the proposed outfall site.

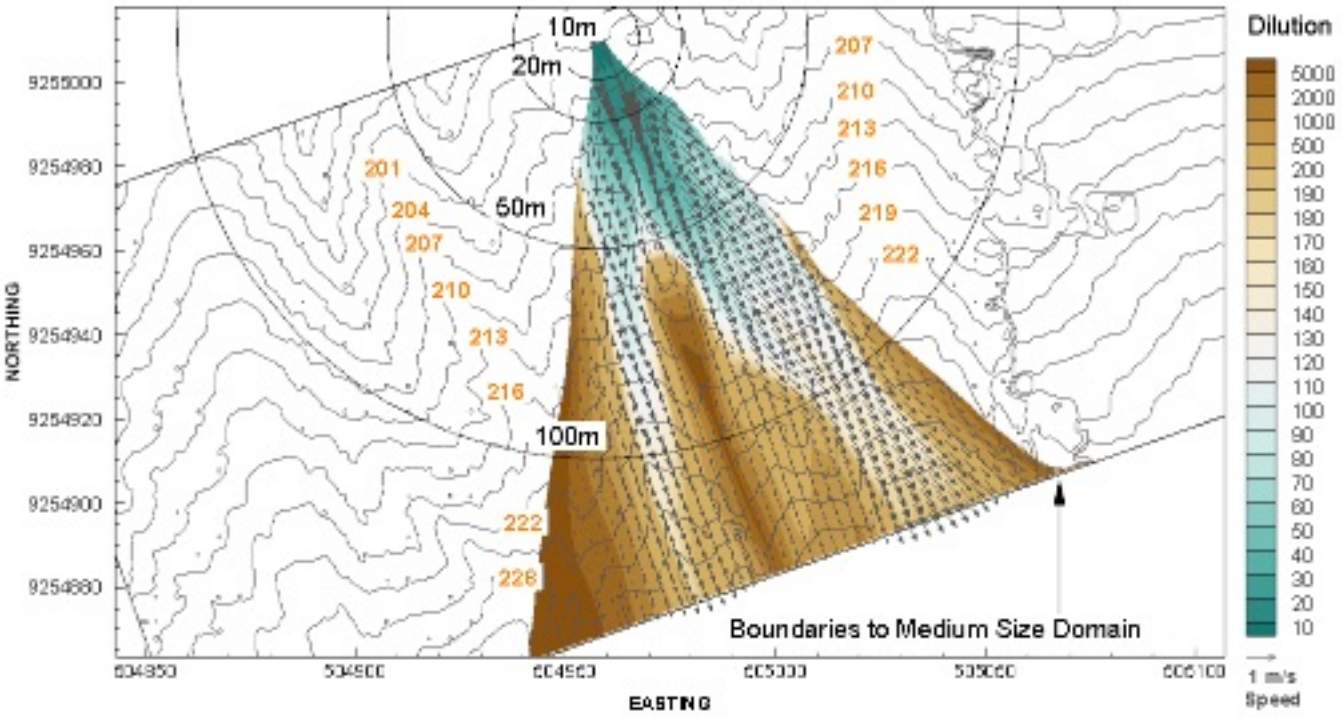

Figure 3.5 Predicted Total Dilutions in the Near-Field Density Current

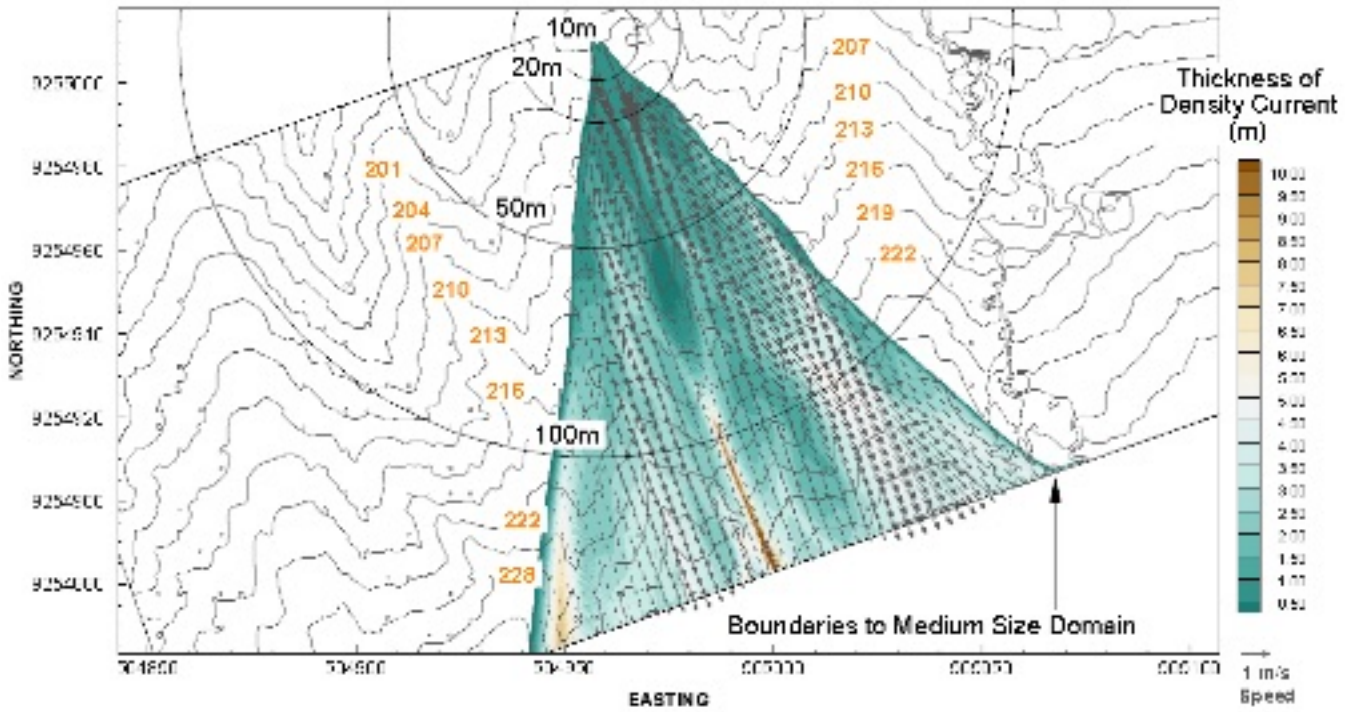

Figure 3.6 Predicted Thickness of the Density Current in the Near-Field after Reaching Steady State

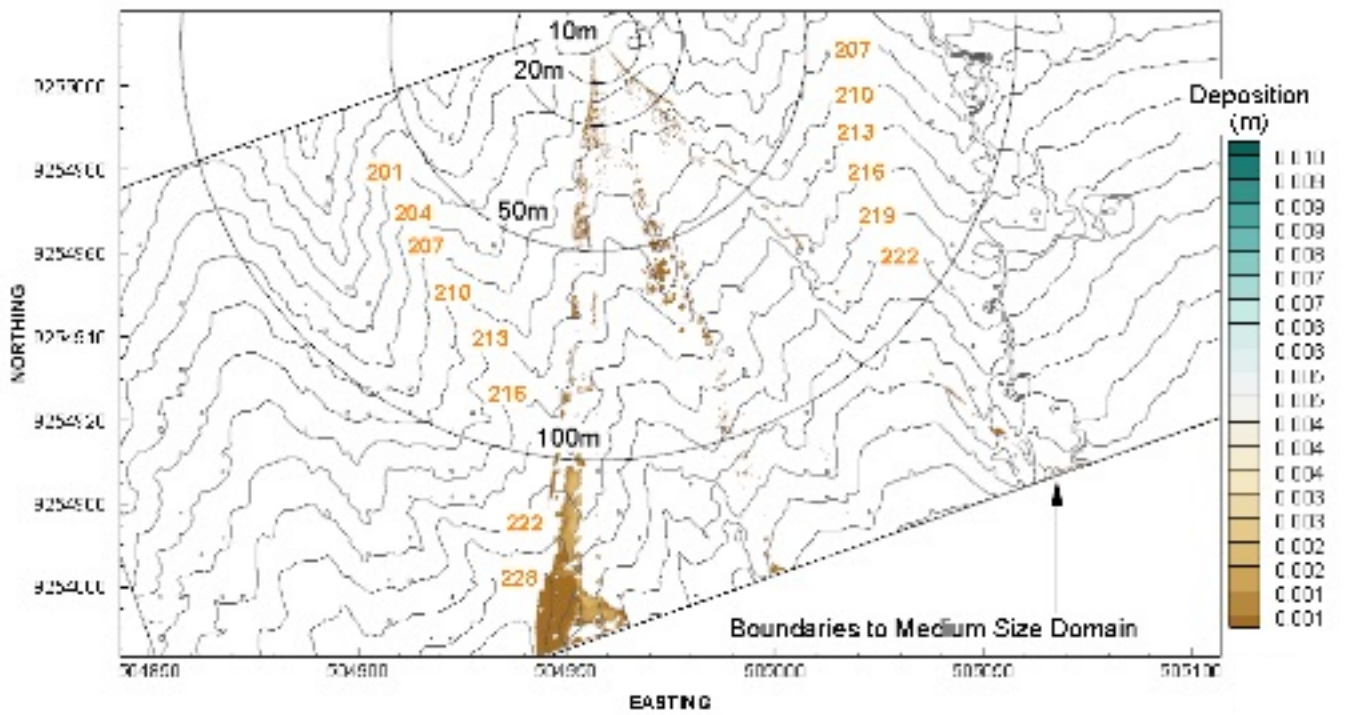

Figure 3.7 Predicted Deposition from the Density Current in the Near-Field after Reaching Steady State

3.2 Intermediate-Field Density Current Model

The characterization of the density current in the intermediate-field domain is slightly different from the near-field domain. While a steady-state was reached quickly in the near-field domain model, the establishment of a steady-state in the intermediate-field domain is impossible, primarily because of the time-varying forcing from the oceanic currents in the Huon Gulf. A more adequate term to characterize this density current behaviour is a "*quasi-steady-state*". Due to the loss of momentum by the density current in the near-field domain, oceanic currents have a major impact on the trajectory of the density current. The speed and direction of oceanic currents vary, and hence so does the behaviour of the density current. These changes are characterized by sudden collapse of levees, resulting in the generation of sub-surface plumes or the transport of the material further downslope and the settling in deeper water or the material exiting the boundaries of the intermediate-field model.

3.2.1 Mass Balance

Since a multi-year simulation was not possible from a computing and data availability point of view, a one-month simulation was conducted. A representative one month period was selected and considered adequate for the Huon Gulf considering the limited seasonal variability in temperature and salinity profiles and other major forcings that control the hydrodynamics within the Huon Gulf. The critical period of time to consider when modelling the transport, deposition, and scouring of the density current is the ability to reach the quasi-steady-state. The quasi-steady-state was reached within a very few days. Figure 3.8 shows the mass balance and illustrates this quasi-steady-state: a near-constant rate of tailings exiting through sub-surface plumes (grey curve and subsequently modelled in the 3D section) and depositing (orange curve). Note that tailings exiting through sub-surface plumes is also called "depleted material", since it represents material leaving the density current. A very minimal amount of tailings exits the geographical boundaries of the domain, less than 1% and shown as the yellow curve on Figure 3.8. Table 3.3 shows the quasi-steady state mass balance for the intermediate-field model.

Table 3.3: Mass Balance for the Intermediate-Field Density Current Model

Item	Percent
Tailings exiting the boundaries of the Intermediate-Field domain	0.8%
Tailings depositing within the boundaries of the Intermediate-Field domain	60.0%
Tailings exiting through sub-surface plumes within the Intermediate-Field domain and subsequently modelled in the transport, deposition, and scour of sub-surface plumes section	39.2%

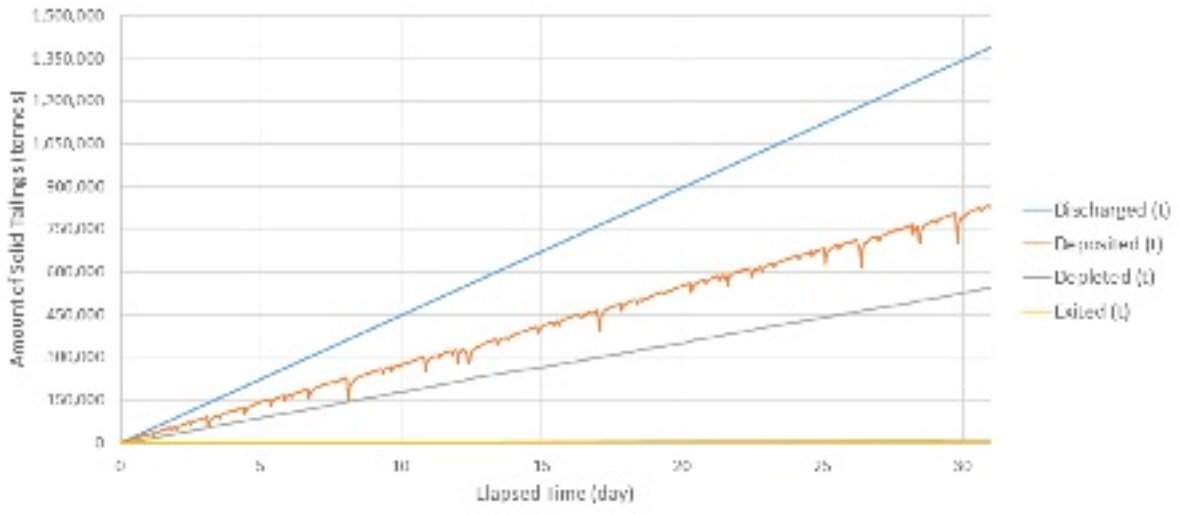

Figure 3.8 Mass Balance in the Intermediate Field Density Current Model

3.2.2 Predicted Tailings Settling Depths and Sub-Surface Plume Generation Depths

An analysis of the depths at which tailings is predicted to settle and the depths at which sub-surface plumes are predicted to be generated was conducted. Figures 3.9 and Table 3.4 show the depth distribution where tailings solids are predicted to exit the density current and form sub-surface plumes. Only fines are predicted to exit the model through sub-surface plumes. Note that Figures 3.9 and 3.10 show the depleted and deposited fractions of tailings expressed as *relative percentages* of the corresponding fraction within the density current. Only the fine fraction forms sub-surface plumes, the coarse fraction is assumed to be concentrated at the bottom of the density current, i.e., has negligible concentration at the interface between the density current and the overlying sea water.

Figure 3.10 and Table 3.5 show the depth distribution where deposition of both the fine and coarse fractions of the tailings solids is predicted to occur within the density current model. One can read that most of the coarse deposition (about 63% of the coarse fraction of tailings in the density current) is predicted to occur at depths greater than 700m. On the other hand, the bulk of the fine deposition (about 75% of the fine fraction of the tailings remaining in the density current that do not exit the density current through subsurface plumes) is predicted to occur in shallower water between 300m and 600m depth. Note that the majority of the fine tailings exit the density current as subsurface plumes, whereas, the coarse fraction can only exit the density current via deposition. Stated somewhat differently, the fine fraction is exhausted from the density current in shallower depths, mainly between 300m and 400m, so that relatively little is available for deposition at depths greater than about 700m.

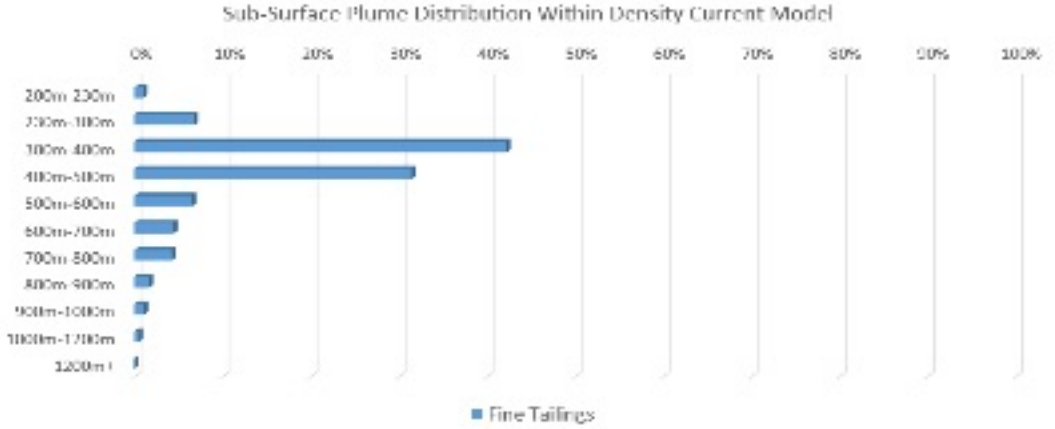

Figure 3.9 Predicted Depths Associated with Sub-Surface Plumes Creation (expressed as relative percentage of the fine fraction of tailings in the density current)

Table 3.4: Summary of Predicted Sub-Surface Plumes Depth Creation

Depth Range	Relative Percentage of Solid Tailings Exiting the Intermediate-Field Domain via Sub-Surface Plumes
200m-230m	1.2%
230m-300m	6.6%
300m-400m	42.3%
400m-500m	31.4%
500m-600m	6.5%
600m-700m	4.4%
700m-800m	4.3%
800m-900m	1.7%
900m-1000m	1.1%
1000m-1200m	0.5%
1200m+	0.0%

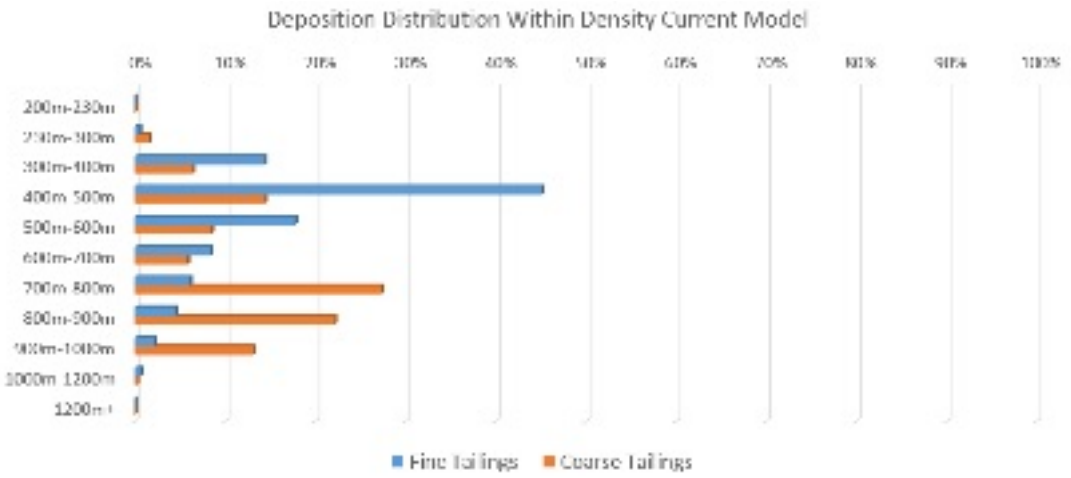

Figure 3.10 Predicted Depth Distribution of Fine and Coarse Tailings Deposition (expressed as relative percentages of respective fraction remaining in density current)

Table 3.5: Summary of Predicted Depth at Which Tailings Deposit from the Density Current

Depth Range	Relative Percentage of Coarse Deposition	Relative Percentage of Fine Deposition
200m-230m	0.0%	0.0%
230m-300m	1.6%	0.6%
300m-400m	6.5%	14.4%
400m-500m	14.5%	45.1%
500m-600m	8.5%	17.8%
600m-700m	5.9%	8.5%
700m-800m	27.4%	6.2%
800m-900m	22.2%	4.5%
900m-1000m	13.1%	2.2%
1000m-1200m	0.3%	0.7%
1200m+	0.0%	0.0%

3.2.3 Predicted Total Dilutions and Concentrations

Statistics were produced in order to characterize the total dilutions and concentrations of both the liquid and solids fractions of the tailings. These statistics were based on one month of density current modelling, capturing the daily variability in the behaviour of the density current.

Figure 3.11 shows the predicted 95th and 50th concentration percentiles of the tailings solids fraction (as mg/L of total suspended solids) within the density current at various distances from the outfall discharge point. As an example, 3km away from the outfall terminus, the predicted tailings solids concentrations are lower than 1,000mg/L 95 percent of the time. The large difference between the 50th percentile and the 95th percentile predictions is due to slumping of levees around 1km from the outfall, which result in episodic high solids concentrations within the density current.

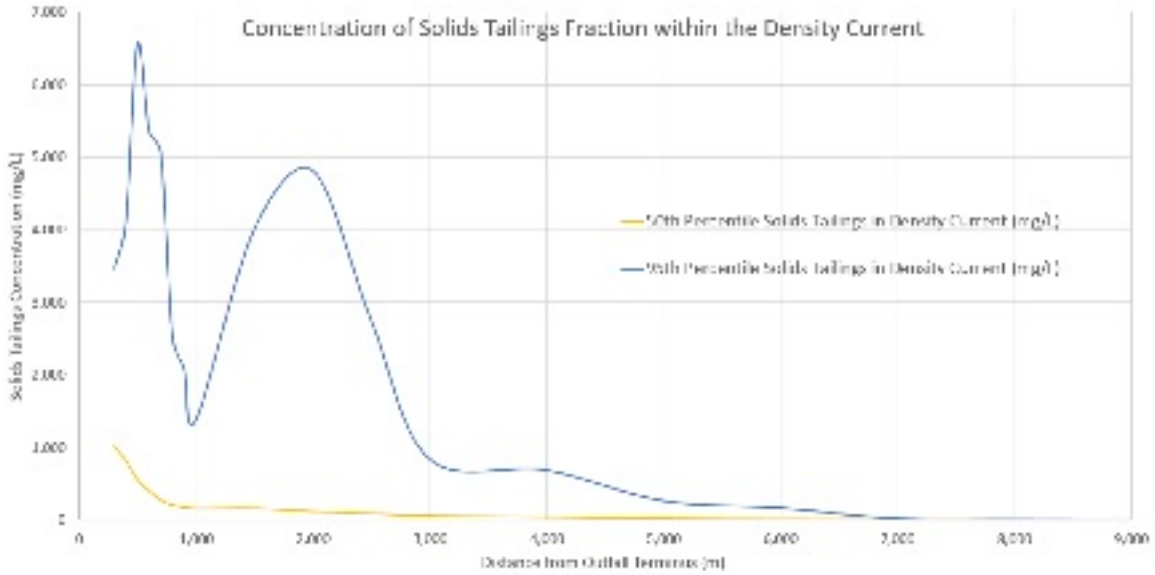

Figure 3.11 Predicted Concentrations of Tailings Solids within Density Current

The predicted distance from the outfall required for the tailings to travel in order to achieve total dilutions between 300:1 and 5,000:1 for the tailings liquid fraction are shown in Table 3.6. This table was generated by extracting the distance to reach specific dilutions, e.g., 300:1 as a time-series of distances, then sorting these distances and extracting the 50th and 95th percentile values. Note that these dilutions are total dilutions, i.e. they include the pre-discharge dilution. Distances reported in the table indicate the maximum distance the tailings would need to travel from the discharge point to be certain of reaching various target dilutions. For example, 95% of the time, the tailings would need to travel 2.1km from the discharge point to achieve a dilution of 1,800:1 whereas for 50% of the time (i.e., the median) the tailings would need to travel only 1.4km from the discharge point.

Table 3.6: Predicted Distances to Achieve Target Dilutions of Tailings Liquid Fraction within Density Current

	300:1	1,000:1	1,800:1	2,000:1	5,000:1
50th Percentile	227m	693m	1,412m	1,577m	2,871m
95th Percentile	240m	1,008m	2,111m	2,309m	4,381m

3.2.4 Predicted Tailings Depositional Footprint from Density Current

Following a one-month simulation during which quasi-steady-state was reached, a scaling and sliding procedure was applied to the predicted depositional footprint in order to scale up the deposition to a one-year period, allowing areas of deposition with steep slopes to collapse once they exceed their angle of repose. Figure 3.12 shows the predicted tailings depositional footprint after one year of tailings discharge and subsequent settling from the density current (without any natural mass movement event). This depositional footprint corresponds to about 10Mt of tailings solids depositing directly from the density current, and does not include the 6Mt of tailings from the subsurface plumes. The top panel of Figure 3.12 presents the entire Huon Gulf, while the bottom panel shows a zoom in to the study area. The red dotted line in the bottom panel shows the boundaries of the intermediate-field model domain. A cut-off at 5mm deposition (over one year) was applied in Figure 3.12.

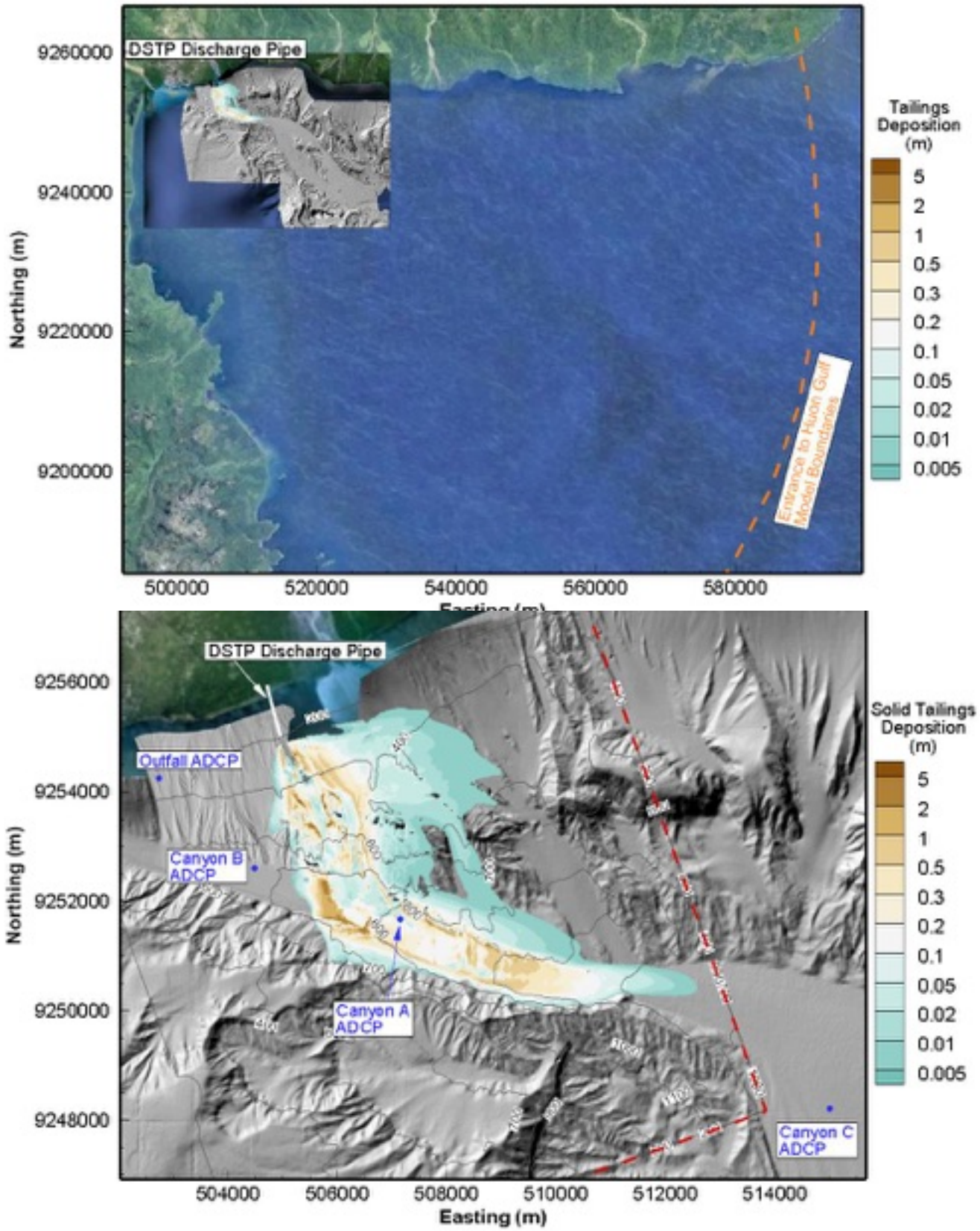

Figure 3.12 Predicted Tailings Depositional Footprint from the Density Current in the Intermediate-Field Model after 1 Year

3.3 Transport, Deposition and Scour of Sub-surface Tailings Plumes

As the density current propagates down-slope, a considerable amount of dissolved and fine suspended material is transferred from the density current into the water column by the generation of subsurface plumes. As shown in Section 3, about 39% of the discharged tailings is predicted to leave the density current in the form of sub-surface tailings plumes.

A three-dimensional circulation model was used to track the liquid and solid fractions of the tailings once they have separated from the density current, thus completing the tailings behaviour modelling. As for the density current modelling, a one-month simulation was conducted and then scaled up to a full year.

3.3.1 Predicted Solids Concentrations and Total Dilutions an

The solids component of the sub-surface tailings plumes is discussed first. Figure 3.13 illustrates the spatial extent of predicted concentrations of suspended tailings solids in sub-surface plumes through a plan view (top panel) and a section view (bottom panel). Note that this figure is not a statistical representation of the plume, but rather it is a snapshot in time. The top panel shows the spatial distribution of concentration of suspended tailings solids (mg/L) in the water column within the near-bed layer of the 3D hydrodynamic model (i.e. bottom layer of the hydrodynamic model, that is, within between 10m and 50m of the seabed, depending on local depth) at one point in time. One can observe that, within a 10km radius, concentrations are predicted to drop to around or below 1mg/L. A cut-off at 1mg/L was applied to Figure 3.13, since 1mg/L generally represents a minimum detectable TSS concentration for instrumentation. The blue line shows the transect along which the section of the bottom panel was made and follows the central pathway for the descending density current. The bottom panel indicates that the maximum concentrations can be found near the seabed, because the suspended solids are undergoing both horizontal transport by currents and sinking because their density is greater than that of sea water. That is, the downward slope of these sediment plumes is an indication that the sediment is slowly sinking to the seabed.

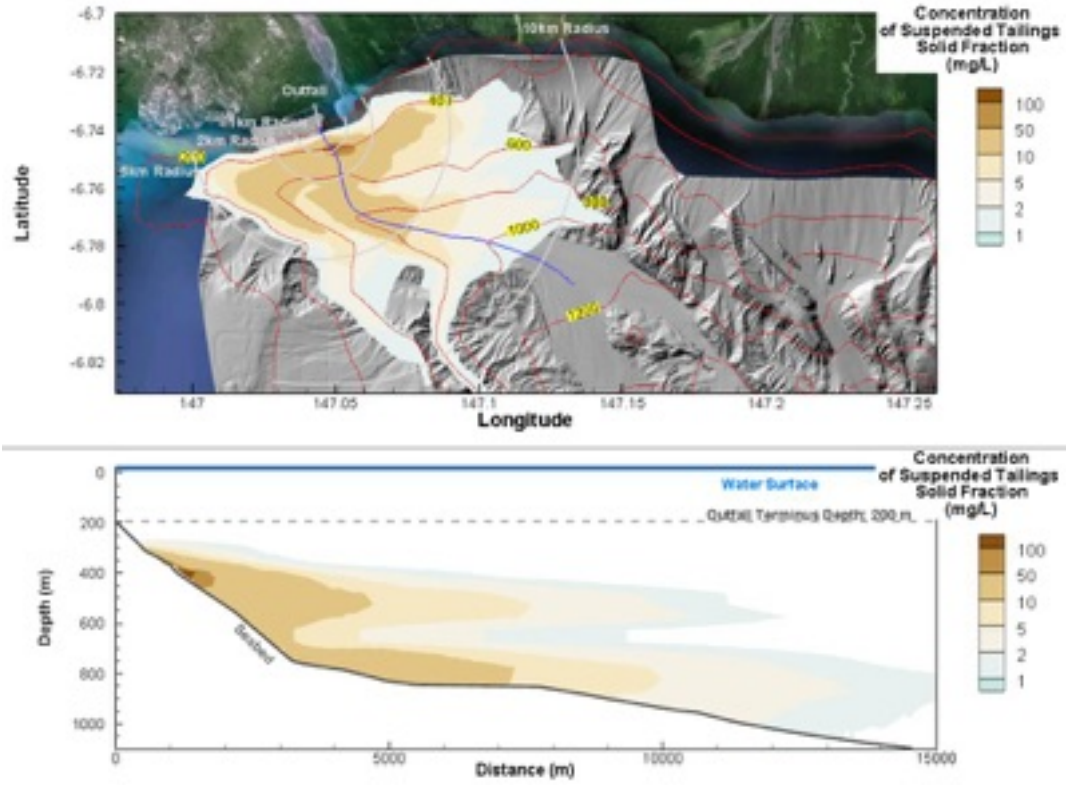

Figure 3.13 Plan and Section View of Predicted Suspended Tailings Solids Concentrations in Sub-Surface Plumes

Similarly, a snapshot of predicted total dilutions of the tailings liquid fraction within sub-surface tailings plumes is presented in Figure 3.14. Total dilutions greater than 5,000:1 are not shown. One can observe that predicted total dilutions less than 1,800:1 are contained within a 1km radius, for this snapshot. Figure 3.15 presents the same results as in Figure 3.14 but with a zoom-in on the area of study for better readability. Note that in the section plots, the liquid fraction plumes travel horizontally and do not sink, whereas in Figure 3.13, the sediment component of the plumes does sink.

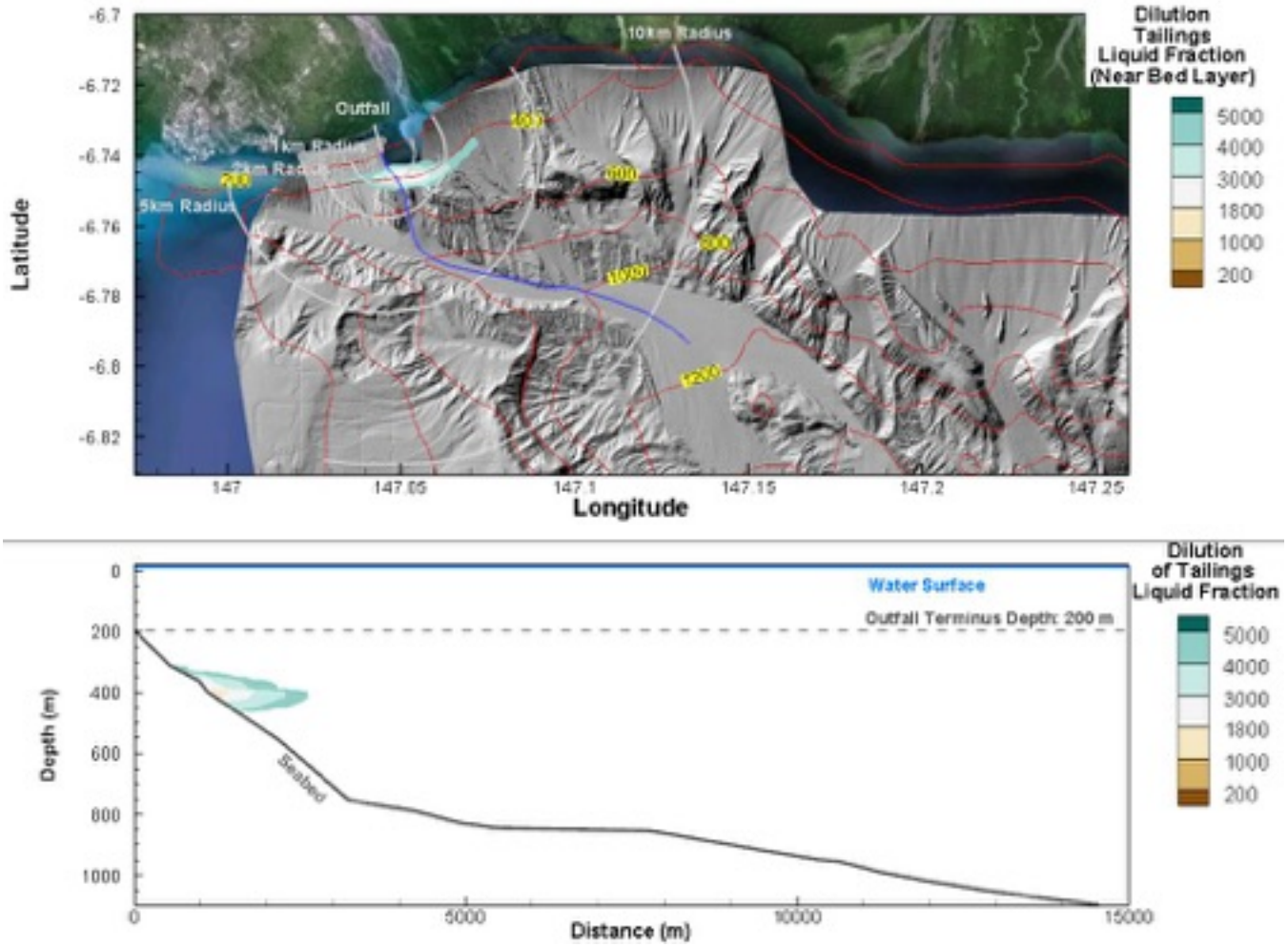

Figure 3.14 Plan and Section View of Predicted Tailings Liquid Fraction Total Dilutions in Sub-Surface Plumes

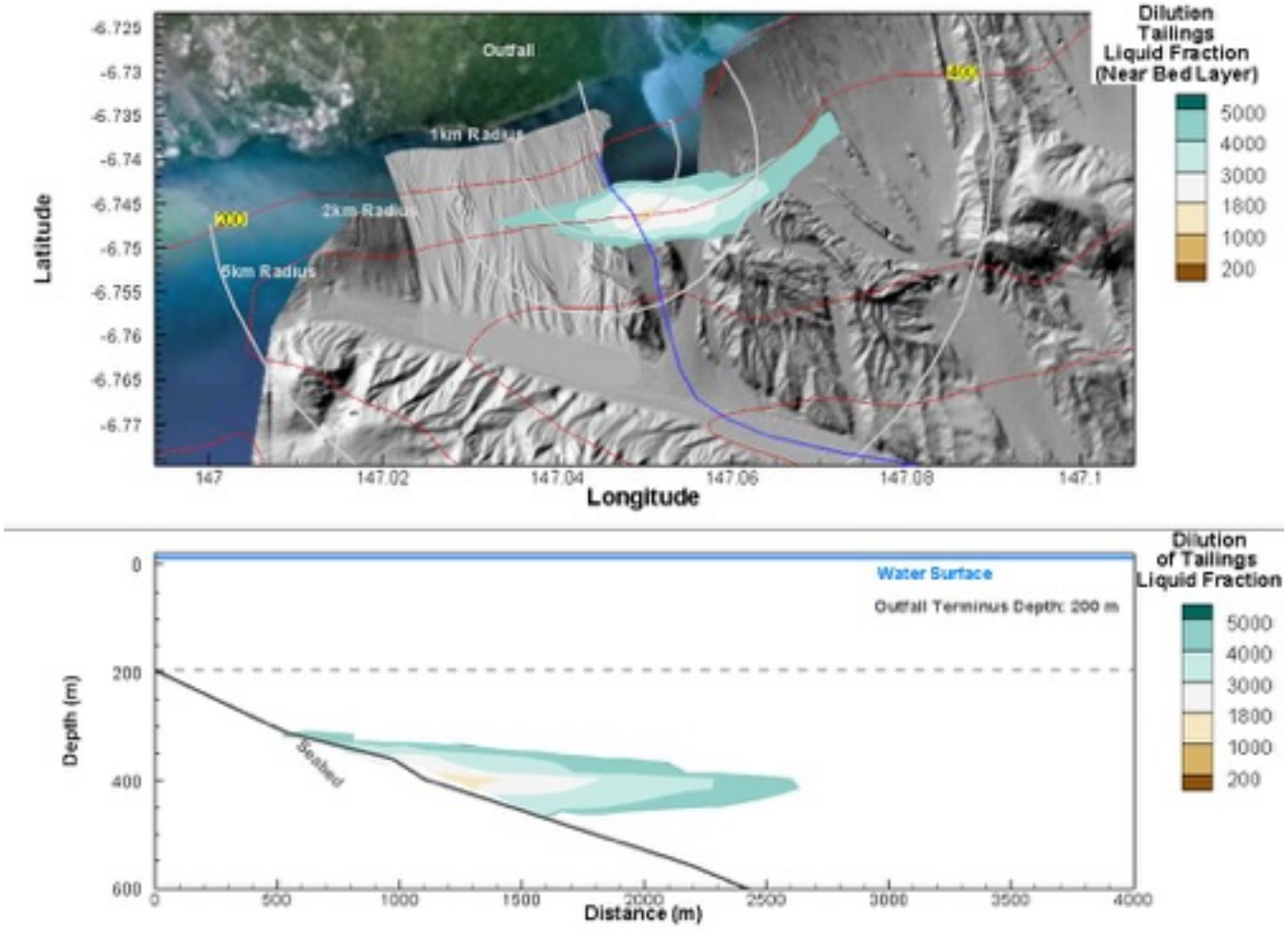

Figure 3.15 Zoom-in on Plan and Section View of Predicted Tailings Liquid Fraction Total Dilutions in Sub-Surface Plumes

Next, combining the information on solids concentrations available in snapshots such as Figure 3.13, statistics were generated. Statistics on the predicted concentrations at various depths were extracted, based on one month of density current modelling, capturing the daily variability in the behaviour of density current and sub-surface tailings plumes. Figure 3.16 plots the 50th and 95th percentile statistics for the maximum suspended tailings solids concentrations in sub-surface plumes against depth. As expected based on Section 3.2, since sub-surface plumes are generated predominantly at depths of 300m to 500m, the greatest concentrations are predicted for this depth range. For 95% of the time, suspended tailings solids concentrations would have a maximum predicted concentration less than 190mg/L.

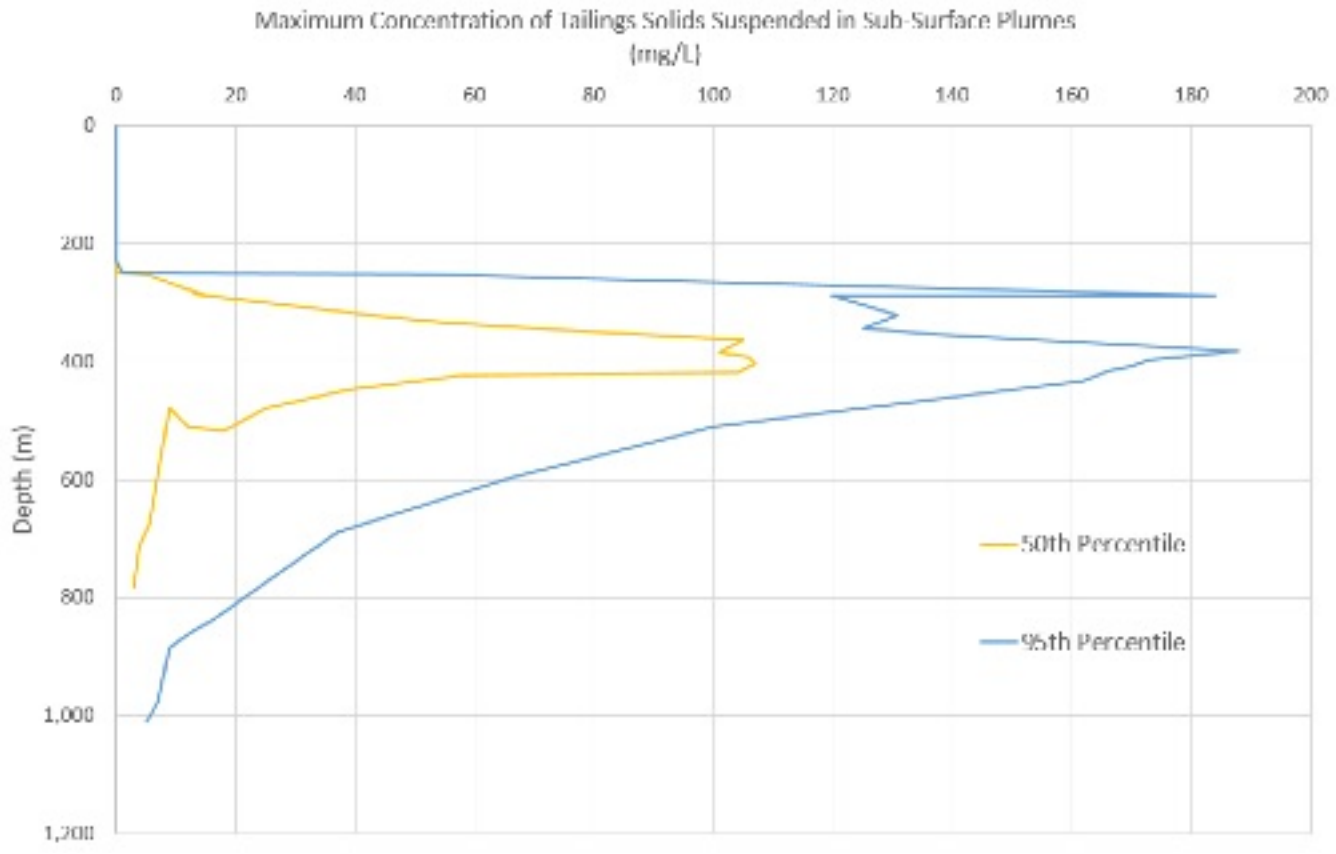

Figure 3.16 Predicted Maximum Concentration Profiles of Suspended Tailings in Sub-Surface Plumes

Figure 3.17 shows predicted maximum concentrations of tailings solids in subsurface plumes versus distances from the outfall pipe terminus for both the 50th and 95th percentiles. Predicted maximum concentrations are reached within the first kilometre from the outfall terminus.

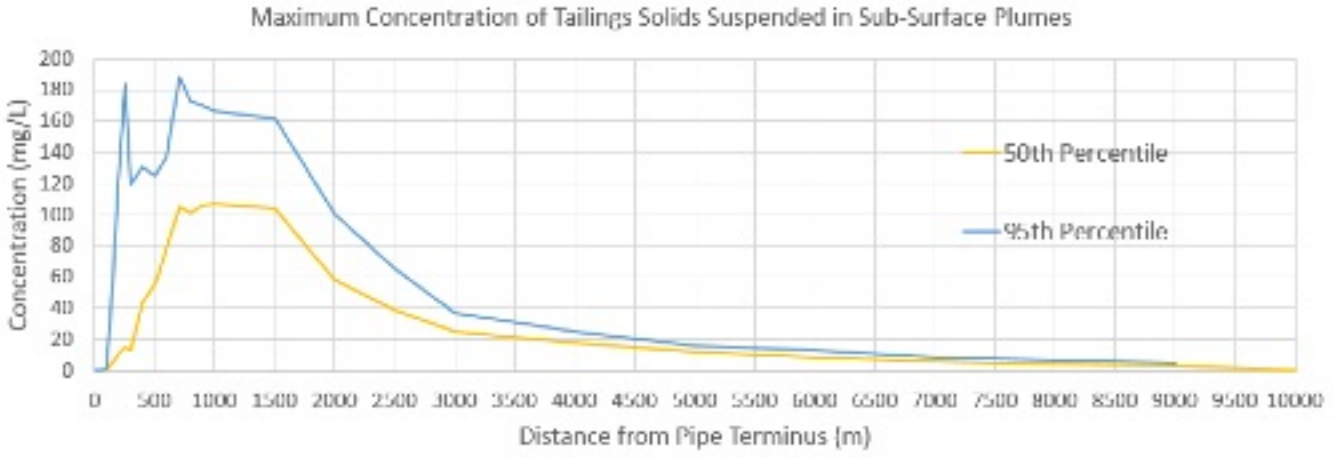

Figure 3.17 Predicted Maximum Concentration of Suspended Tailings in Sub-Surface Plumes versus Distance from Discharge Point

3.3.2 Predicted Depositional Footprint from Sub-Surface Tailings Plumes

Following this one-month tracking, the predicted depositional footprint was, similar to the density current, scaled up to one year. This sliding process was required for the tailings deposited directly from the density current to allow areas of deposition with steep slopes to collapse once they exceed their angle of repose. However, this function was not required for the scaling of the depositional footprint from the sub-surface plumes, due to their more widely distributed, thinly blanketing nature (i.e. the side slopes resulting from differential deposition within adjacent cells did not exceed the angle of repose, even considering the natural slope of the seabed). Figure 3.18 shows the predicted depositional footprint after one year of tailings settling from the sub-surface tailings plumes. This deposition corresponds to about 6.5Mt of solids tailings.

This figure is shown on a separate page for better readability. The top panel of Figure 3.18 presents the entire Huon Gulf, while the bottom panel shows a zoom in the area of study. A cut-off at 5mm was applied on Figure 3.18. One can observe that all predicted deposition from the sub-surface tailings plumes occurs at depths greater than 200m.

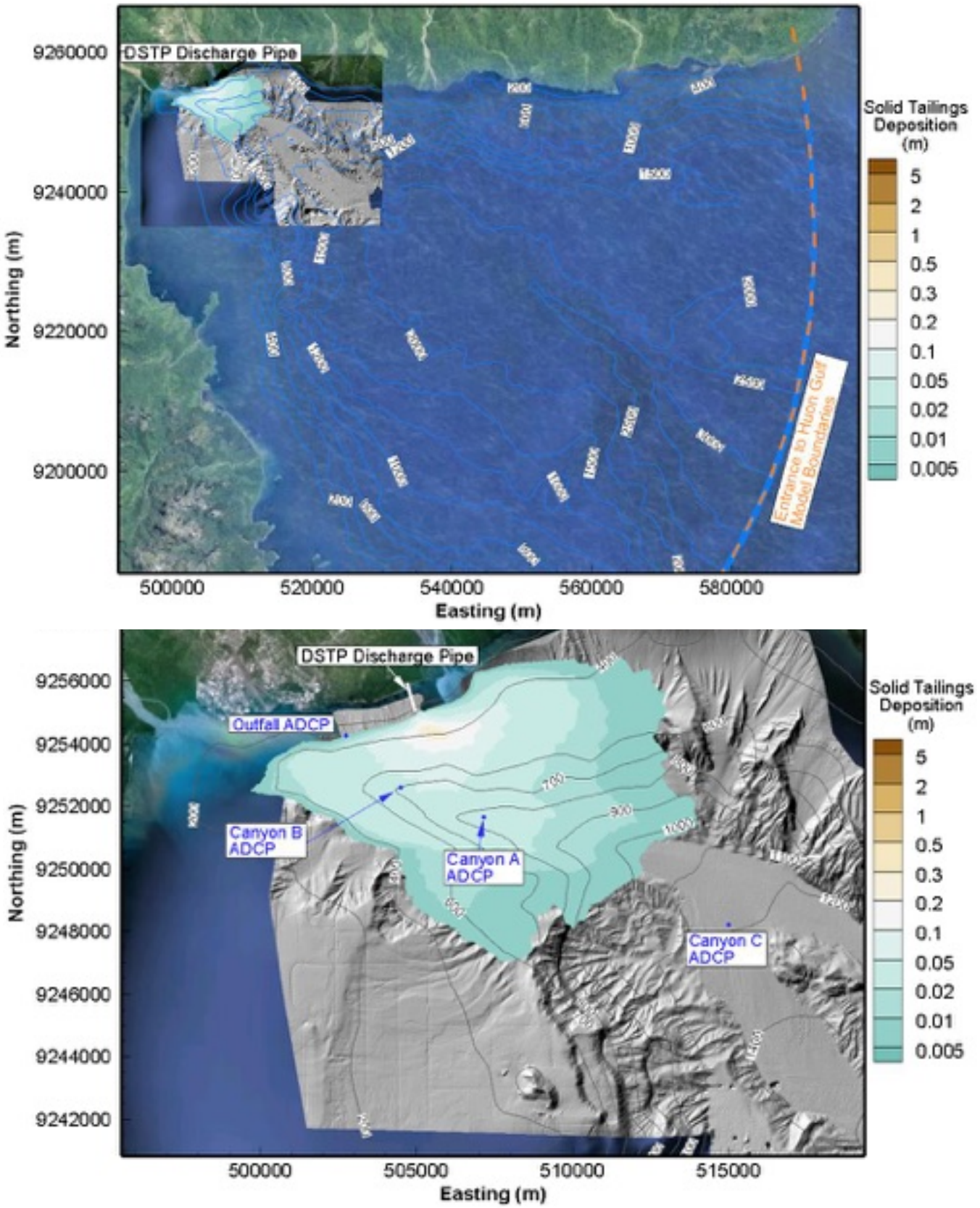

Figure 3.18 Predicted Depositional Footprint from Sub-Surface Tailings Plumes after 1 Year

3.4 Predicted Total Tailings Depositional Footprint Before an Episodic Mass Event

The predicted tailings depositional footprint corresponding to settling from the density current (estimated at about 10Mtpa) and settling from sub-surface tailings plumes (estimated at about 6.5Mtpa) were combined together to obtain a total tailings depositional footprint. Figure 3.19 shows the predicted total tailings depositional footprint corresponding to one-year of deposition, in the absence of any episodic mass movement events.

As one can observe, the bulk of the tailings deposition is predicted to occur along the density current pathway which runs down the steeply sloping (~20°) north wall of the Markham Canyon to the floor of the canyon and then turns left and continues in the down canyon direction to over 1,000m water depth. The model predicts only limited deposition on the canyon floor despite its shallow gradient (~3°), due to presence of a persistent near-bed current which reduces deposition in the centre of the canyon floor and push the tailings solids to the sides of the canyon.

This figure is shown on the next page for better readability. The top panel presents the predicted total tailings deposition footprint before an episodic mass event after one year in the Huon Gulf, and the bottom panel zooms in on the area of interest.

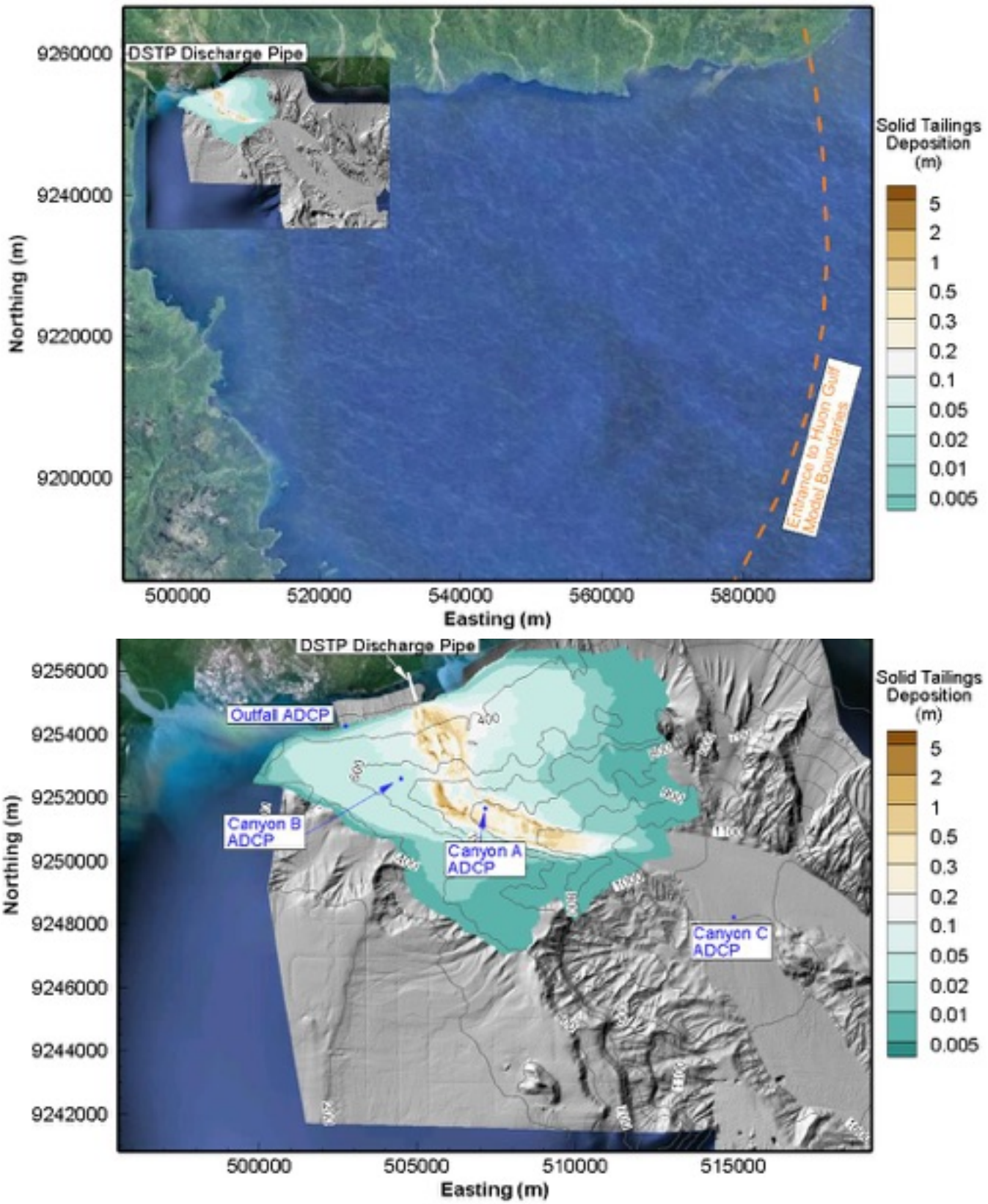

Figure 3.19 Predicted Total Tailings Depositional Footprint after 1 Year in the Absence of Episodic Mass Movement Events

3.5 Episodic Mass Movement Events

Over the course of one year of oceanographic measurements, subsea mass movement events have been identified in the Huon Gulf and described in the IHAconsult oceanographic report (IHAconsult, 2017). In particular, IHAconsult (2017) identified the following:

"*The speed of the front of the turbidity current for significant events has been estimated by extracting the time that high current speeds were first recorded at two locations and measuring the distance along the canyon thalweg, as is summarised in Table 5-1 below. The speed estimates are high, varying from 1.8 to 8.4 m/s (3.5 to 16.3 kn) and have the capacity to entrain and transport high concentrations of sediment.*"

The following table was extracted from the IHAconsult (2017) report:

Table 3.7: Estimated Speed of Turbidity Current Fronts

Date	Canyon Section	Time of Travel (min)	Distance (km)	Estimated Turbidity Current Speed (m/s)
8Jan17	Canyon A to Basin A	40	18.710	7.8
3Jun17	Canyon B to Basin B	87	43.903	8.4
1Aug17	Canyon C to Basin B	302	32.789	1.8
2Sep17	Canyon C to Basin B	188	32.592	2.9

The potential for episodic mass movement events to mobilize natural sediment and tailings deposits on the floor of the Markham Canyon appears highly likely. As a result, modelling of these episodic mass movement events was undertaken, with the total one-year footprint map (Figure 3.19) used as the basis for this analysis.

3.5.1 Inputs

The density current model was used to simulate the turbidity currents generated by mass movement events and the simulation was set up on the coarse resolution grid, i.e. 50m resolution. A hypothetical seabed failure located at approximately 400m depth on the southern side of the Markham Canyon was simulated. The location was selected near the amphitheater identified in the seabed slope stability analysis (Tetra Tech, 2017), which was interpreted as a very active area characterized by with numerous slumping events. Figure 3.20 shows this seabed failure location. Model assumptions were the following:

- Both fine and coarse natural sediments were released during this slumping event with a volumetric concentration of 20%;
- Composition of sediments was based on Box Core #4 (IHAconsult & GDA Consult, 2018), shown on Figure 3.20 with
    - 90% natural coarse (d_{50} = 144µm, d_{90} = 398µm)
    - 10% natural fine (d_{50} = 20µm, d_{90} = 32µm)
- The duration of this slumping event was assumed to be 10 minutes;
- The amount of fines released over this event was 408,000m^3, i.e. about 1.08Mt. In the modelling, this amount corresponds to a slump of three cells (150m length) by 2 cells (100m width) over a 27m depth range.

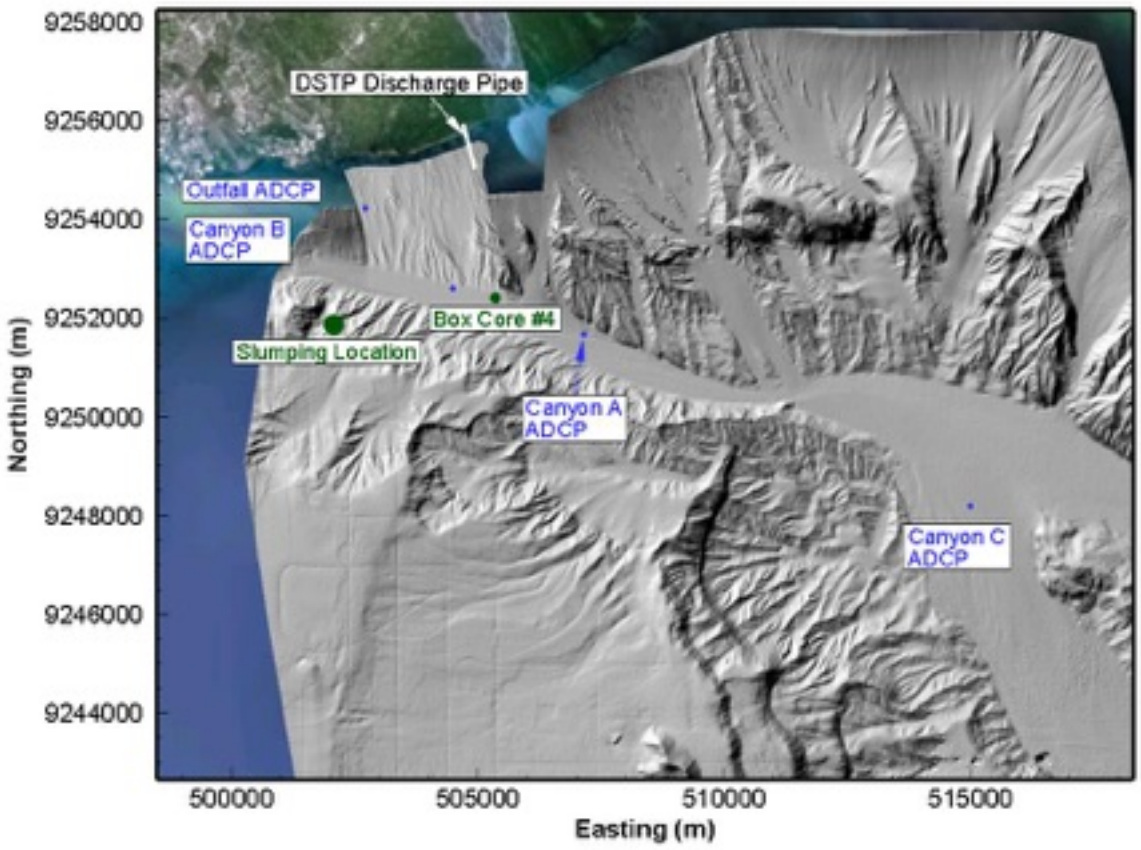

Figure 3.20 Slumping and Box Core #4 Locations

3.5.2 Comparison with Observed Episodic Events

Figures 3.21 to 3.23 present the results of this simulation, in terms of a longitudinal section through the turbidity current event created from this submarine landslide, and being advected to deeper depths in the Markham Canyon, reaching over 2,000m depth by the time the turbidity current dissipates. The front of the simulated turbidity current is very distinct and travels at high velocities. Note that the axis range for Figures 3.21 to 3.23 are different. All three figures present a profile of the turbidity current with colouring representing the simulated turbidity current event velocity.

- Currents of 6-7m/s were between the slumping location and 500m depth (Figure 3.21) 10min following the initiation of the slumping;
- About 2 hours following the slumping, velocities of about 2.5m/s were simulated at 1,000m depth (Figure 3.22);
- Down to 2,000m depth, velocities exceeding 1m/s were predicted (Figure 3.23).

The travel speed of the turbidity current event compares well with observed episodic events, with observed speeds of about 7-8m/s near Canyon A (700m depth) and 1.8 to 3m/s in deeper areas (1,000 to 2,000m depth).

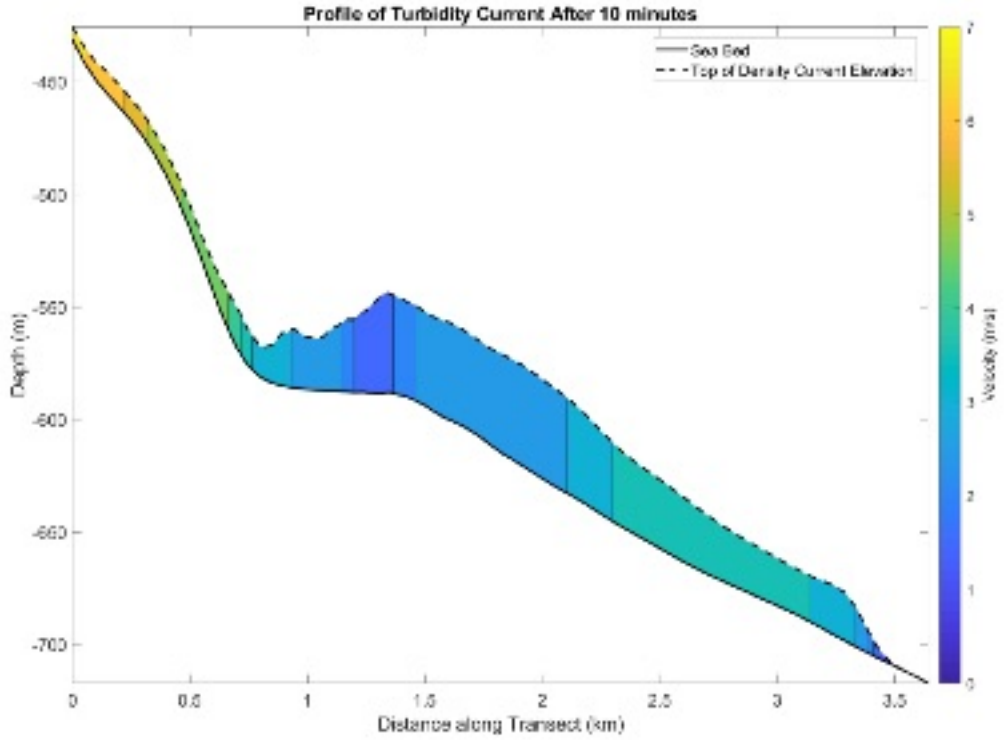

Figure 3.21 Profile of Turbidity Current Event after 10min

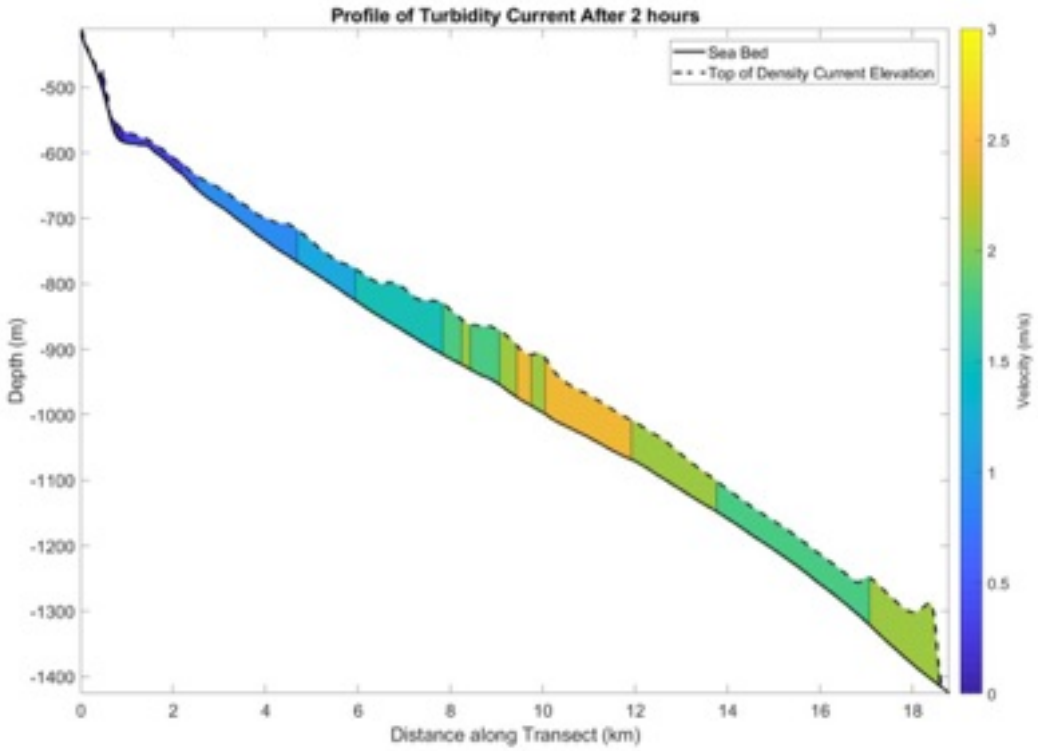

Figure 3.22 Profile of Turbidity Current Event after 2hours

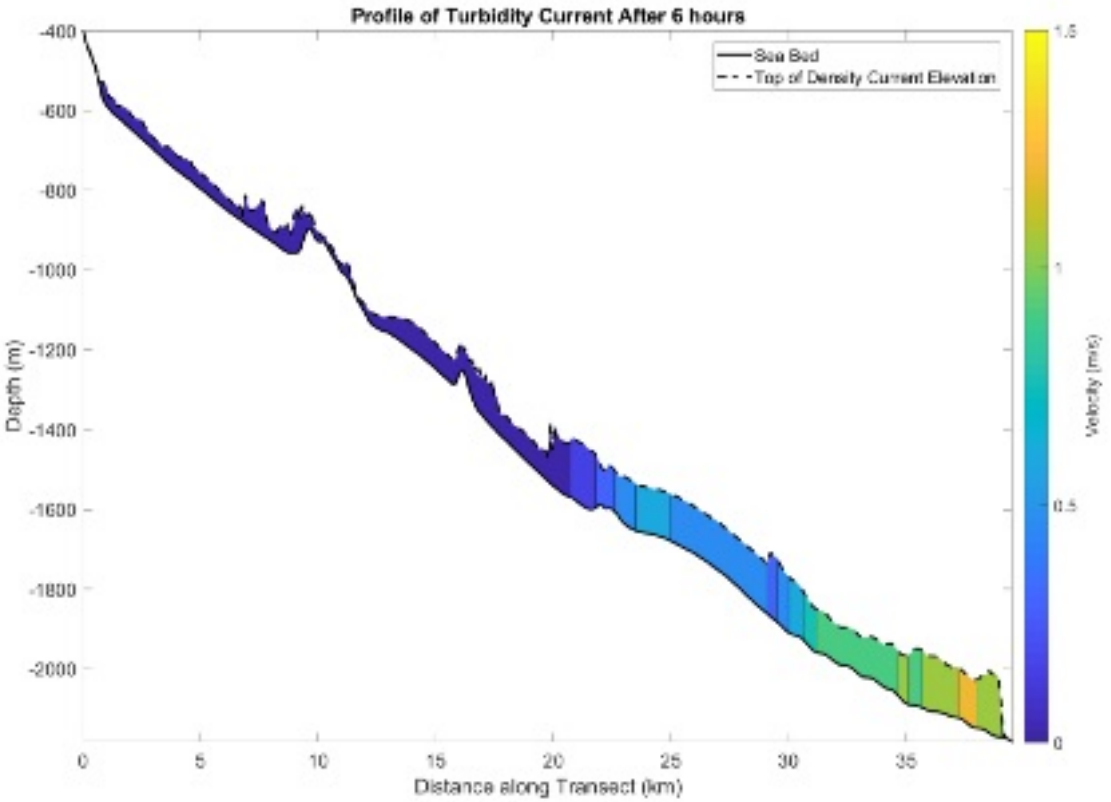

Figure 3.23 Profile of Turbidity Current Event after 6hours

3.5.3 Mass Balance

Table 3.8 presents the mass balance of the simulation. Three types of sediments were considered in this simulation: tailings (fine and coarse), natural sediments discharged from rivers (fine) and natural sediments from slumping event (fine and coarse).

Due to the large amount of sediment carried by the turbidity current in this slumping event and combined with the momentum, a large quantity of sediment/tailings is put in suspension during the passage of the turbidity current. However, after two days, due to the loss of momentum of the turbidity current, a large majority of these re-suspended natural sediments and tailings solids are predicted to have re-deposited on the seabed, but at a considerable distance further down the Canyon. A minority (less than 5%) exited the model domain through the generation of sub-surface plumes at deep depths.

Table 3.8: Mass Balance of Episodic Mass Movement Event Simulation

	Tailings	Natural Sediments from Rivers	Natural Sediments from Slumping
In episodic current	0.5%	3.8%	1.3%
On seabed	94.8%	96.1%	91.7%
Generated sub-surface plumes	4.7%	0.0%	7.0%
Exited model's boundaries	0.02%	0.1%	0.0%

3.5.4 Predicted Combined Tailings Solids and Natural Sediment Depositional Footprint after 27 Years

While the IHAconsult oceanographic report (IHAconsult, 2017) shows that episodic mass movement events are initiated at different times through the year, and with different volumes, the assumption was made that the same event, i.e. a slumping near the amphitheater at 400m depth (Figure 3.20) on the south bank of the Markham Canyon, would be reproduced on a yearly basis. This assumption is conservative since many mass movement events were recorded in the IHA oceanographic report (IHAconsult, 2017) over the period of a year, which were reduced to one event a year for the purpose of the modelling.

Following the first episodic mass event, after one-year of tailings and natural sediment deposition, the redistributed depositional footprints were, similar to the density current, scaled up to 27 years for both tailings and natural sediments, allowing areas of deposition with steep slopes to collapse once they exceed their angle of repose.

It was also assumed that the depleted near-bed sub-surface plumes generate by the passage of this episodic mass event (less than 5%) deposited from the water column onto the seabed. The flat slope of the Markham Canyon, about 2º to 3º, was not sufficient for sub-surface plumes to head far off the seabed.

Figure 3.24 shows the predicted tailings solids deposition after 27 years: the top panel presents the entire Huon Gulf while the bottom panel is a close-up of the study area. On the steeply sloping north wall of the Markham Canyon, at depths shallower than 500m, the predicted tailings deposition is thickest (exceeding 10m) since no episodic mass movement event swept that area. On the other hand, the model predicts that tailings solids deposited in the Markham Canyon, will be re-suspended during these episodic mass movement events and redeposited at greater depths, mostly deeper than 1,700m. The ultimate thickness of predicted tailings solids deposition is less than 0.5m in most deep areas deeper than 1,000m.

A couple of limitations to this approach should be noted. First, given the morphology of the northern slope of the Markham Canyon both east and west, small slumping events are expected to occur and would mobilise the accumulations of tailings and natural sediments and move them in deeper waters into the canyon. Since these small slumping events are not quantified, they were not incorporated into this present modelling. On this aspect, the results present a conservative approach for amount of tailings deposition on the banks of the canyon. Second, over the 27 years of mine activity, it is expected that these episodic events will occur from various locations and depths, which would result in re-suspending some of the material at depths of 1,500m and carry them even deeper. This limitation to the modelling framework results again in a conservative approach in terms of deposition in depth shallower than 2,000m.

Figure 3.25 similarly shows the predicted natural sediment deposition after 27 years. The largest patch of predicted deposition is near the Markham River. Note that the 10m of predicted natural sediment deposition in the vicinity of the Markham River mouth is very likely overestimated and reflects an approximate bathymetry that was used in this part of the domain. Finally, Figure 3.26 shows the same results in close-up around the discharge area. The top panel presents the predicted deposition from tailings while the bottom panel shows the predicted deposition from natural sedimentation.

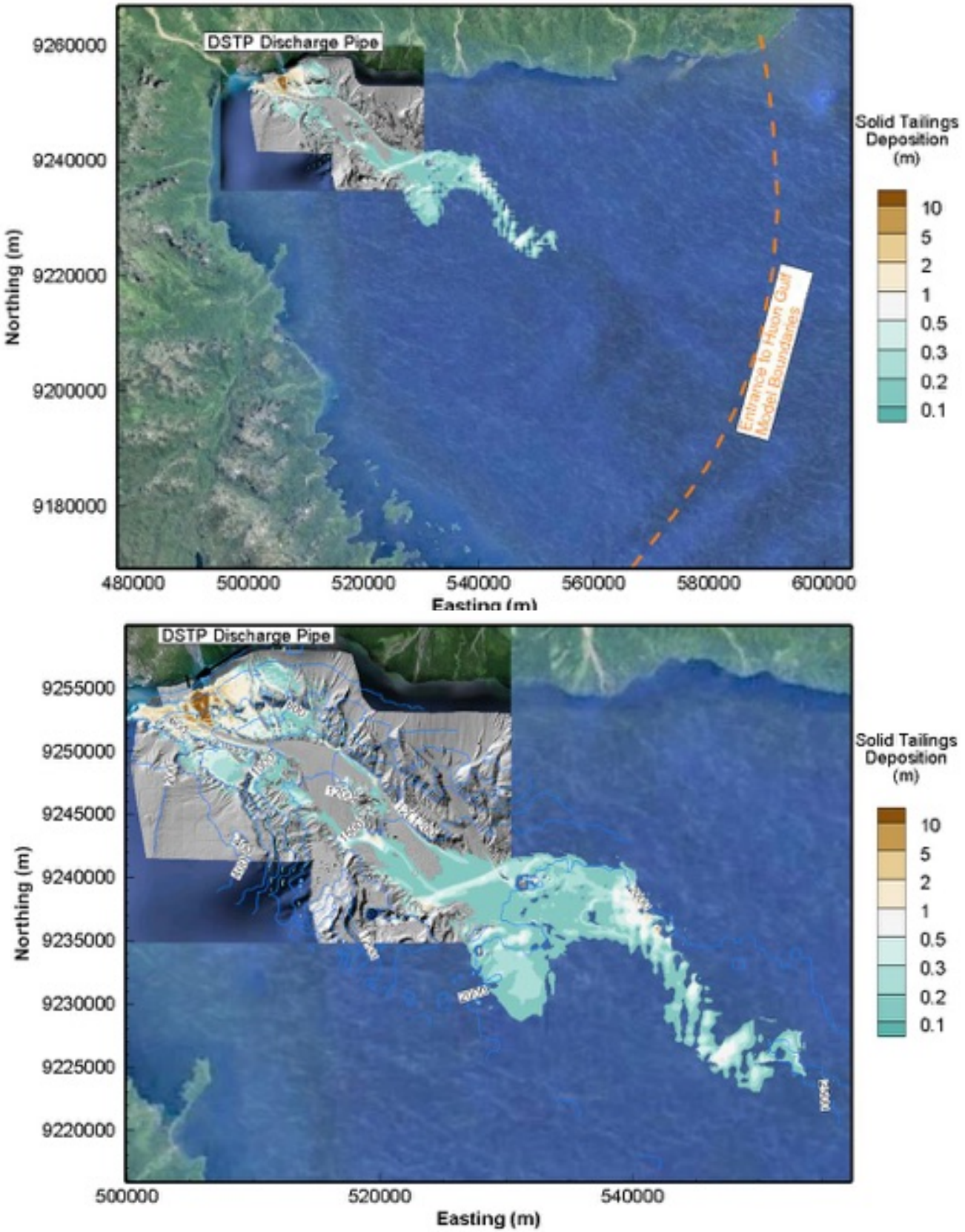

Figure 3.24 Predicted Total Tailings Depositional Footprint after 27 Years (with annual mass movement events; natural sediments not shown)

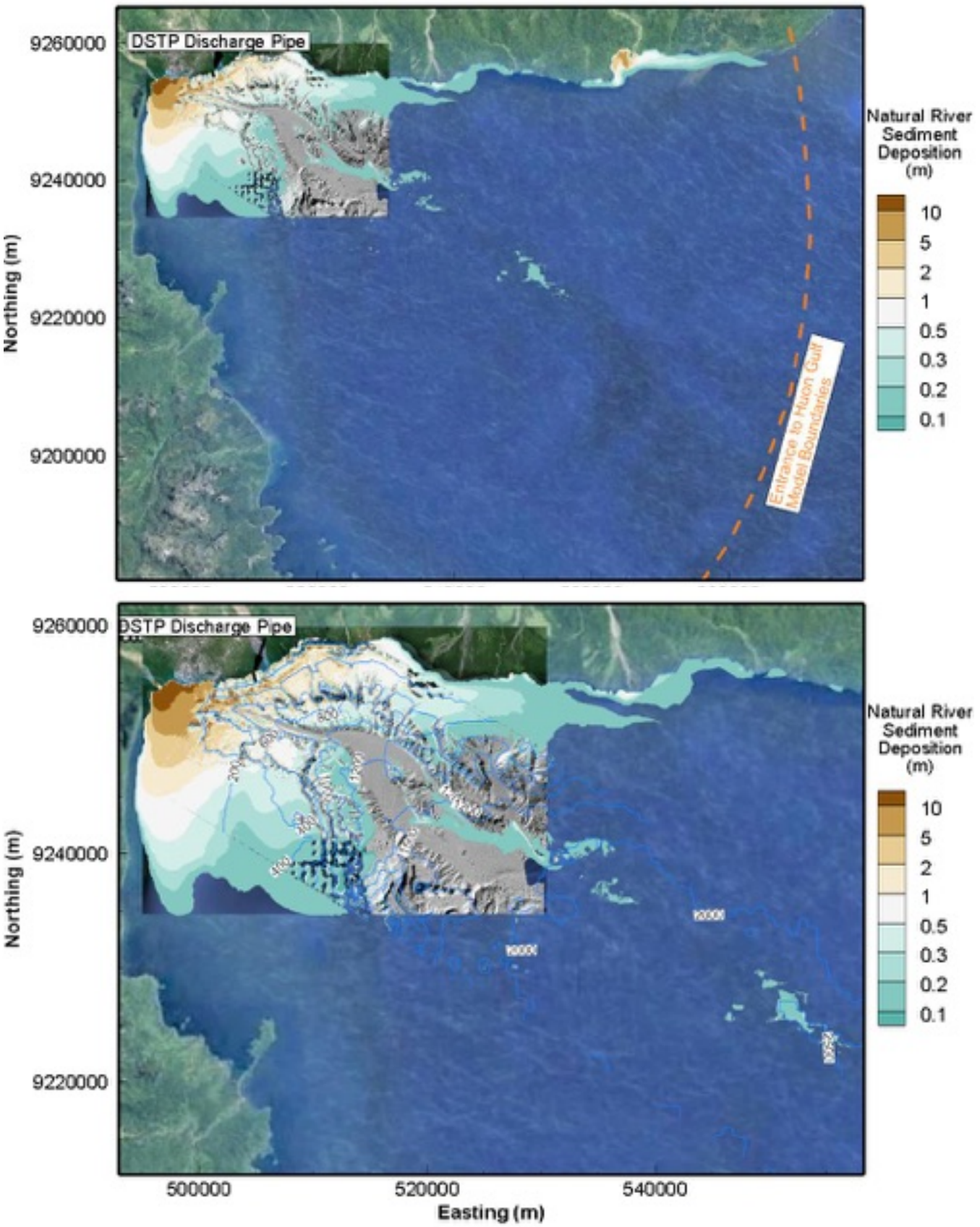

Figure 3.25 Predicted Natural Sediment Depositional Footprint after 27 Years (with annual mass movement events)

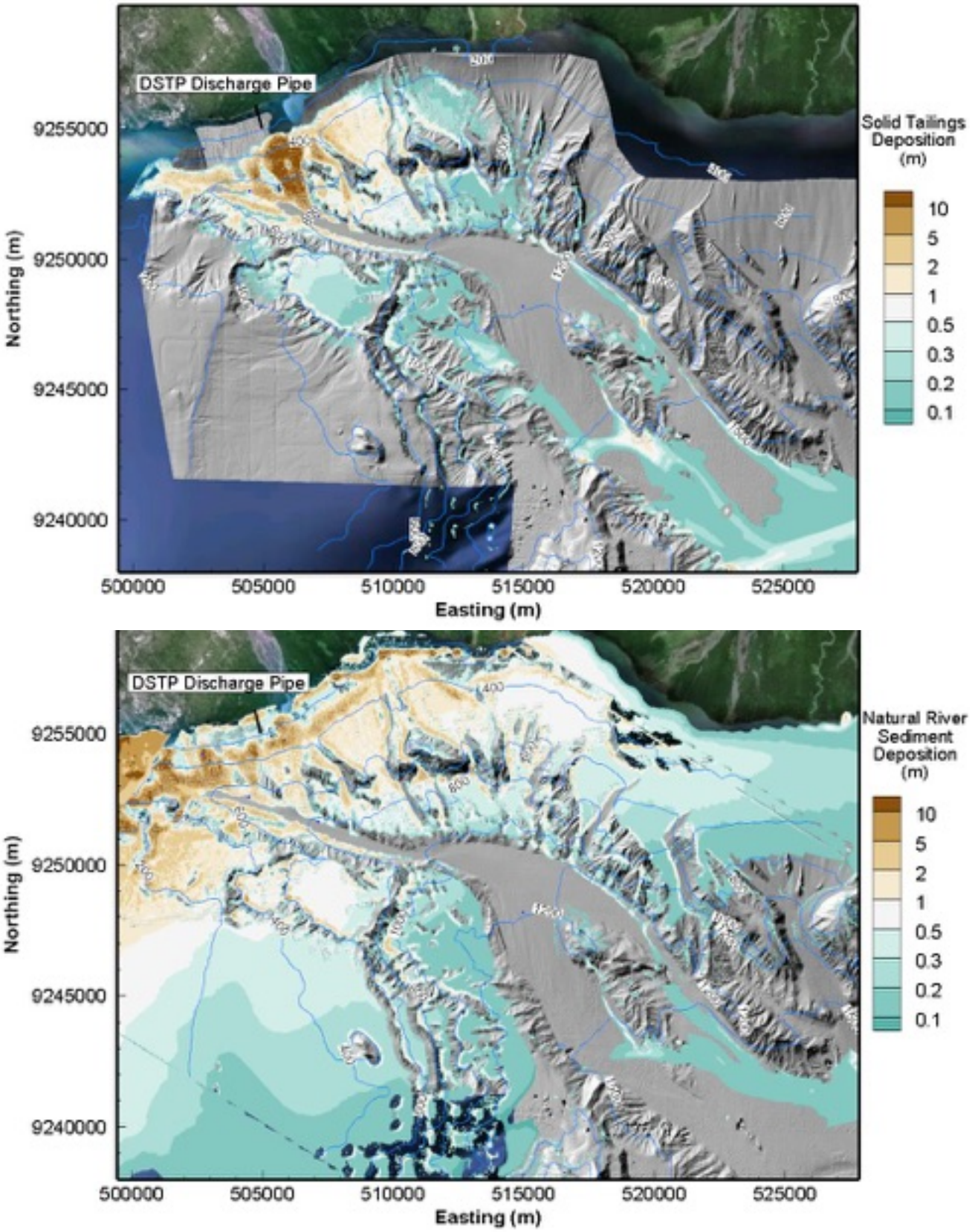

Figure 3.26 Predicted Total Tailings (top panel) and Natural Sediment (bottom panel) Depositional Footprint after 27 Years

4.0 COMPARISON BETWEEN PREDICTED TAILINGS AND NATURAL SEDIMENT DEPOSITION

4.0 Increment in TSS Concentrations Resulting from Tailings Sub-Surface Plumes

Figure 4.1 (from IHAconsult (2017)) summarizes the locations of the different ADCP moorings in the upper Huon Gulf (left panel) and CTD casts (right panel). For selected CTD locations, modelled natural sediment concentrations in the water column were extracted over a one-year period, allowing computation of 50th and 95th percentile concentrations through the water column. Figures 4.2, 4.4 and 4.6 show the increment in TSS concentrations resulting from suspended tailings in sub-surface plumes at locations of CTD B1/B4/B5, CTD A1/A2/A3 and ADCP Outfall/Canyon/Basin, respectively.

The blue line on Figure 4.2 shows the modelled concentration of natural sediment, while the orange dotted line shows the modelled total natural sediment plus suspended tailings concentration. For comparison purposes, Figure 4.3 presents IHA's CTD turbidity data at Location CTD B1, a location relatively close to the river plumes. While the two figures cannot be directly compared (turbidity in FTU is not exactly equivalent to TSS concentration in mg/L), one can still infer the areas where high turbidity indicates greater TSS concentrations. Most profiles on Figure 4.3 indicate low turbidity though the first 300m of the water column. However, a few profiles do show some strong, but episodic, sediment plumes captured at depth of 100m to 200m depth. These higher episodic turbidity events at 100m-200m depth have been reproduced by the 3D model: one can observe, as shown on the modelled concentration of natural concentration at location CTD B1 (left panel of Figure 4.2).

Similarly, Figure 4.4 shows the modelled concentrations and Figure 4.5 presents the observed turbidity at location CTD A1. Turbidity profiles indicate that this is a very low turbidity location, with the exception of some events in which turbidity spikes up by over two orders of magnitude. A reasonable agreement is observed between modelled and observed at location A1, in particular between 50m and 100m depth.

Figure 4.6 finally shows modelled concentrations at the outfall, canyon and basin ADCP locations.

Figure 4.1 IHA's ADCP (left panel) and CTD (right panel) Locations

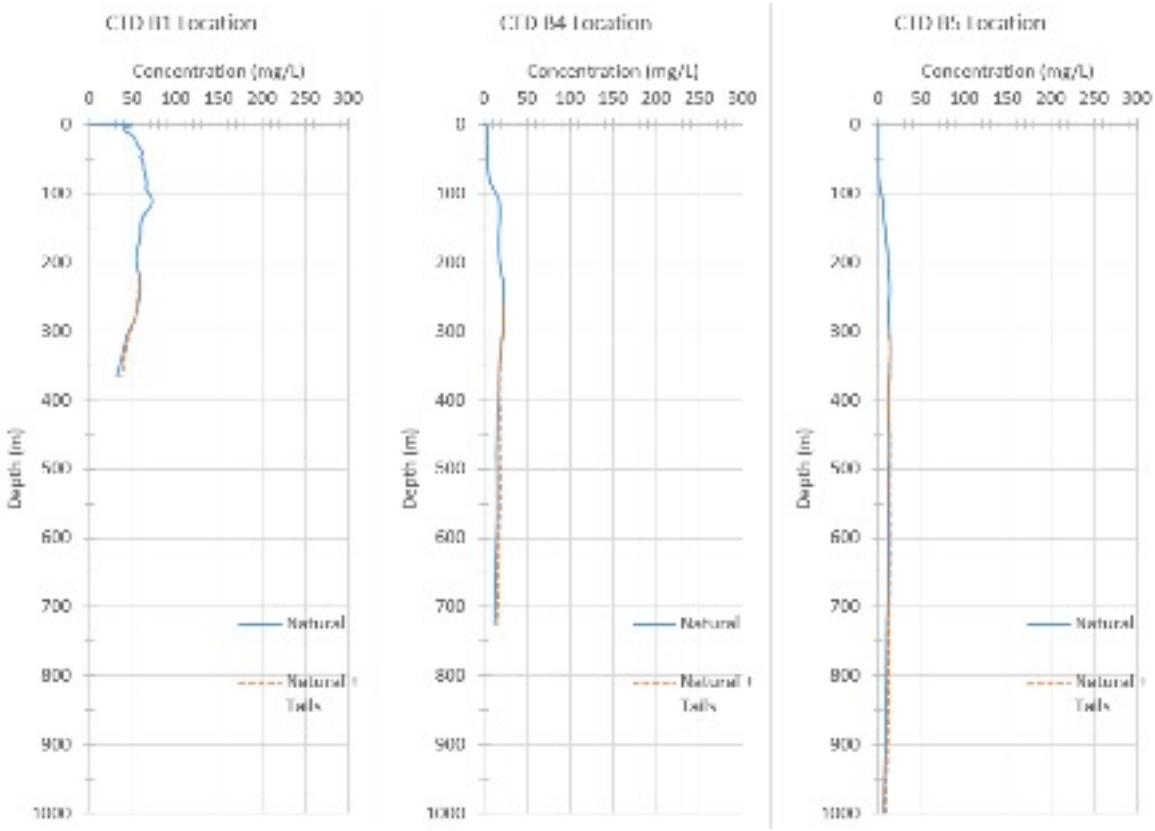

Figure 4.2 Modelled TSS Concentrations at CTD B1/B4 and B5 Locations

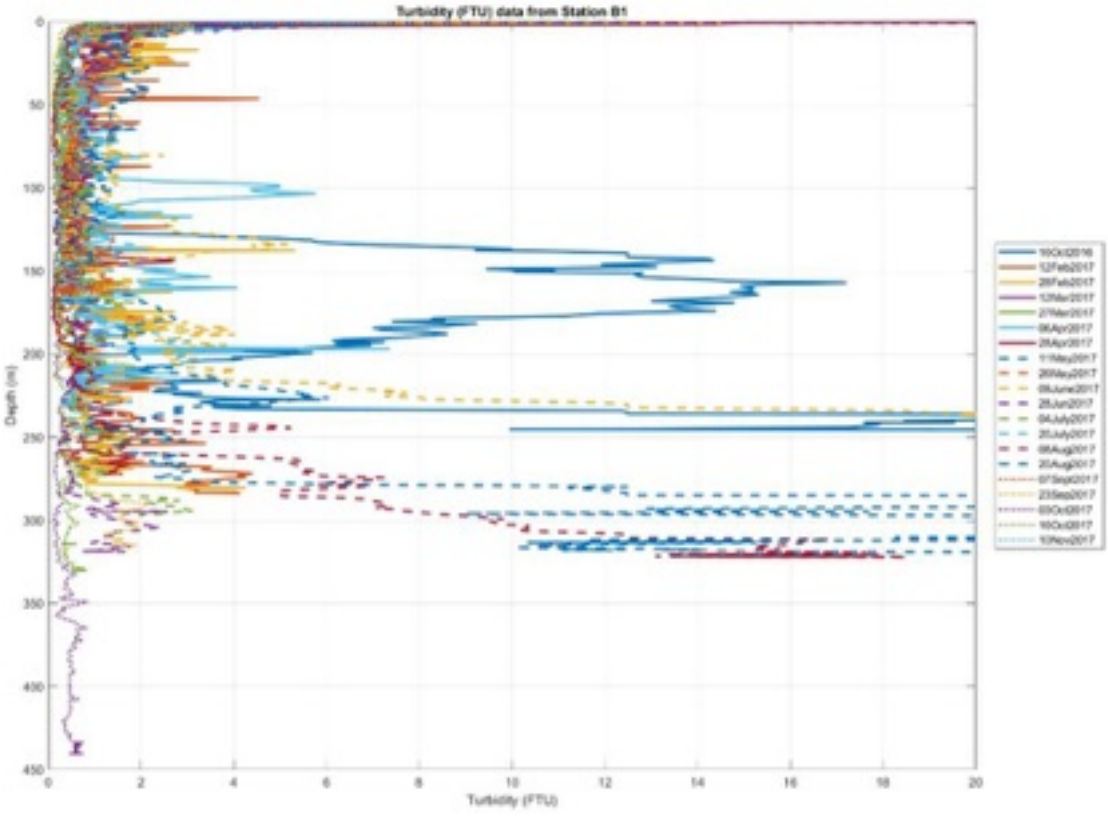

Figure 4.3 IHA's Measured Turbidity at CTD B1 Location

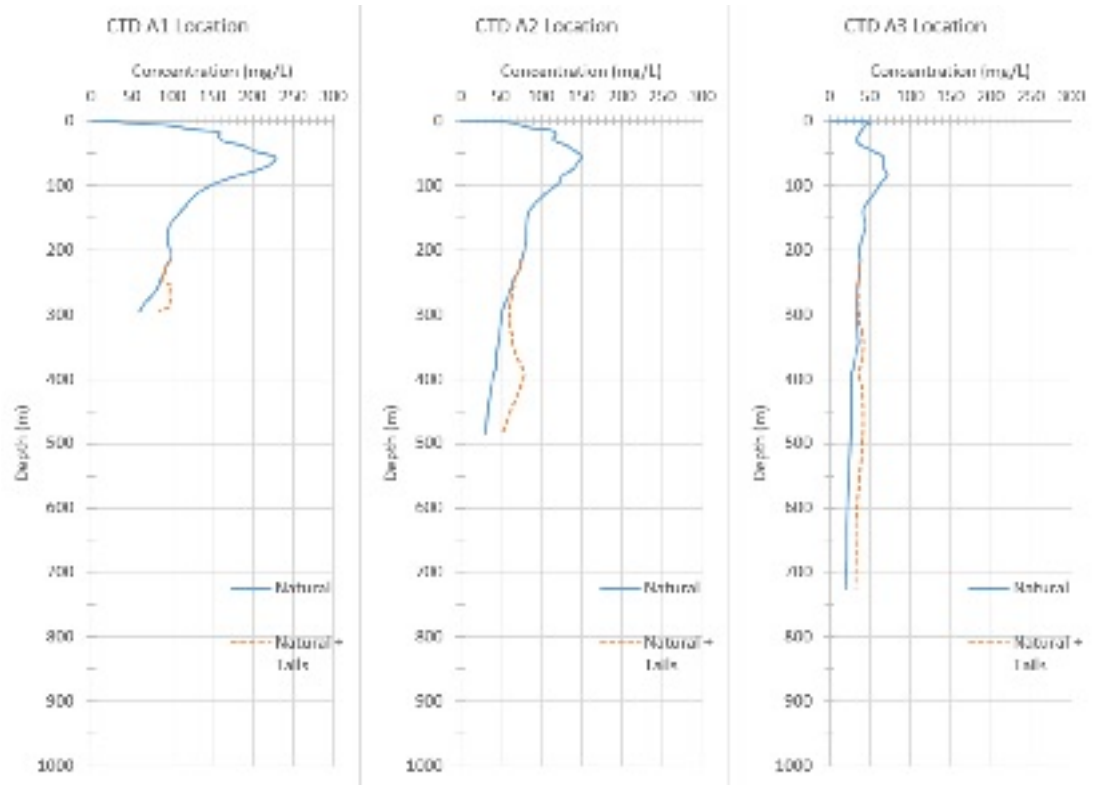

Figure 4.4: Modelled TSS Concentrations at CTD A1/A2 and A3 Locations

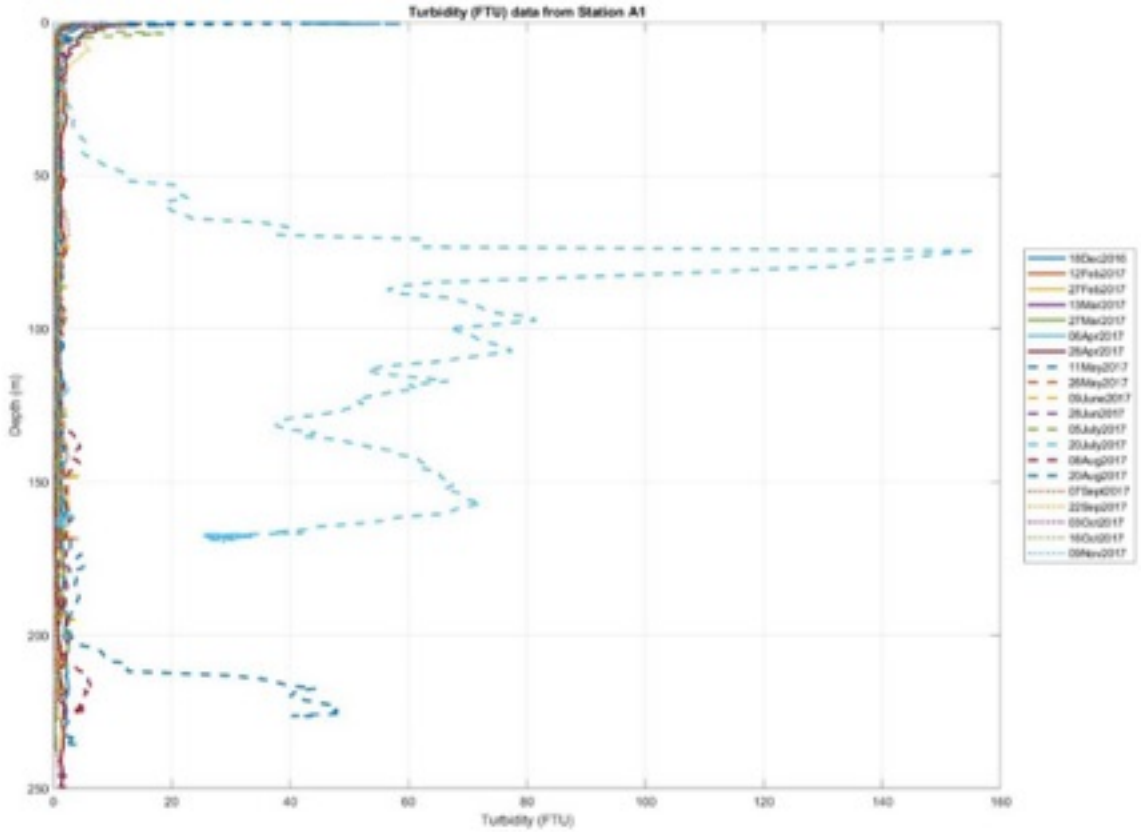

Figure 4.5 IHA's Measured Turbidity at CTD A1 Location

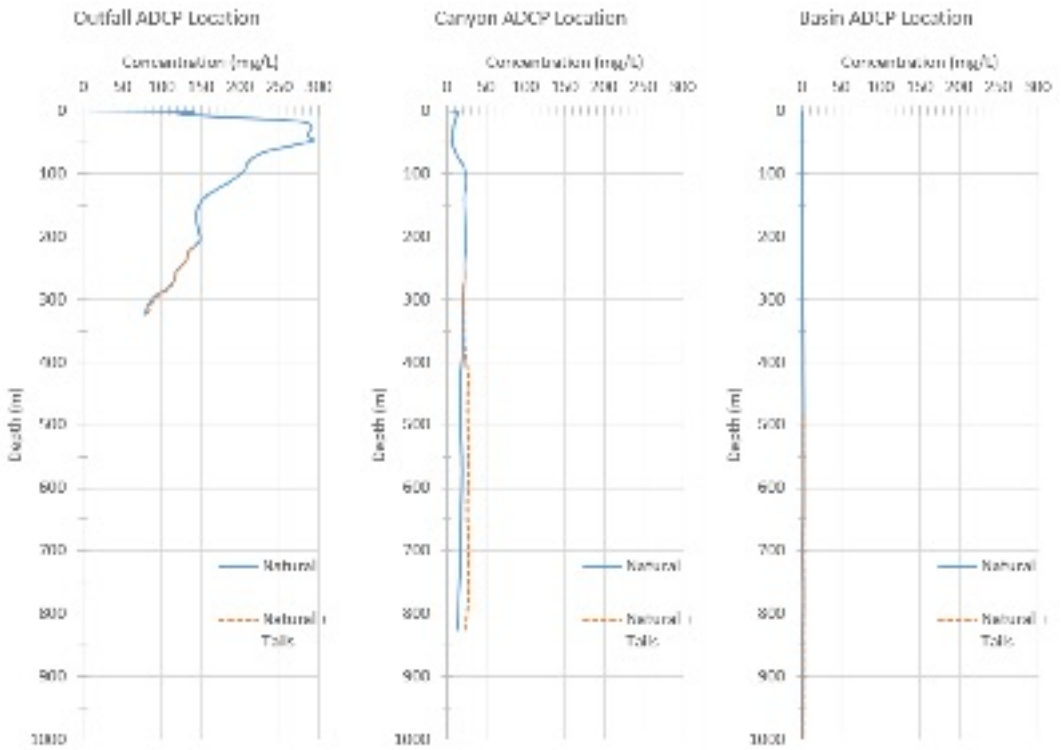

Figure 4.6 Modelled TSS Concentrations at ADCP Outfall/Canyon and Basin Locations

In Summary, both model and observations indicate that the waters of the Huon Gulf, in the area north of Markham Canyon, which is also the area over which the Markham, Busu and other river plumes propagate, are subject to significant but episodic sub-surface plumes, This behaviour of the natural sediments is quite logical, as it demonstrate the pathway by which the sediment in the sub-surface plumes sinks to the seabed. The simulations also show that the turbidity levels will not be significantly increased by the generation of sub-sea plumes by the proposed DSTP system.

4.1 Ratio of Tailings Deposition to Natural Deposition

To appreciate the incremental deposition that the proposed future discharge of tailings solids will bring to the Huon Gulf, the ratio of future tailings deposition to existing natural deposition was computed and displayed in Figure 4.7. The top panel of Figure 4.7 displays the ratio of tailings to total deposition from both natural sediment and tailings following 27 years of simulated tailings discharge (Figure 3.23), and the bottom panel zooms-in on the area of study. A brown colour indicates that more tailings than natural sediment have deposited, whereas a green colour indicates that more natural sediment deposited than tailings. A value of 10% means that the deposition in this area is made of 10% tailings and 90% natural sediment. A value greater than 50% means that there are more tailings deposited on this location than natural sediments, while a value less than 50% means more natural sediment. Note that this ratio is not shown for cells where the deposition from both natural sediment and tailings are each less than 10cm after 27 years.

As an example, towards the mouth of the Markham River, the colour is green and indicates that 100% of deposition consists of natural sediment. On the other hand, at a depth of 2,000m, the brown colours indicate that deposition is predominantly composed of tailings. That said, Figure 4.8 shows the predicted tailings deposition thickness after 27 years: in deep areas (i.e. below 2000m depth) the tailings deposition is predicted to be predominantly concentrated in a laterally constrained region approximately between the Far-Field and Trench mooring locations (Figure 2.27) with deposited layer thicknesses after 27 years less than 0.5m. The natural sediment is much more

widely dispersed throughout the Huon Gulf (i.e. refer to predicted average natural sedimentation rate per year in Figure 5.1, Section 5.0). By design, the tailings is released along an initial trajectory that is directed into the Markham Canyon where it travels downslope via the density current, and is subsequently swept down-canyon by the episodic mass movement events, generally following the thalweg of the Huon Gulf. Therefore, the ratio of tailings to natural sediment below about 2000m depth is high within the localized area shown in Figure 4.7. These tailings are expected to be ultimately covered by natural river sediment thereafter (Section 5.0) and to also continue to progress downslope as a result of subsequent mass movement events and downslope turbidity currents.

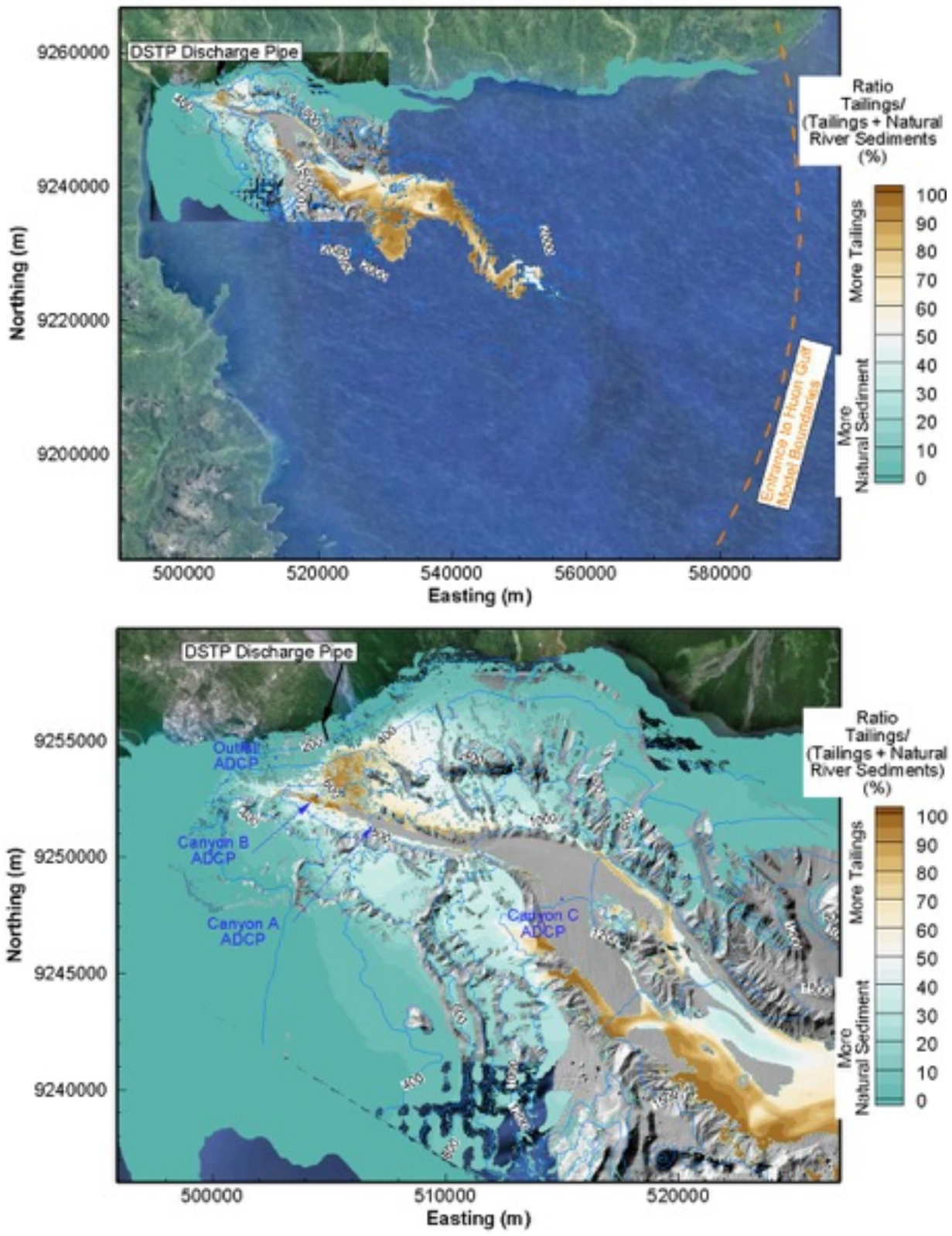

Figure 4.7 Ratio of Tailings/(Natural Sediments + Tailings) (top panel) and Zoom-in (bottom panel) after 27 years (Ratio not shown where tailings and natural sediment are each < 10cm deposition)

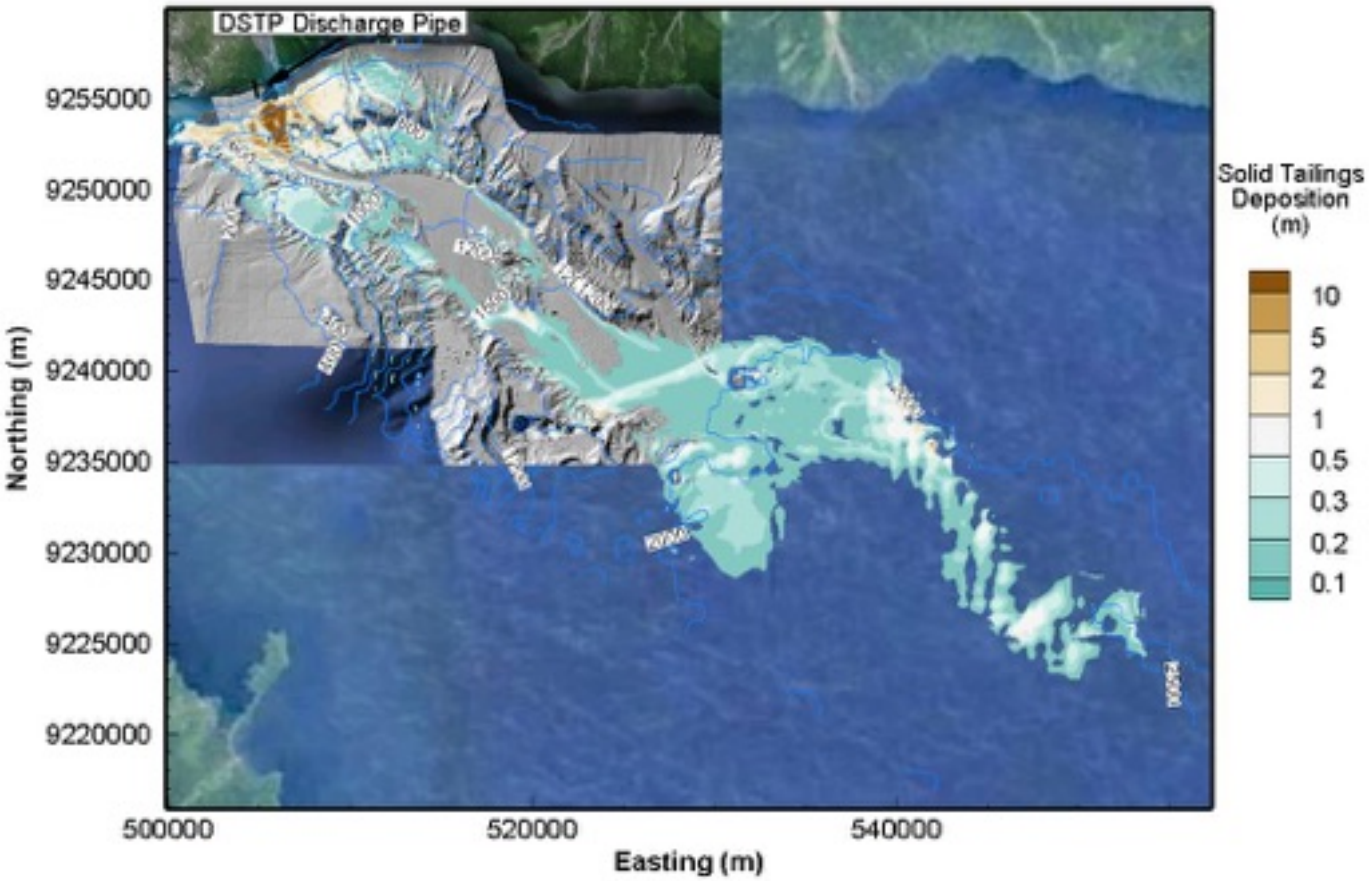

Figure 4.8 Predicted Tailings Depositional Thickness after 27 years

5.0 POST-CLOSURE SEDIMENTATION

Post-closure configuration of the deposited tailings was conservatively modelled based solely on river-derived sedimentation. Following the closure of the mine after 27 years of DSTP discharge, the post closure sedimentation was predicted based on the average natural sedimentation rate per year. In the area with the greatest thickness of tailings deposition, along the density current pathway from the outfall pipe to the floor of the Markham Canyon, predicted rates of post closure sedimentation of natural sediments shown in Figure 5.1 range from 0.01m/year to 0.10m/year, and will rapidly build up a layer of natural sediment to cover any exposed tailings, (or mix of tailings and natural sediment), and inhibit any residual release of metals from the deposited tailings solids.

As discussed in this report and in GDA&IHAC, another powerful process acting in the Huon Gulf is the occurrence of both episodic mass movement events and more persistent bottom turbidity currents. Note that the figures in this section are based only on average natural sedimentation from rivers. No additional episodic mass events following the closure of the mine have been considered. It has been demonstrated that these mass movement events can readily transport deposited tailings outside of the Huon Gulf, toward the New Britain Trench. Given the rates of natural sedimentation throughout the model domain within the Huon Gulf, it is predicted, that even in the absence of episodic mass movement events of natural sediment in subsequent years following mine closure, the tailings remaining within the Huon Gulf would be quickly buried by natural sediment.

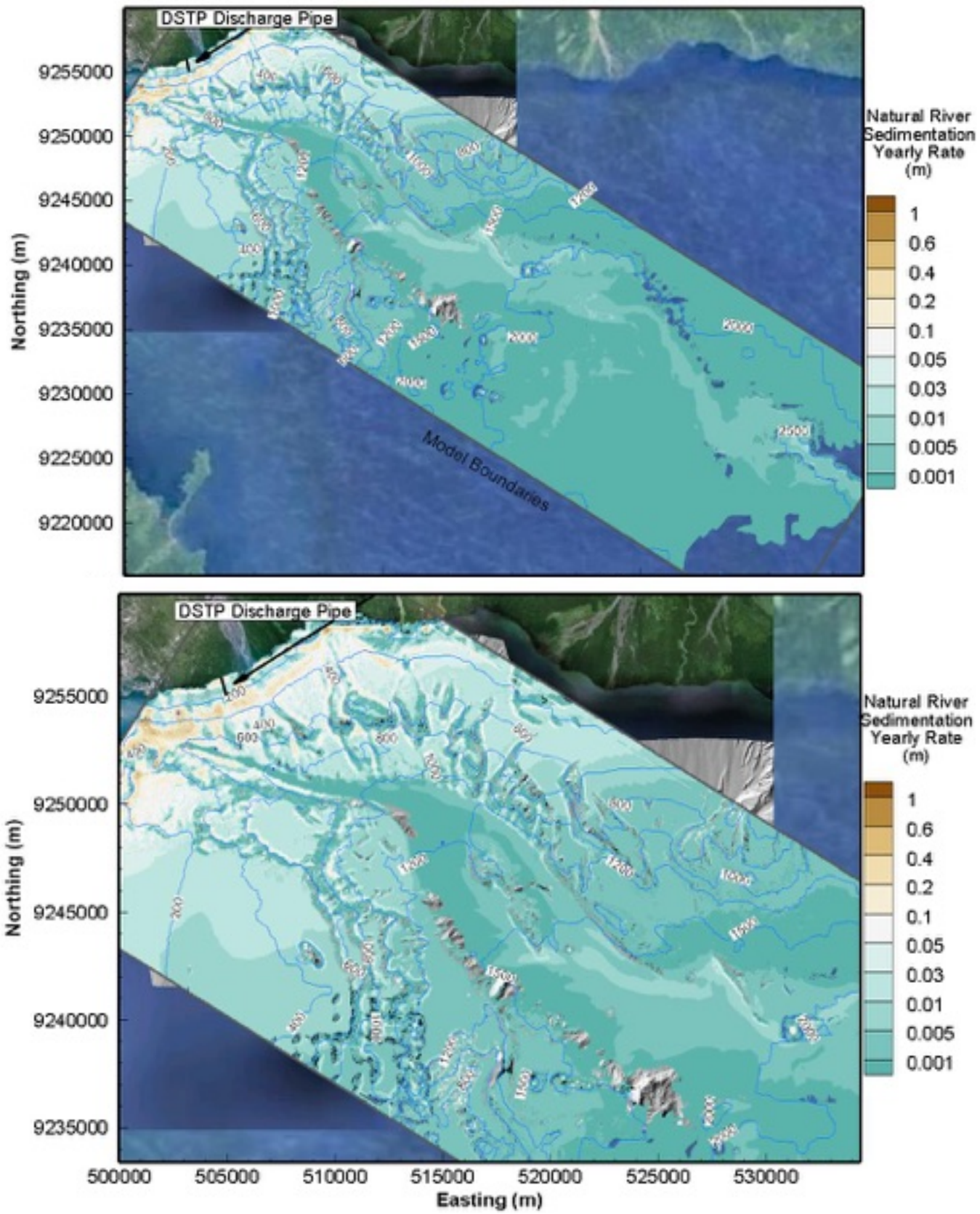

Figure 5.1 Predicted Average Natural Sedimentation Rate per Year

6.0 CONCLUSIONS

This report describes the work completed and results obtained from both the density current and 3D hydrodynamic modelling for the Wafi-Golpu project DSTP system.

To simulate the transport, deposition and scouring processes that govern the extent of the tailings in the marine environment, two models were used: a density current model, and a 3-D hydrodynamic model called H3D. The density current model simulates the behaviour of the density current and the transport, deposition, and scour of the tailings. The H3D model simulates the transport, deposition, and scouring of subsurface plumes that are generated by the depleted tailings as they separate from the density current en route to the bottom of the Markham Canyon, hence completing the tailing behaviour modelling. H3D also incorporates thermal, salinity, and mass fluxes from the eleven rivers along the north shore of the Huon Gulf, including the Markham and Busu Rivers, as these variables have been shown to have significant impact on the hydrodynamics within the Huon Gulf.

Inputs to the numerical models include:

- High resolution bathymetry as a compilation between Multi-beam AUV surveys and GEBCO data.
- HYCOM water temperature and salinity data validated with CTD profiles.
- Busu and Markham river flows and sediment concentrations as well as 10 other rivers on the north shore of the Huon Gulf.
- WAVEWATCHIII wind data.
- Solar radiation (theoretically derived) validated with Wagang Station observations.
- GFS air temperature and relative humidity validated with Wagang Station observations.
- Physical tailings and DSTP system characterization.

The three-dimensional model shows good agreement with observed data, thus giving confidence in the model's ability to respond to the wide range of environmental forcing in the Huon Gulf, and confidence in the ability to realistically simulate the transport, deposition and scouring processes governing the tailings distribution. Taking into account the limitations of numerical modelling, i.e. extrapolation of one year of deposition into 27 years, a conservative approach was undertaken with respect to modelling tailings transport, deposition, and scouring. That is, several large mass movement events have been observed to occur in one year, but the modelling only assumed one per year. This one event was able to sweep almost all the yearly tailings deposition in the Markham Canyon to the deeper basin, indicating that there will be minimal build-up within the Canyon. Based on the current modelling work, as well as oceanographic data collected during 2016 – 2017, and past literature review (i.e. Buleka et al., 1999) that describe the persistent nature of the down-canyon turbidity current within the Huon Gulf, it is expected that the majority of the tailings that is initially deposited within the Markham Canyon will be conveyed to greater depths thereafter by way of these natural episodic events and down-canyon turbidity currents. However, there will be significant build-up on the slopes leading away from the outfall pipe, at depths of 300 to 500m. Two processes serve to mitigate this tailings deposition. First, this side-slope area is also an area of significant natural deposition, so that the tailings footprint will be covered over with natural sediments in a relatively short time after mine cessation, thereby inhibiting release of metals from the deposited tailings. Second, morphological analysis of the sloping sea bottom from the outfall terminus to the Markham Canyon (Tetra Tech Updated Slope Stability Assessment, 2018) indicates that there are a number of down-slope channels, both active and abandoned, that serve to enable the down-slope migration of natural sediments. These channels would similarly serve to allow deposited tailings to move downslope to the Markham Canyon, on an episodic basis. It is shown in this report that any material that arrives at the Markham Canyon is ultimately transported down-canyon towards the New Britain Trench.

7.0 CLOSURE

We trust this report meets your present requirements. If you have any questions or comments, please contact the undersigned.

Respectfully submitted,
Tetra Tech Canada Inc.

Prepared by:

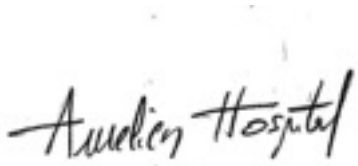

Aurelien Hospital, M.Eng., M.Sc.
Hydrotechnical Specialist
Direct Line: 778.945.5747
Aurelien.Hospital@tetratech.com

Chris Young, M.Sc., EIT
Junior Hydrotechnical Engineer
Direct Line: 778.945.5788
Chris.Young@tetratech.com

Reviewed by:

Jim Stronach, Ph.D., P.Eng.
Senior Oceanographer
Direct Line: 778.945.5849
Jim.Stronach@tetratech.com

/ah

REFERENCES

Ahmad, Q. A. 1979. Solar Radiation at Lae. Papua New Guinea, Papua New Guinea University of Technology, Dept. of Mechanical Engineering.

Arakawa A, Lamb VR. 1977. Computational design of the basic dynamical processes of the UCLA general circulation model. Methods in computational physics. 1977 Jan 1; 17:173-265.

Backhaus JO, and E. Maier-Reimer. 1983. On Seasonal Circulation Patterns in the North Sea. North Sea Dynamics. 1983.Betasolo, M. L., Gore, S., & Bii, A. (2014, August). Design of Sustainable Use and Management of Groundwater in Morobe Province. In Proceedings of the 3rd International Workshop on Design in Civil and Environmental Engineering (p. 27).

Backhaus JO. 1983. A semi-implicit scheme for the shallow water equations for application to shelf sea modelling. Continental Shelf Research. 1983 Sep 1; 2(4):243-54.

Ellison TH, Turner JS. 1959. Turbulent entrainment in stratified flows. Journal of Fluid Mechanics. 1959 Oct; 6(3):423-48.

IHAconsult & GDA Consult (2018). Physical, Chemical and Biological Sedimentology of the Huon Gulf. WAFI Document No. 532-1104-FS-REP-0003.

IHAconsult (2018). Oceanographic Investigations of the Huon Gulf. Wafi-Golpu Project Document No. 532-1104-FS-REP-0001_RevC.

Slurry Systems (2017a). Rheology and Laboratory Tests on Wafi-Golpu Tails. (April 21, 2017). Wafi-Golpu Project Document No. 532-3800-PP-REP-30006_1.

Slurry Systems (2017b). Hydraulic Feasibility Design, Terrestrial Tailings Pipeline. (April 21, 2017). Wafi-Golpu Project Document No. 532-3800-PP-REP-30007_1.

Tetra Tech Canada (2016). Preliminary Slope Stability Assessment for Deep Sea Tailings Placement (DSTP) Pipes. (November 16, 2016). Wafi-Golpu Project Document No. 532-1214-PF-REP-0002 REV0.

Tetra Tech Canada (2018). Wafi-Golpu DSTP Pipeline – Updated Slope Stability Assessment. (February 8, 2018). Wafi-Golpu Project Document No. 532-1214-FS-REP-0012.

Van Rijn LC. 1993. Principles of sediment transport in rivers, estuaries and coastal seas. Amsterdam: Aqua publications; 1993.

Wallcraft, A. J., Metzger, E. J., & Carroll, S. N. (2009). Software design description for the hybrid coordinate ocean model (HYCOM), Version 2.2 (No. NRL/MR/7320--09-9166). Naval Research Lab Stennis Space Center MS Oceanography Div.

APPENDIX A

DENSITY CURRENT MODEL

The tailings behaviour numerical model also called density current model is a two-dimensional reduced-gravity model of the density current created by the tailings discharge. That is, it considers the two-layer flow consisting of the density current flowing under the receiving water as if it were a one-layer flow, the density current itself, but with the acceleration of gravity in the equations of motion modified according to:

$$g_{reduced} = g \,.\frac{(D-h)}{D} \,.\frac{(\rho - \rho_{ambient})}{\rho_{ambient}}$$

Where:

- *D* is the total water depth;
- *h* is the thickness of the density current;
- $\rho_{ambient}$ is the ambient seawater density; and
- ρ is the density of the density current, including both the effects of entrained ambient seawater and the solids load.

Commonly, the layer thickness is much less than the overall depth, and the above equation reduces to:

$$g_{reduced} = g \,.\, \frac{(\rho - \rho_{ambient})}{\rho_{ambient}}$$

The model is a time-stepping model, and uses a spatial grid of uniformly spaced cells. Typically, the near-field density current model considers five cells to represent the pipe diameter, which results in a grid size of 20cm for assessment the behaviour of the discharged slurry in the near-field. The simulation starts with a bare seabed, and with all cells devoid of the denser tailing bearing fluid. As tailings are discharged, more and more computational cells are turned on as the density current distribution builds in a down-slope direction with time. Ultimately, a quasi-steady state is reached, with the solids settling out within the model domain, or being carried off in subsurface plumes.

In order to simulate the frontal advance of the density current, an algorithm similar to the algorithm for flooding and drying banks of tidal models in shallow water is used. At each timestep (i.e the simulated period is broken down in smaller intervals with limited changes from one time interval to the next – these intervals are called timesteps), each active cell is first examined to see if it should be de-activated because the density current has retreated from that particular cell.

Next, de-activated cells are examined to see if they should be re activated, because the thickness of the density current in an adjacent cell is sufficient to flood into that cell. The simulation then proceeds to evaluate the fluxes of mass into each cell, velocity components, and concentrations of dissolved scalars and sediment. The net result is that the density current readily flows in the downstream direction, but spreads laterally much more slowly, the expected behaviour for a density current discharging down a slope, and similar to the configuration of a turbulent wall jet.

Strongest speeds are usually located along the outfall pipe main axis; flows spread laterally with decreasing velocities. Since seawater is entrained into the density current, its thickness grows as it progresses downstream. The further from the outfall, the thicker the density current becomes. In terms of dilution, the lowest dilution is found along the main axis leading from the pipe, and increases laterally and with distance from the pipe. Dilutions of 10:1 are usually achieved within 20m to 30m from the outfall terminus. Also, the sediment concentration pattern is similar to the dilution pattern with high concentrations at the terminus of the outfall pipe. The similarity reflects the fact that very little sediment deposits in the near field

The model hydrodynamics include:

- advective terms;
- Coriolis term;
- bottom friction;
- interfacial friction, expressed as a fixed fraction of bottom friction;
- entrainment of ambient fluid based on a fit to the Ellison and Turner (1959) observations:

  $$E = E_0 . e^{-k.R_i}$$

  where E_0 and k are adjustable constants and R_i is the local Richardson number;
- depletion, which removes material from the top of the density current when it is unstable, based on a Richardson Number criteria;
- horizontal eddy viscosity, and
- drag by ambient currents.

The model resolves the sediment field into a number of components, each with a specific grain size and hence settling velocity w_m. Deposition is determined by a balance of upward and downward fluxes of sediment at the interface between the density current and the sea bed, using methodology similar to that described in Wu et al. (2000), with modification of some of the equations and parameterizations based on the results presented in Van Rijn (1993). Essentially, the downward flux of sediment is taken to be w_mC, the product of the settling velocity w_m and the sediment concentration C at a reference level, a, just above the sea bed. The reference level is usually taken to the local roughness length. The upward flux is taken to be w_mCa, the product of the settling velocity w_m and the equilibrium concentration at the reference level, Ca. Ca has been determined in a number of laboratory and field studies, and is given as a function of grain size, viscosity, sediment specific gravity, and the excess of bed stress over that required for mobilization, the latter based on the Shield's curve. If the system is at equilibrium, the two rates are equal, and neither scour nor deposition occurs. If the sediment concentration is lower than the reference level, and sediment is available, scouring occurs. Similarly, if the sediment concentration is higher than the reference level, deposition occurs.

Two important processes in the density current model are depletion and entrainment, represented in terms of corresponding velocities normal to the density current. Close to the outfall terminus, the high velocities lead to a high entrainment of the overlying water into the density current. This process leads to an increase in thickness of the density current in the downstream direction as well as to dilution of the density current by seawater. As the density current moves away from the outfall terminus, velocities become lower and differences in density between the density current and the overlying water column become smaller, leading to lower entrainment and higher depletion velocities. When the depletion velocities become greater than the entrainment velocities, a flux from the density current towards the overlying water column occurs, generating sub-surface plumes. Sub-surface plume generation usually does not occur in the near-field density model, because the density of the density current usually remains well above seawater density, stabilizing the density current/seawater interface over this small domain (100m x 100m in this case). The competing processes of entrainment and depletion were validated against data reported by Hurzeler et al. (1996).

As the density current exits the pipe, the central core maintains a high velocity, but the flow along the two outer boundaries, to either side of the main core, is slower, and generally, small levees form along these lateral boundaries. However, their height is limited, because once they are tall enough to exceed a critical slope, they collapse into the main core of the flow, where the high turbulence and velocities usually carry the collapsed sediment away from the pipe. The levee cycle is simulated in the model by allowing the levees to grow based on the sediment dynamics described above, until the slope exceeds the angle of repose. The levees then collapse before starting growing again. The angle of repose depends on the angle of repose in stationary water, as well as on the velocity of the flow moving past the levees, and is considerably less than the angle of repose in stationary water. This specific parameter is a key item in the near-field density current modelling to ensure that the levees do not plug up the system.

The model has been validated against laboratory data (Stronach et al., 1999, Stronach et al., 2000). As well, aspects of the model such as the depositional footprint and the production of subsurface plumes have been shown to compare well with field observations at the Lihir Gold Mine, Papua New Guinea (Hay & Company, 2009).

H3D Model

H3D is a three-dimensional time stepping numerical model that computes the three components of velocity (u, v and w) for ocean water on a regular grid in three dimensions (x, y and z). The spatial grid may be visualized as a number of interconnected computational cells collectively representing the water body. Figure 3.1 shows a schematic of a typical grid. The model also computes scalar fields such as temperature, salinity and various introduced contaminants. A time stepping numerical model is one in which the period of interest (e.g., a year-long simulation of currents in the Bay of Fundy) is broken up into a number of small time intervals (e.g., 30 seconds each). The model takes advantage of the fact that over a short time interval, or time step, changes in currents, salinities and other properties are small and can be computed in a simple fashion, suitable for coding in a numerical model. The time step length is variable, depending on the maximum velocity present in the model at that particular time step. During each time step, values of velocity, temperature, and salinity are calculated and updated in each model cell. Typically, for spill simulations, data are archived (i.e., saved to disk) every 15 minutes over the course of the simulation, so that the amount of data generated for subsequent spill tracking remains manageable.

The selection of grid size is based on consideration of the scale of the phenomena of interest, the grid domain, and available computational resources. In the vertical, the cells are usually configured such that they are relatively thin near the surface and increase in thickness with depth. The increased vertical resolution near the surface is needed because much of the variability (e.g., stratification, wind mixing, inputs from streams and land drainage) is concentrated near the surface. Water velocities are determined in three dimensions on the faces of each cell. Non-vector variables, such as temperature or salinity, represent an average condition within the cell.

The H3D model is a semi-implicit model, using the numerical scheme described in Backhaus (1983), and using a staggered Arakawa C-grid (Arakawa and Lamb 1977). It uses only two time levels, and computes internal and external modes at the same time. To allow for better simulation of features such as river plumes in conjunction with large tidal excursions, the number of layers represented in the model is allowed to increase and decrease as water level rises and falls. New layers are successively turned on as the water level rises, and are allowed to drain (becoming inactive) as the water level falls. This feature allows river plumes that have vertical dimensions of 1 or 2 metres to be resolved in the presence of tidal ranges of 5 metres. This procedure has been shown to work well for simulations of the Fraser River in British Columbia as it enters the Strait of Georgia (Stronach et al., 2006).

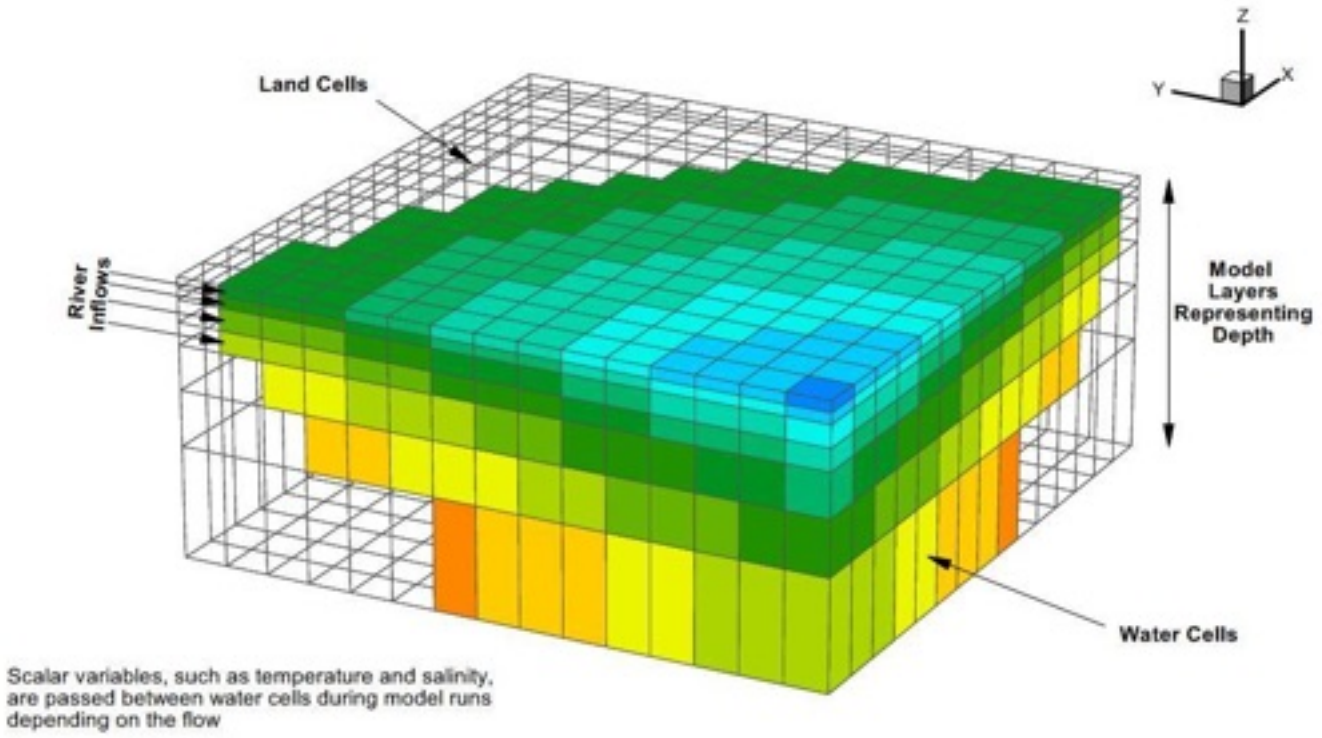

Figure A.1: Typical Grid Mesh

APPENDIX B

IHA'S ADCP CANYON A/B/C AND OUTFALL A LOCATIONS BAR DIAGRAM SUMMARY

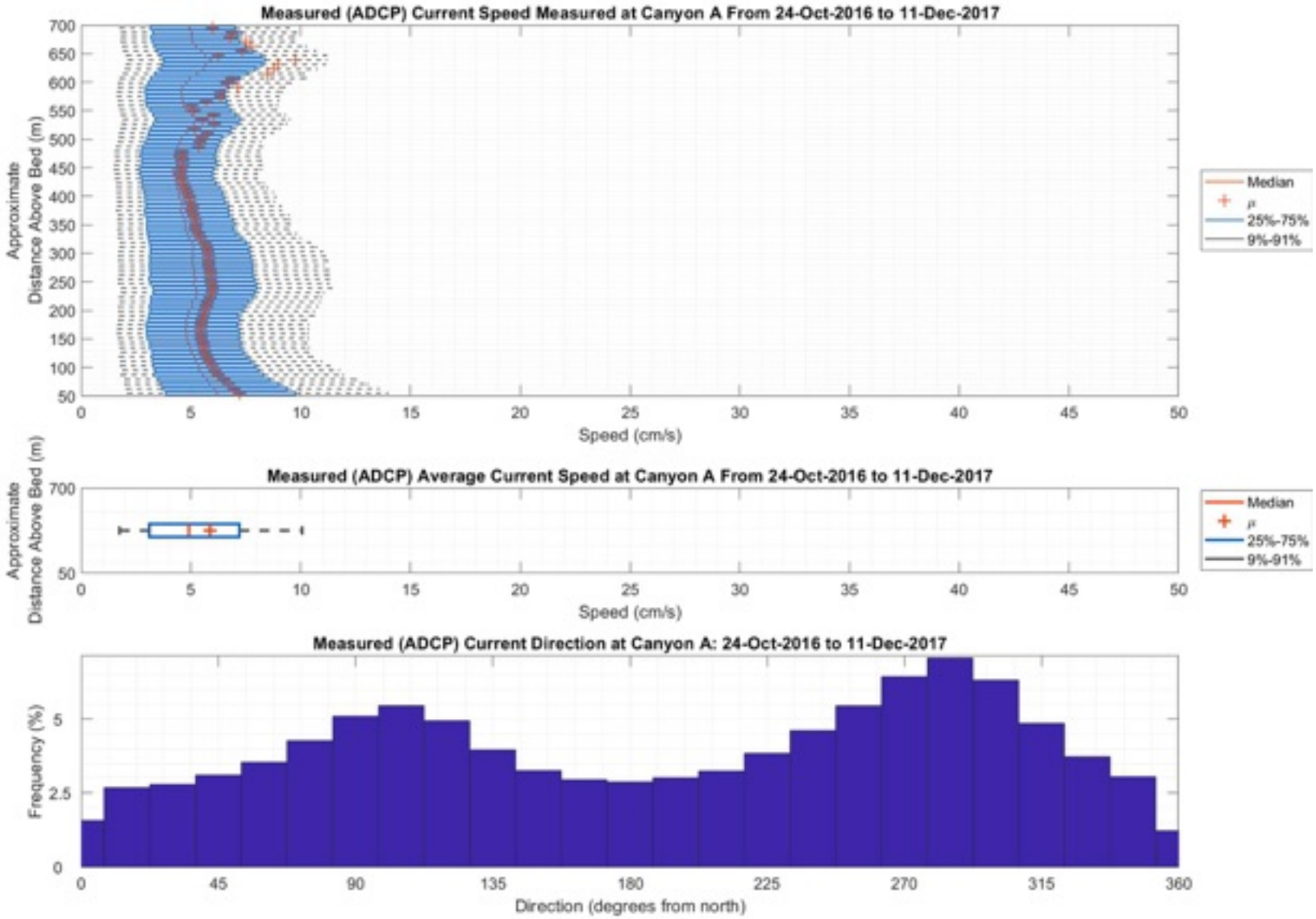

NOTES

IHA ADCP Canyon A Upward Looking Deployment
Dates: 24 Oct 2016 - 11 Dec 2017

STATUS
ISSUED FOR REVIEW

CLIENT

WAFI-GOLPU JOINT VENTURE

TETRA TECH

Wafi-Golpu DSTP Project

Density Current, Plume Dispersion, and Hydrodynamic Modelling

PROJECT NO.	DWN	CKD	APVD	REV
704-TRN.WTRM03037	CY	AH	JAS	JAS

OFFICE: Tetra Tech - VANC
DATE: March, 2018

Figure B-1

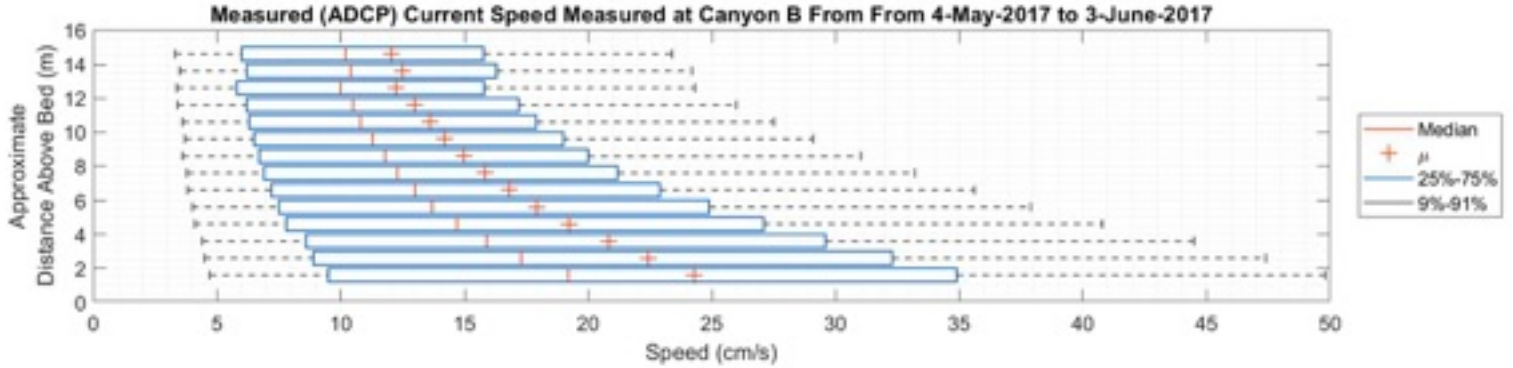

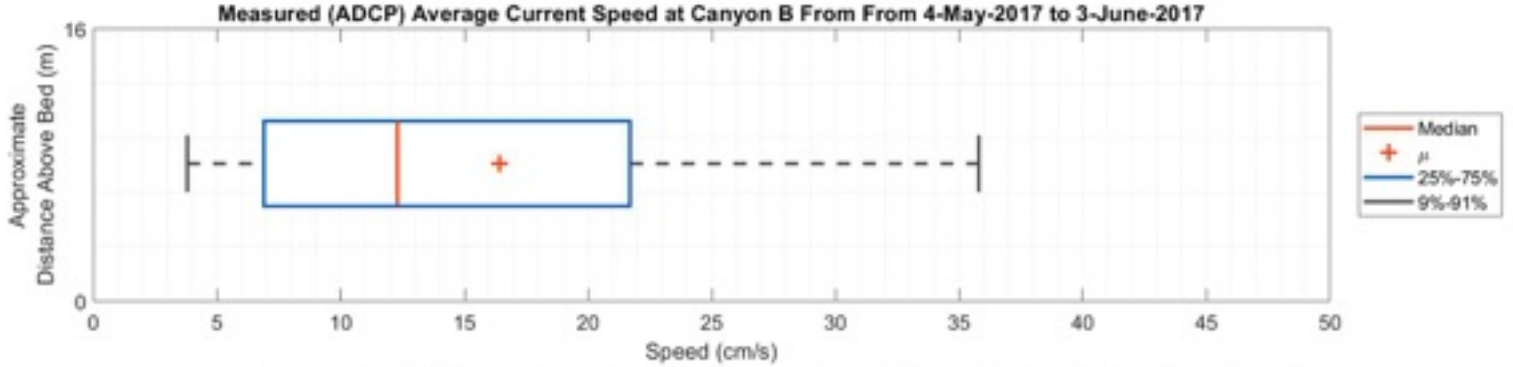

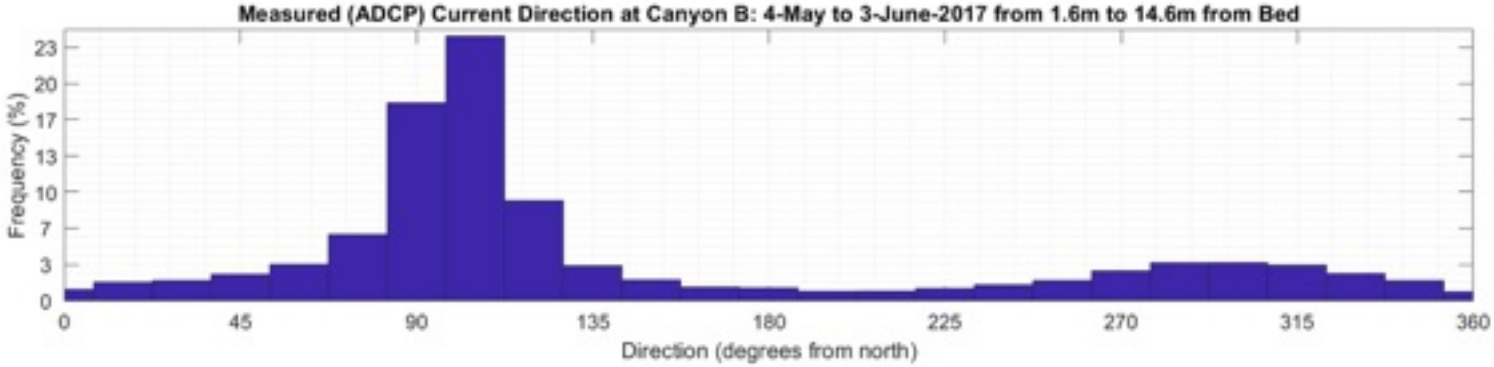

NOTES

IHA ADCP Canyon B Downward Looking Deployment (Before Move)
Dates: 4 May 2017 - 3 Jun 2017

STATUS
ISSUED FOR REVIEW

CLIENT

WAFI-GOLPU JOINT VENTURE

TETRA TECH

Wafi-Golpu DSTP Project

Density Current, Plume Dispersion, and Hydrodynamic Modelling

PROJECT NO.	DWN	CKD	APVD	REV
704-TRN.WTRM03037	CY	AH	JAS	JAS

OFFICE: Tetra Tech - VANC
DATE: March, 2018

Figure B-2

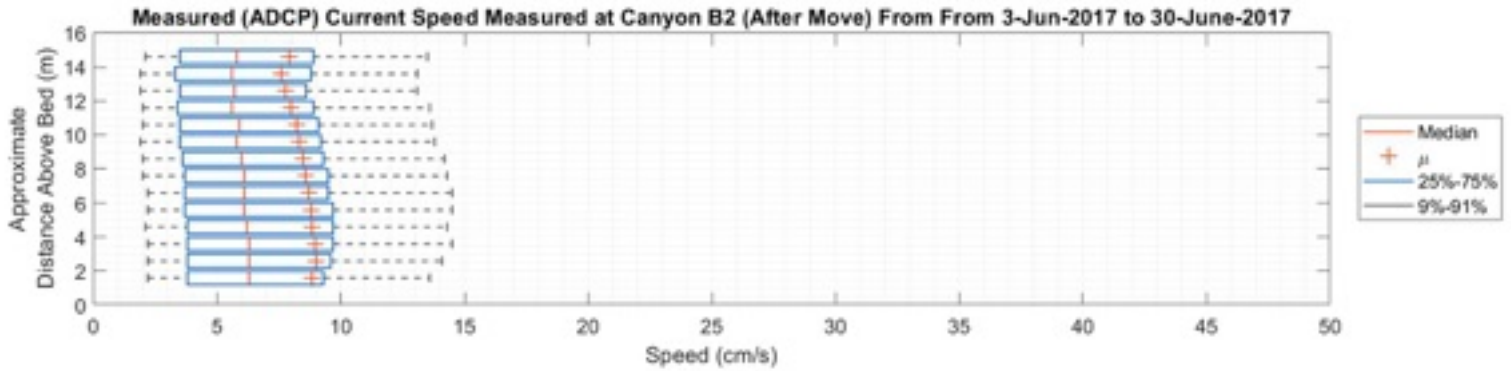

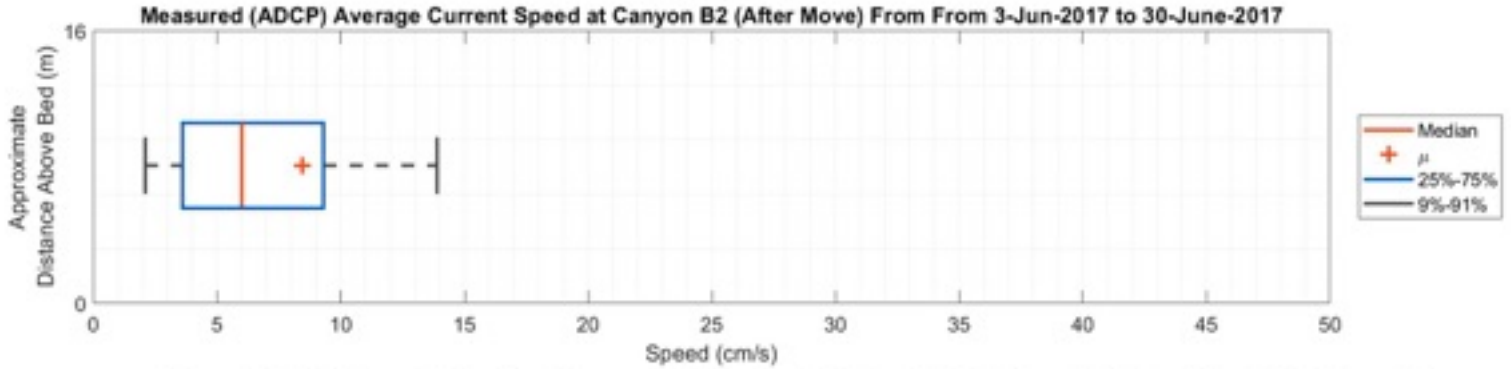

NOTES

IHA ADCP Canyon B Downward Looking Deployment (After Move)
Dates: 3 Jun 2017 - 30 Jun 2017

STATUS
ISSUED FOR REVIEW

CLIENT

WAFI-GOLPU JOINT VENTURE

TETRA TECH

Wafi-Golpu DSTP Project

Density Current, Plume Dispersion, and Hydrodynamic Modelling

PROJECT NO.	DWN	CKD	APVD	REV
704-TRN.WTRM03037	CY	AH	JAS	JAS

OFFICE: Tetra Tech - VANC
DATE: March, 2018

Figure B-3

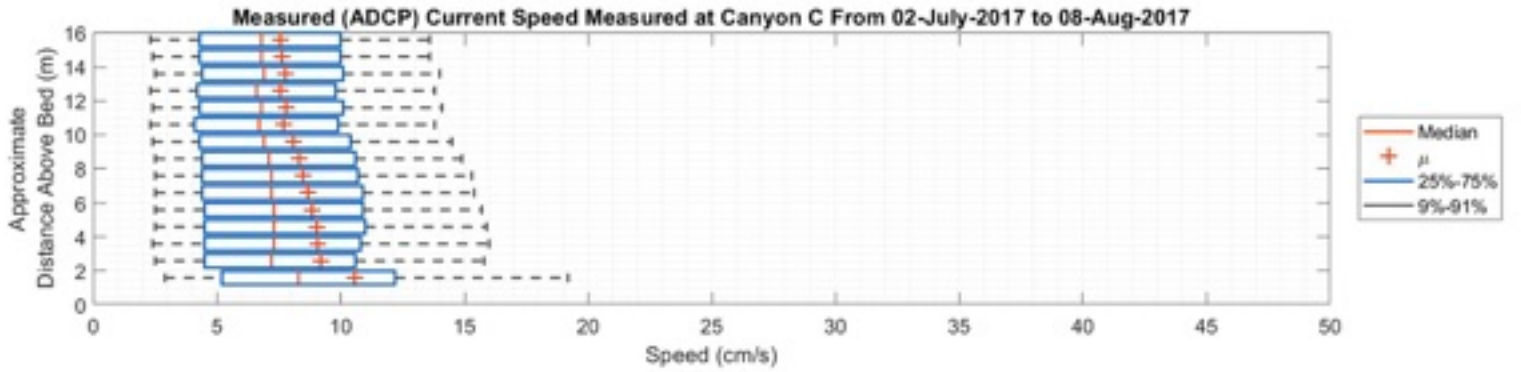

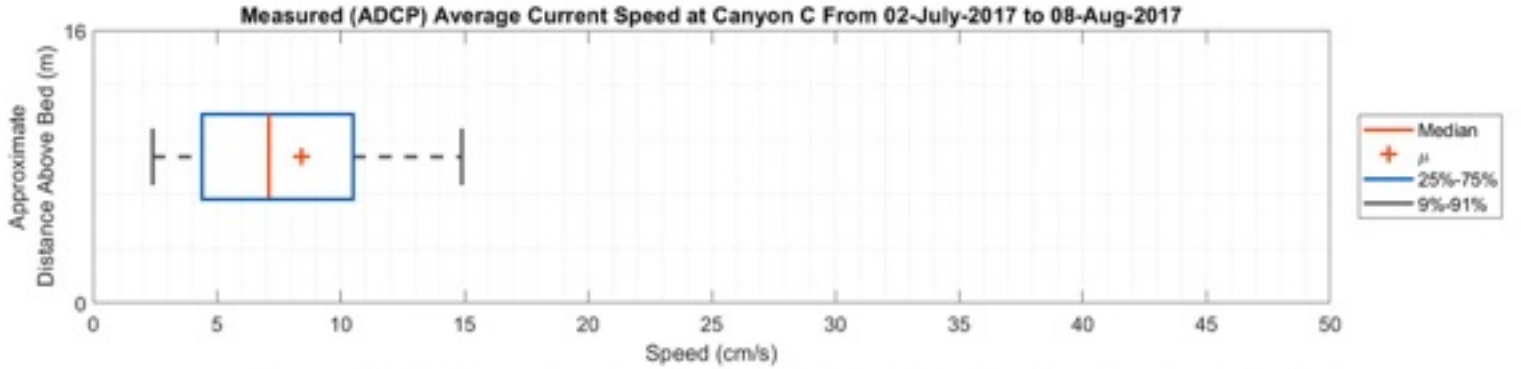

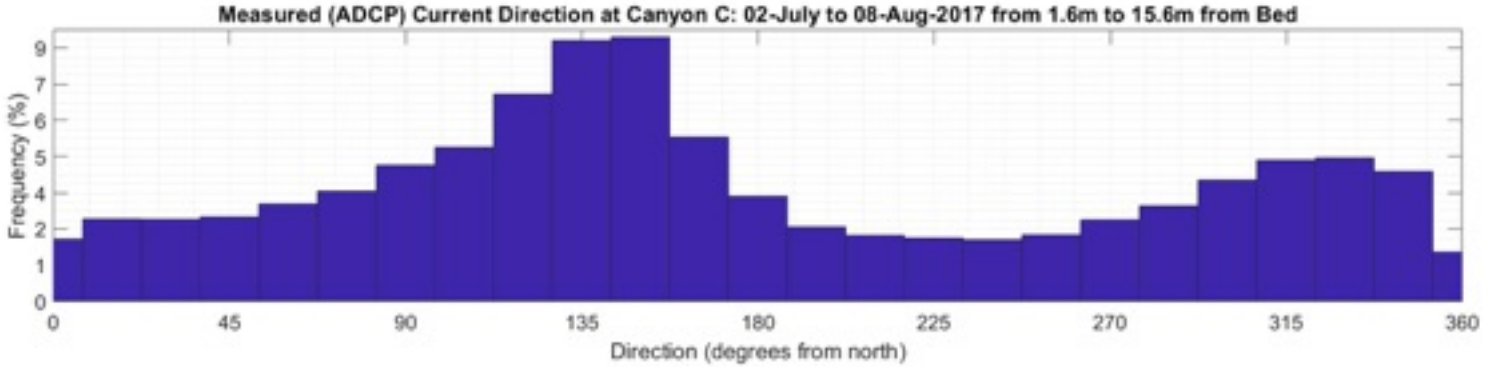

NOTES

IHA ADCP Canyon C Downward Looking Deployment 1
Dates: 02 Jul 2017 - 08 Aug 2017

STATUS
ISSUED FOR REVIEW

CLIENT

WAFI-GOLPU JOINT VENTURE

TETRA TECH

Wafi-Golpu DSTP Project

Density Current, Plume Dispersion, and Hydrodynamic Modelling

PROJECT NO.	DWN	CKD	APVD	REV
704-TRN.WTRM03037	CY	AH	JAS	JAS

OFFICE: Tetra Tech - VANC
DATE: March, 2018

Figure B-4

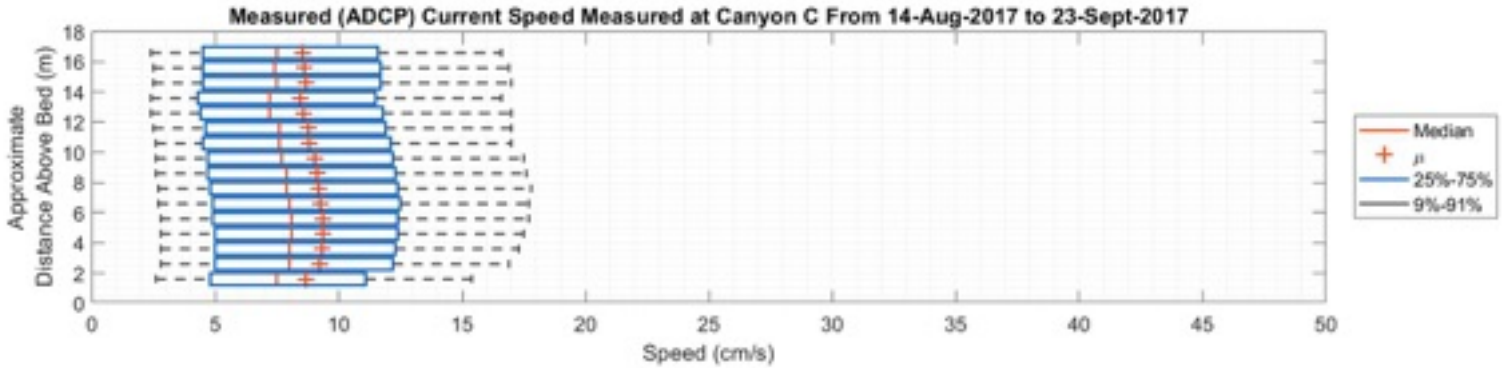

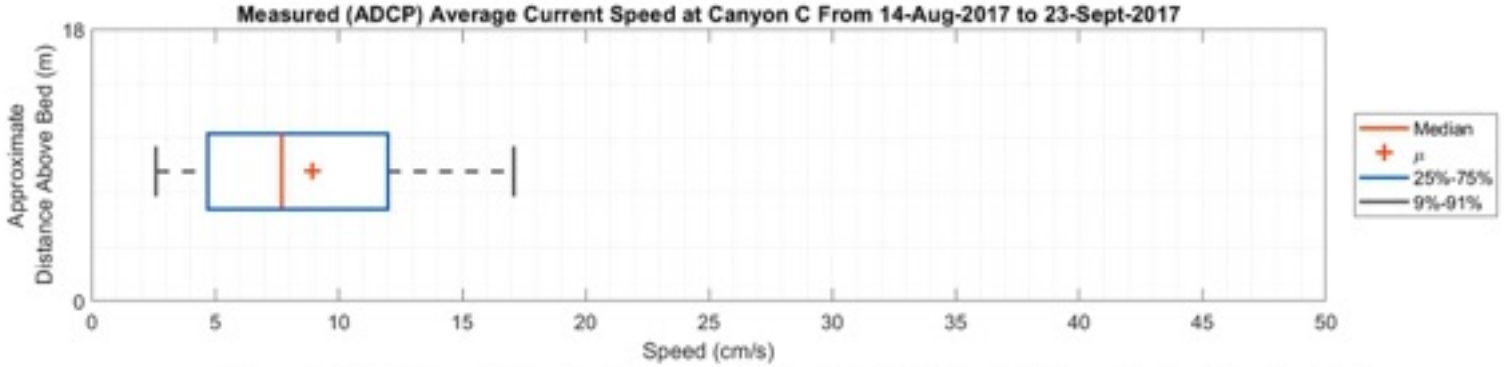

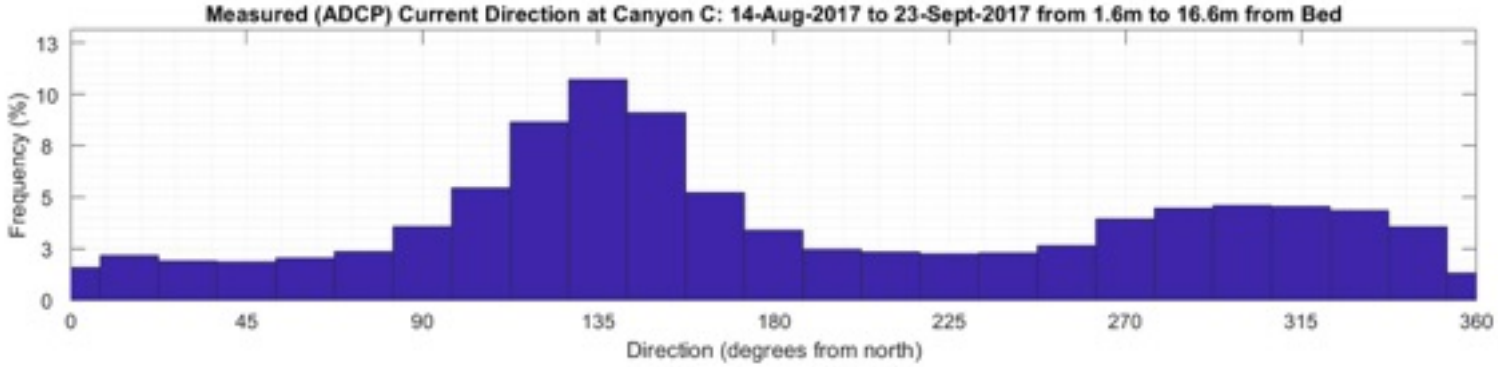

NOTES

IHA ADCP Canyon C Downward Looking Deployment 2
Dates: 14 Aug 2017 - 23 Sep 2017

STATUS
ISSUED FOR REVIEW

CLIENT

WAFI-GOLPU JOINT VENTURE

TETRA TECH

Wafi-Golpu DSTP Project

Density Current, Plume Dispersion, and Hydrodynamic Modelling

PROJECT NO.	DWN	CKD	APVD	REV
704-TRN.WTRM03037	CY	AH	JAS	JAS

OFFICE: Tetra Tech - VANC
DATE: March, 2018

Figure B-5

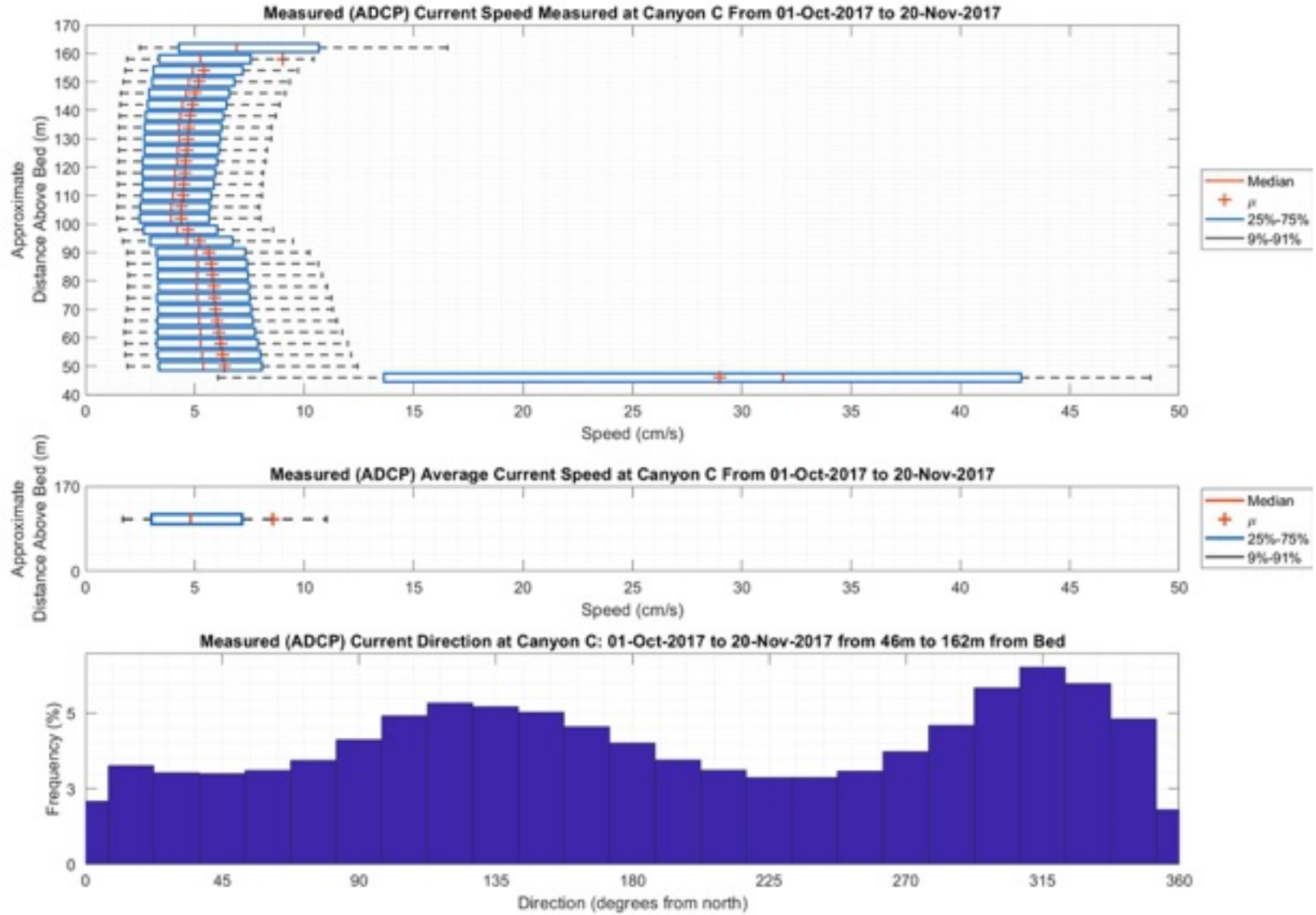

NOTES

IHA ADCP Canyon C Upward Looking Deployment 3
Dates: 01 Oct 2017 - 20 Nov 2017

STATUS
ISSUED FOR REVIEW

CLIENT

WAFI-GOLPU JOINT VENTURE

TETRA TECH

Wafi-Golpu DSTP Project

Density Current, Plume Dispersion, and Hydrodynamic Modelling

PROJECT NO.	DWN	CKD	APVD	REV
704-TRN.WTRM03037	CY	AH	JAS	JAS

OFFICE: Tetra Tech - VANC
DATE: March, 2018

Figure B-6

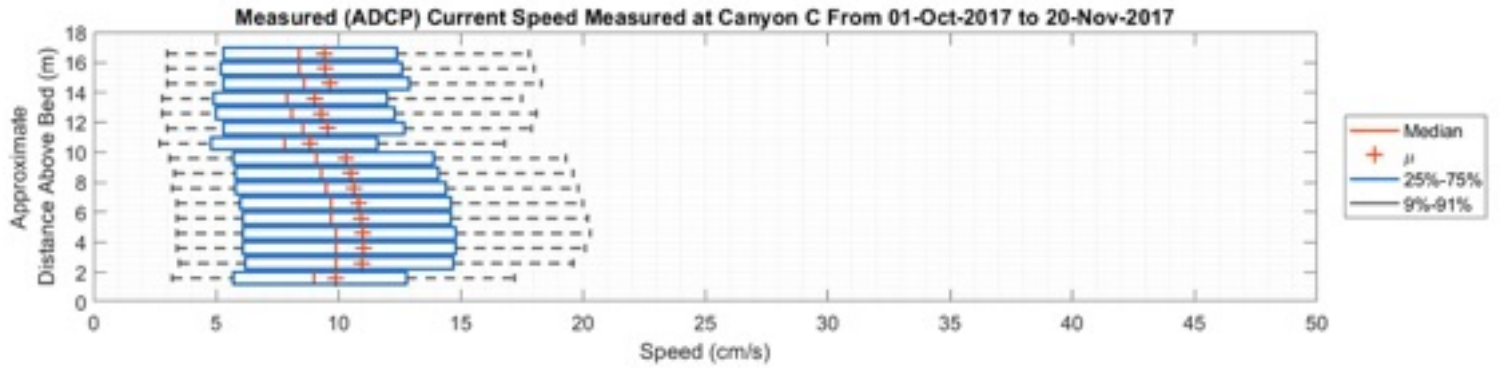

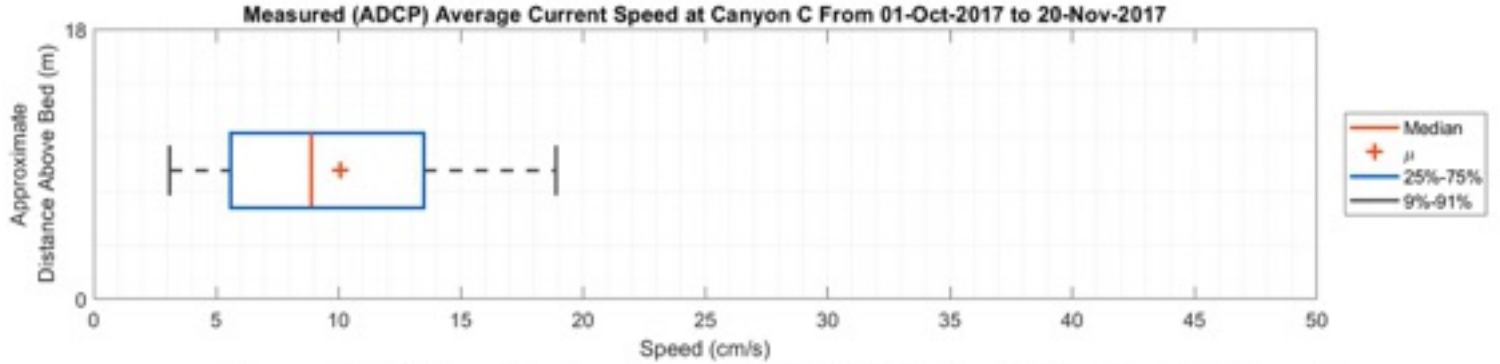

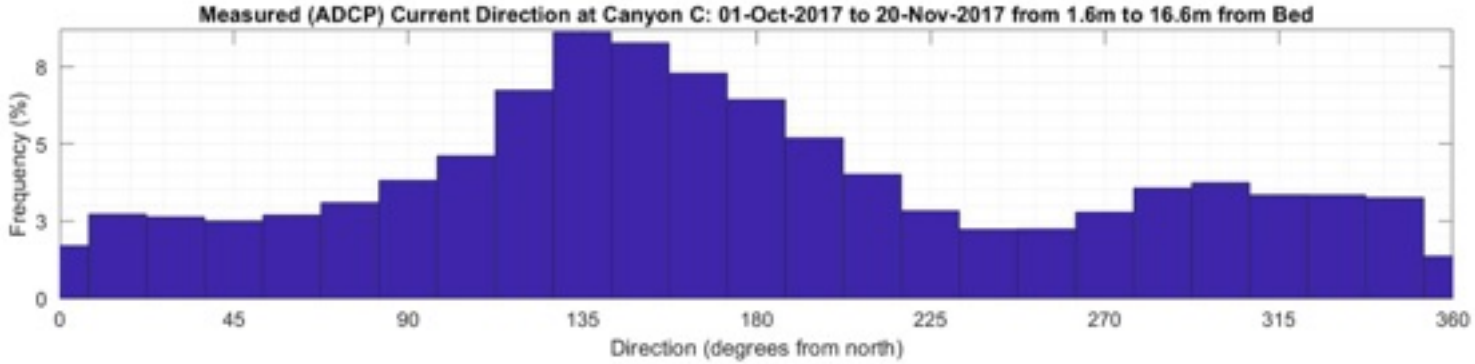

NOTES

IHA ADCP Canyon C Downward Looking Deployment 3
Dates: 01 Oct 2017 - 20 Nov 2017

STATUS
ISSUED FOR REVIEW

CLIENT

WAFI-GOLPU JOINT VENTURE

TETRA TECH

Wafi-Golpu DSTP Project

Density Current, Plume Dispersion, and Hydrodynamic Modelling

PROJECT NO.	DWN	CKD	APVD	REV
704-TRN.WTRM03037	CY	AH	JAS	JAS

OFFICE	DATE
Tetra Tech - VANC	March, 2018

Figure B-7

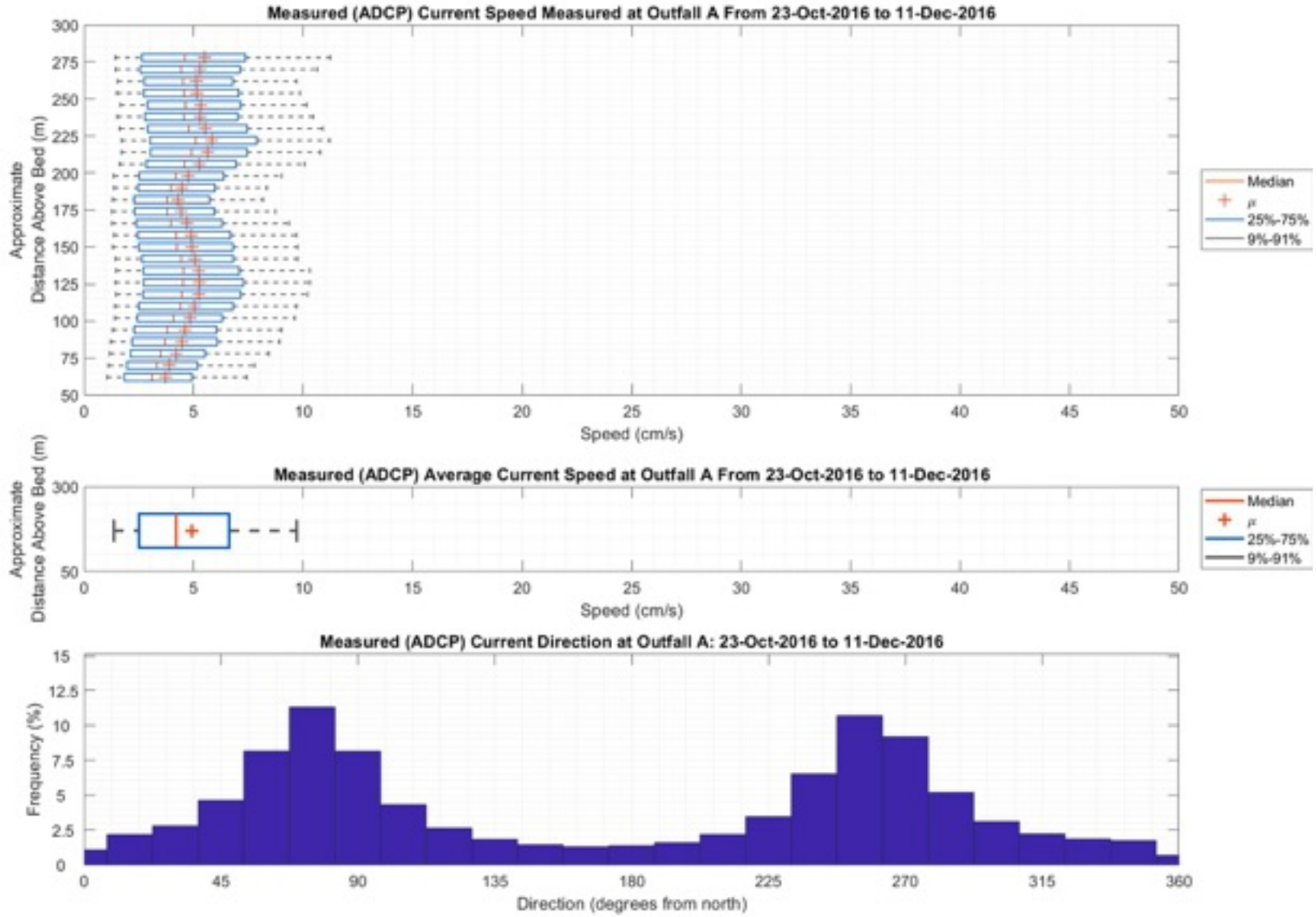

NOTES

IHA ADCP Outfall A Upward Looking Deployment 1
Dates: 23 Oct 2016 - 11 Dec 2016

STATUS
ISSUED FOR REVIEW

CLIENT

WAFI-GOLPU JOINT VENTURE

TETRA TECH

Wafi-Golpu DSTP Project

Density Current, Plume Dispersion, and Hydrodynamic Modelling

PROJECT NO.	DWN	CKD	APVD	REV
704-TRN.WTRM03037	CY	AH	JAS	JAS

OFFICE: Tetra Tech - VANC
DATE: March, 2018

Figure B-8

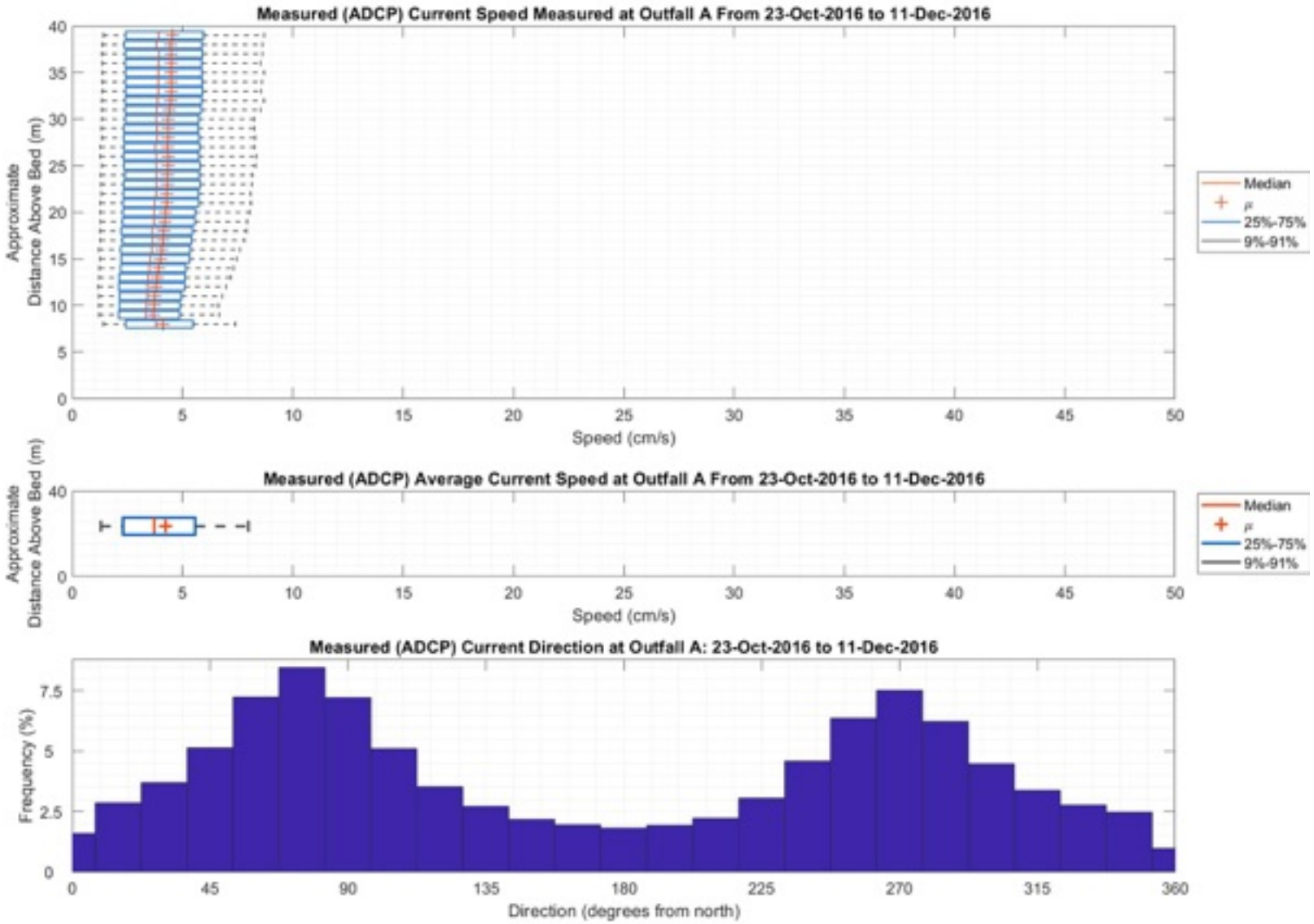

NOTES

IHA ADCP Outfall A Downward Looking Deployment 1
Dates: 23 Oct 2016 - 11 Dec 2016

STATUS
ISSUED FOR REVIEW

CLIENT

WAFI-GOLPU JOINT VENTURE

TETRA TECH

Wafi-Golpu DSTP Project

Density Current, Plume Dispersion, and Hydrodynamic Modelling

PROJECT NO.	DWN	CKD	APVD	REV
704-TRN.WTRM03037	CY	AH	JAS	JAS

OFFICE: Tetra Tech - VANC
DATE: March, 2018

Figure B-9

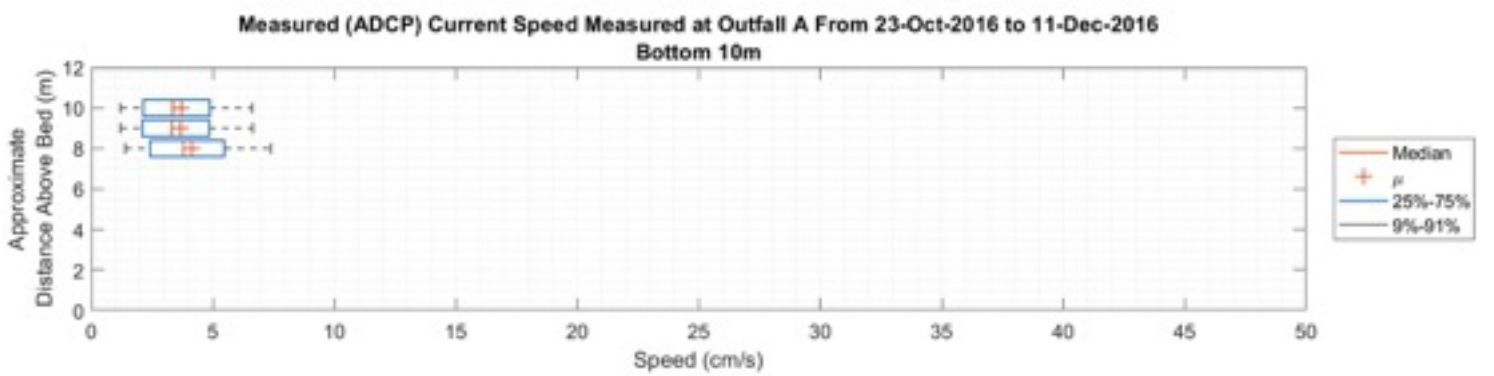

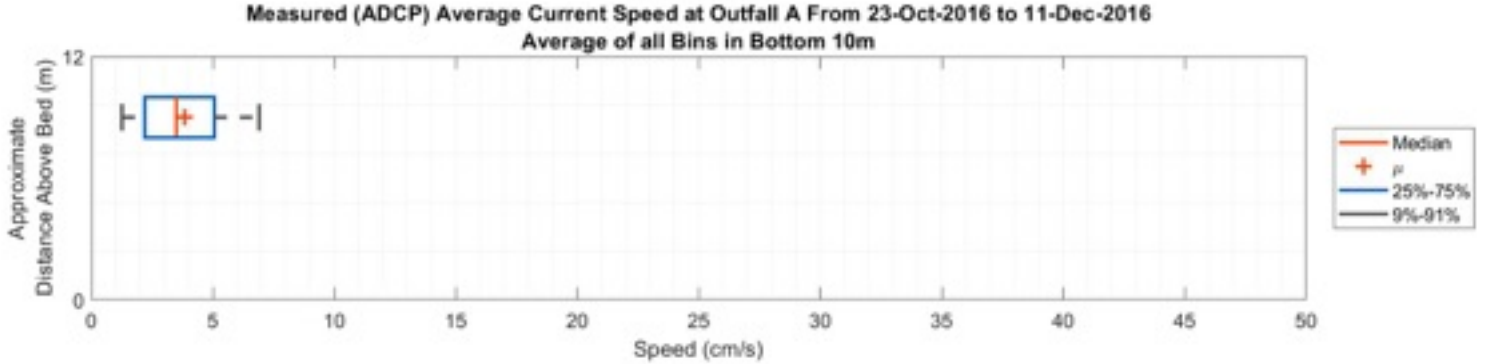

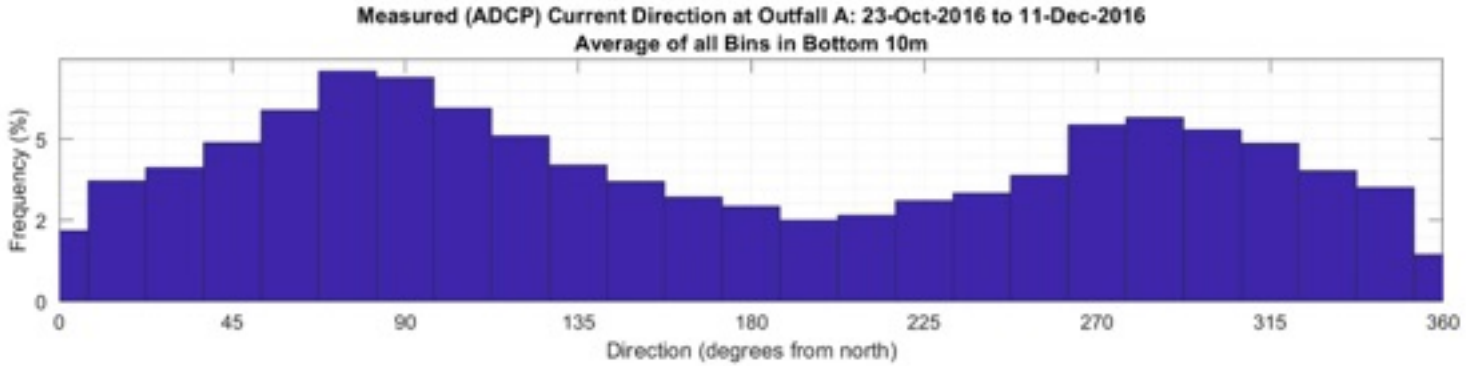

NOTES

IHA ADCP Outfall A Downward Looking Deployment 1 (Bottom 10m)
Dates: 23 Oct 2016 - 11 Dec 2016

STATUS
ISSUED FOR REVIEW

CLIENT

WAFI-GOLPU JOINT VENTURE

TETRA TECH

Wafi-Golpu DSTP Project

Density Current, Plume Dispersion, and Hydrodynamic Modelling

PROJECT NO.	DWN	CKD	APVD	REV
704-TRN.WTRM03037	CY	AH	JAS	JAS

OFFICE: Tetra Tech - VANC
DATE: March, 2018

Figure B-10

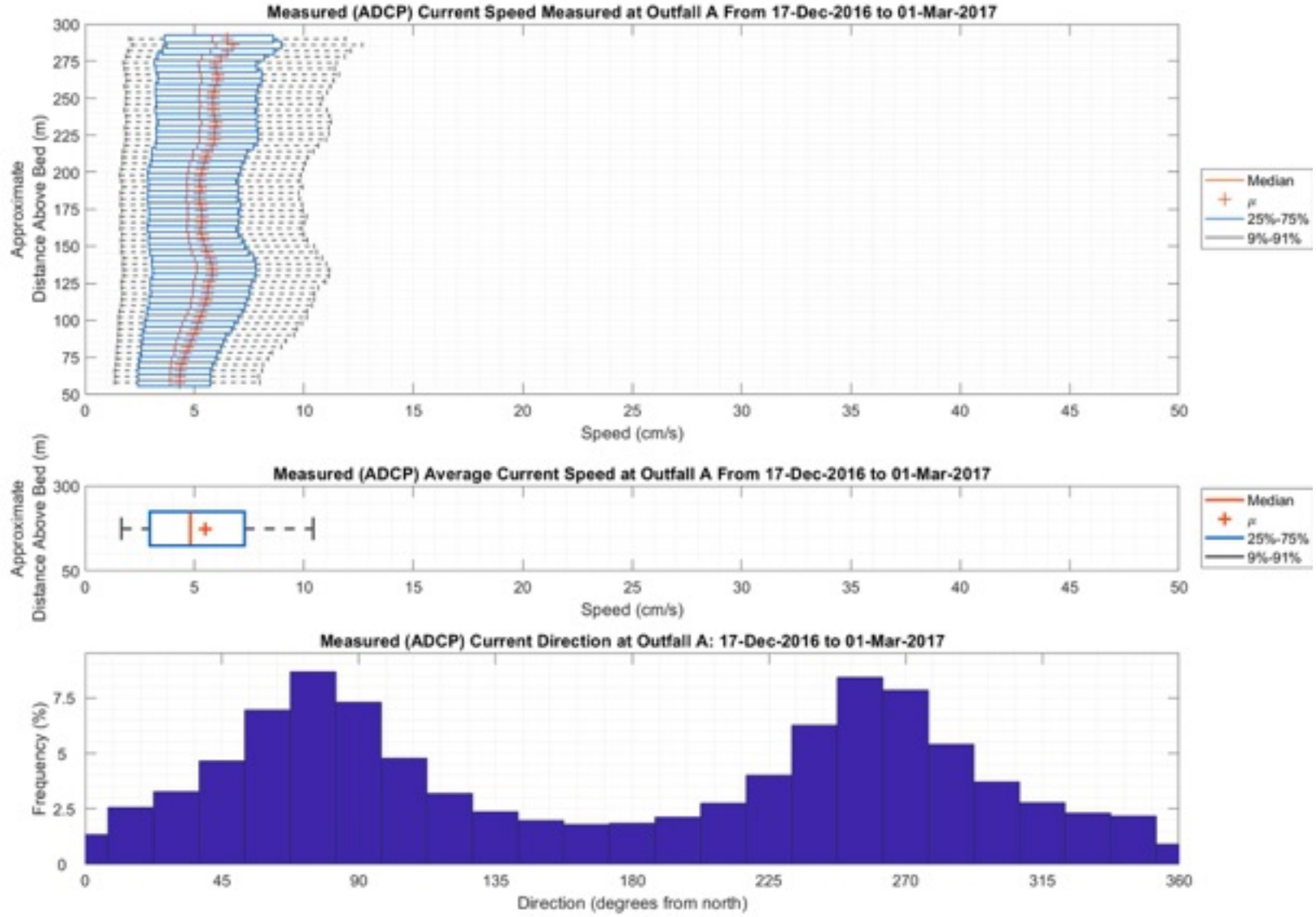

NOTES

IHA ADCP Outfall A Upward Looking Deployment 2
Dates: 17 Dec 2016 - 01 Mar 2017

STATUS
ISSUED FOR REVIEW

CLIENT

WAFI-GOLPU JOINT VENTURE

TETRA TECH

Wafi-Golpu DSTP Project

Density Current, Plume Dispersion, and Hydrodynamic Modelling

PROJECT NO.	DWN	CKD	APVD	REV
704-TRN.WTRM03037	CY	AH	JAS	JAS

OFFICE: Tetra Tech - VANC
DATE: March, 2018

Figure B-11

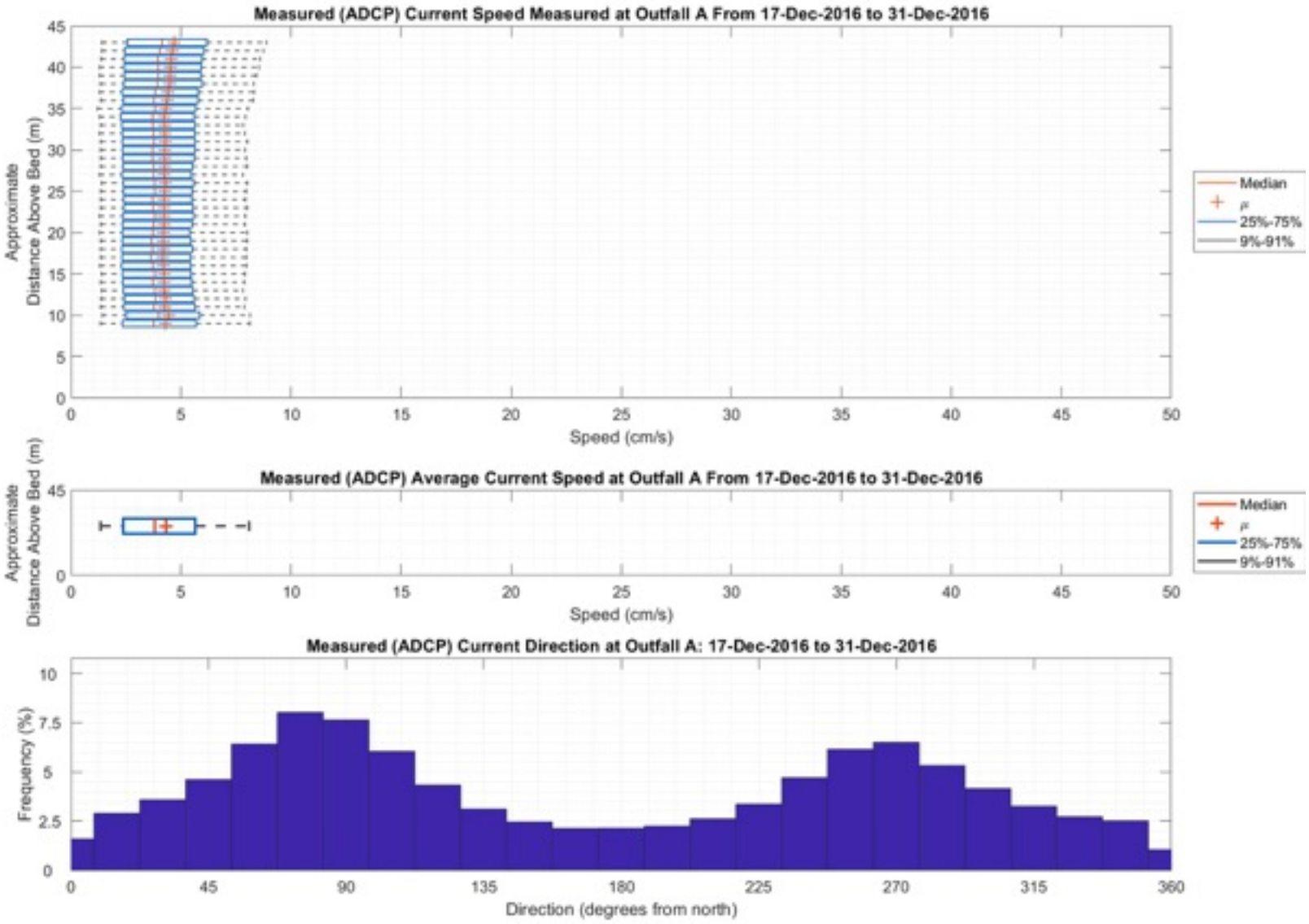

NOTES

IHA ADCP Outfall A Downward Looking Deployment 2
Dates: 17 Dec 2016 - 31 Dec 2016

STATUS
ISSUED FOR REVIEW

CLIENT

WAFI-GOLPU JOINT VENTURE

TETRA TECH

Wafi-Golpu DSTP Project

Density Current, Plume Dispersion, and Hydrodynamic Modelling

PROJECT NO.	DWN	CKD	APVD	REV
704-TRN.WTRM03037	CY	AH	JAS	JAS

OFFICE: Tetra Tech - VANC
DATE: March, 2018

Figure B-12

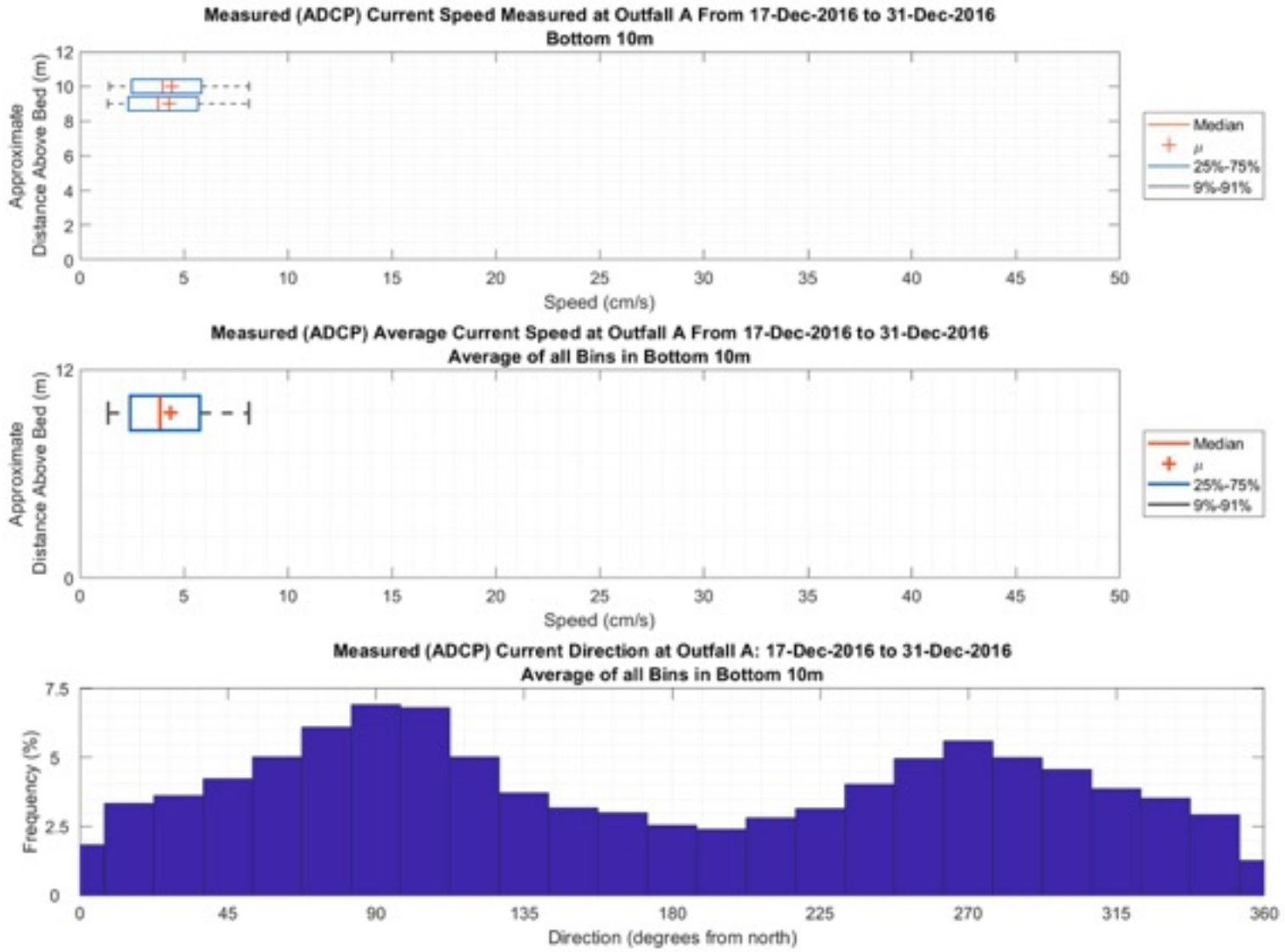

NOTES

IHA ADCP Outfall A Downward Looking Deployment 2 (Bottom 10m)
Dates: 17 Dec 2016 - 31 Dec 2016

STATUS
ISSUED FOR REVIEW

CLIENT

WAFI-GOLPU JOINT VENTURE

TETRA TECH

Wafi-Golpu DSTP Project

Density Current, Plume Dispersion, and Hydrodynamic Modelling

PROJECT NO.	DWN	CKD	APVD	REV
704-TRN.WTRM03037	CY	AH	JAS	JAS

OFFICE: Tetra Tech - VANC
DATE: March, 2018

Figure B-13

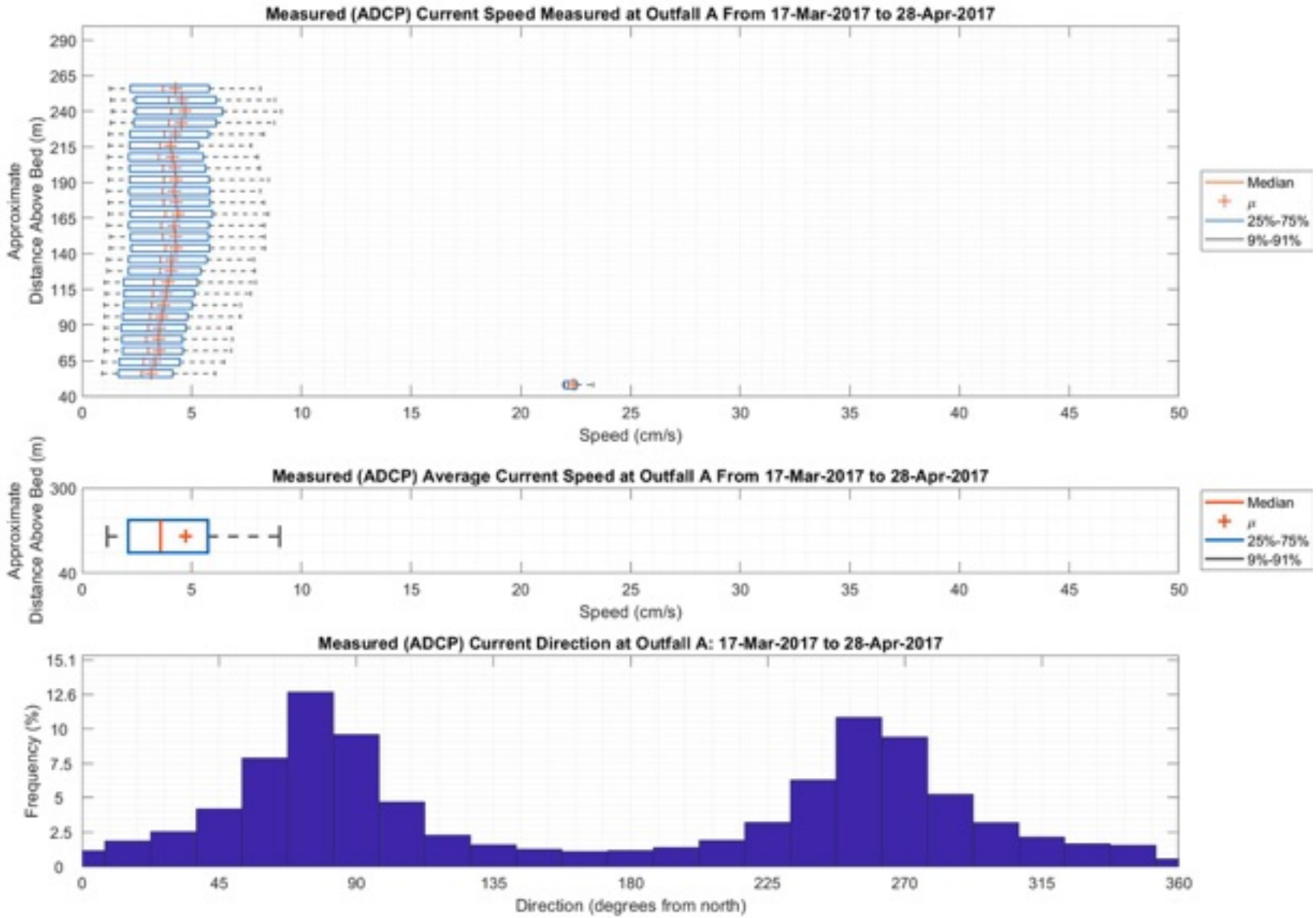

NOTES

IHA ADCP Outfall A Upward Looking Deployment 3
Dates: 17 Mar 2017 - 28 Apr 2017

STATUS
ISSUED FOR REVIEW

CLIENT

WAFI-GOLPU JOINT VENTURE

TETRA TECH

Wafi-Golpu DSTP Project

Density Current, Plume Dispersion, and Hydrodynamic Modelling

PROJECT NO.	DWN	CKD	APVD	REV
704-TRN.WTRM03037	CY	AH	JAS	JAS

OFFICE	DATE
Tetra Tech - VANC	March, 2018

Figure B-14

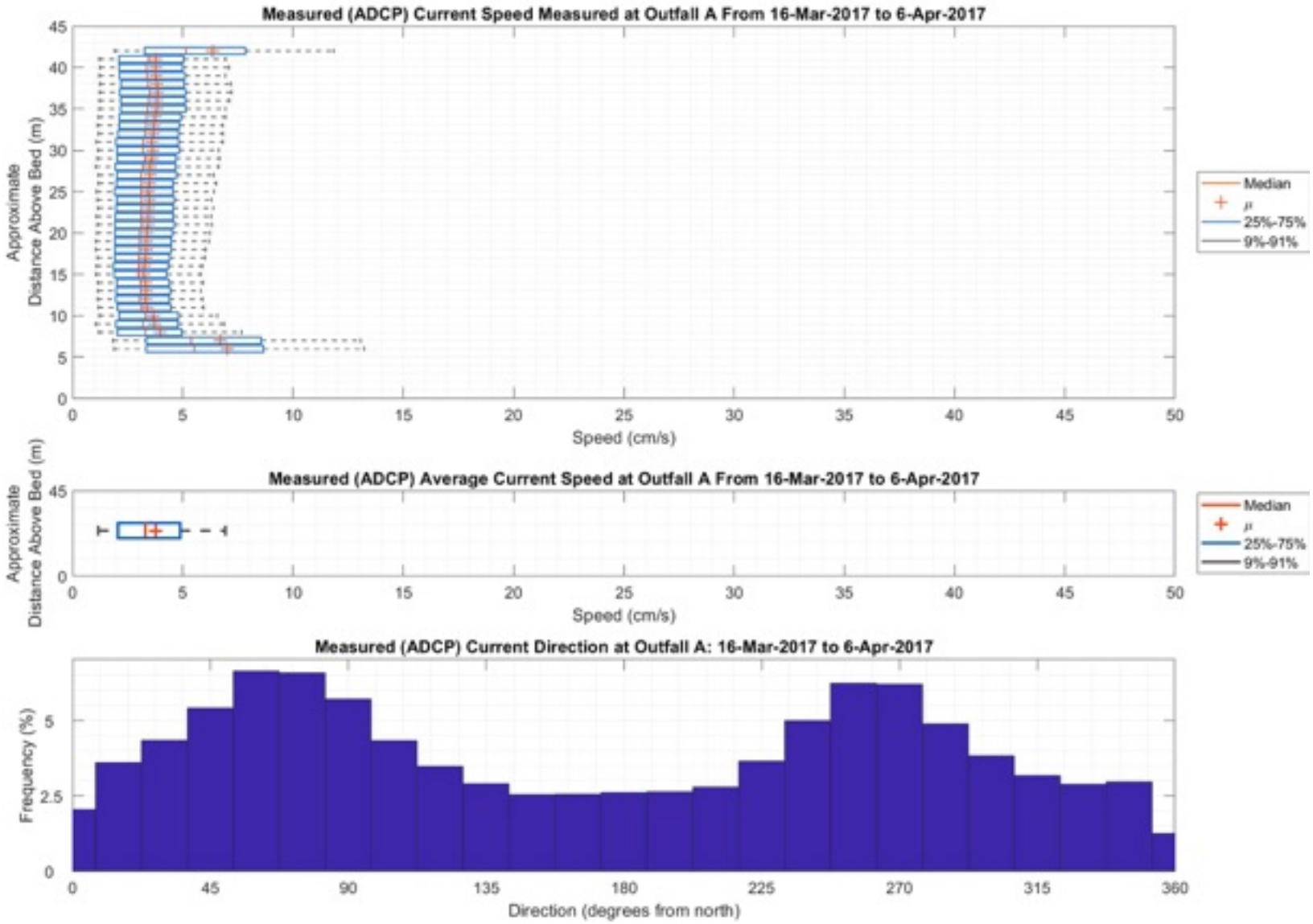

NOTES

IHA ADCP Outfall A Downward Looking Deployment 3
Dates: 16 Mar 2017 - 06 Apr 2017

STATUS
ISSUED FOR REVIEW

CLIENT

WAFI-GOLPU JOINT VENTURE

TETRA TECH

Wafi-Golpu DSTP Project

Density Current, Plume Dispersion, and Hydrodynamic Modelling

PROJECT NO.	DWN	CKD	APVD	REV
704-TRN.WTRM03037	CY	AH	JAS	JAS

OFFICE: Tetra Tech - VANC
DATE: March, 2018

Figure B-15

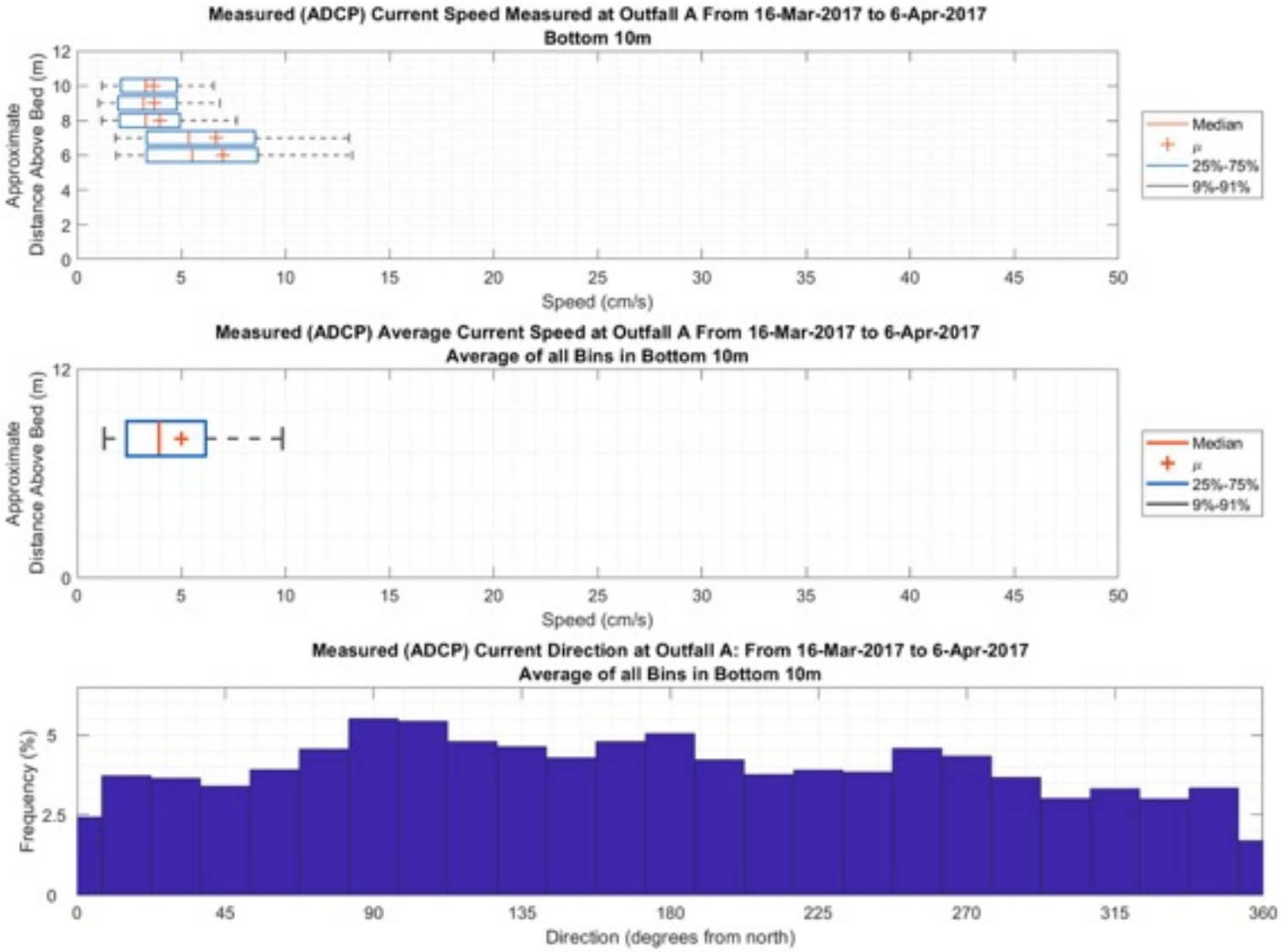

NOTES

IHA ADCP Outfall A Downward Looking Deployment 3 (Bottom 10m)
Dates: 16 Mar 2017 - 06 Apr 2017

STATUS
ISSUED FOR REVIEW

CLIENT

WAFI-GOLPU JOINT VENTURE

TETRA TECH

Wafi-Golpu DSTP Project

Density Current, Plume Dispersion, and Hydrodynamic Modelling

PROJECT NO.	DWN	CKD	APVD	REV
704-TRN.WTRM03037	CY	AH	JAS	JAS

OFFICE: Tetra Tech - VANC
DATE: March, 2018

Figure B-16

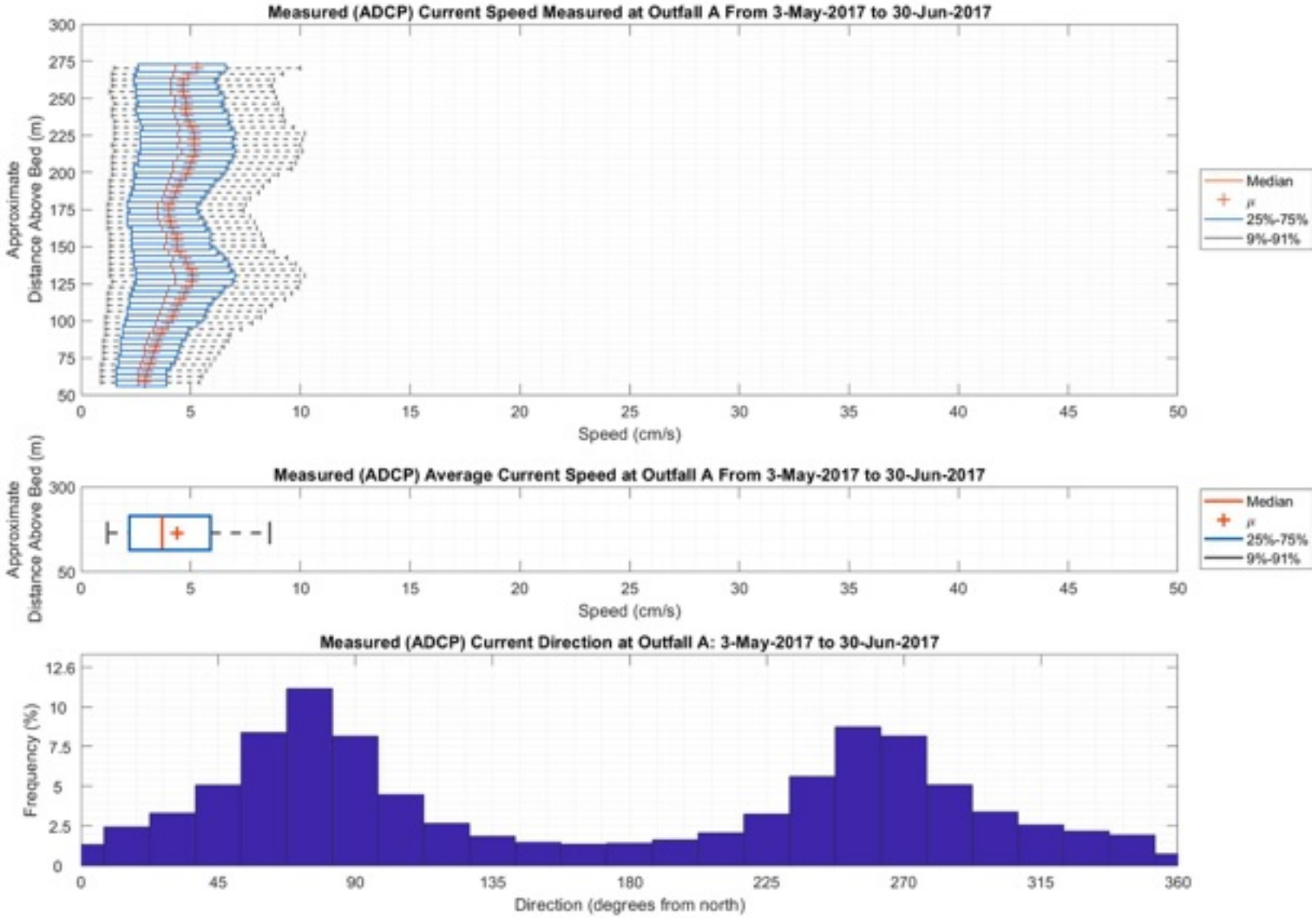

NOTES

IHA ADCP Outfall A Upward Looking Deployment 4
Dates: 03 May 2017 - 30 Jun 2017

STATUS
ISSUED FOR REVIEW

CLIENT

WAFI-GOLPU JOINT VENTURE

TETRA TECH

Wafi-Golpu DSTP Project

Density Current, Plume Dispersion, and Hydrodynamic Modelling

PROJECT NO.	DWN	CKD	APVD	REV
704-TRN.WTRM03037	CY	AH	JAS	JAS

OFFICE: Tetra Tech - VANC
DATE: March, 2018

Figure B-17

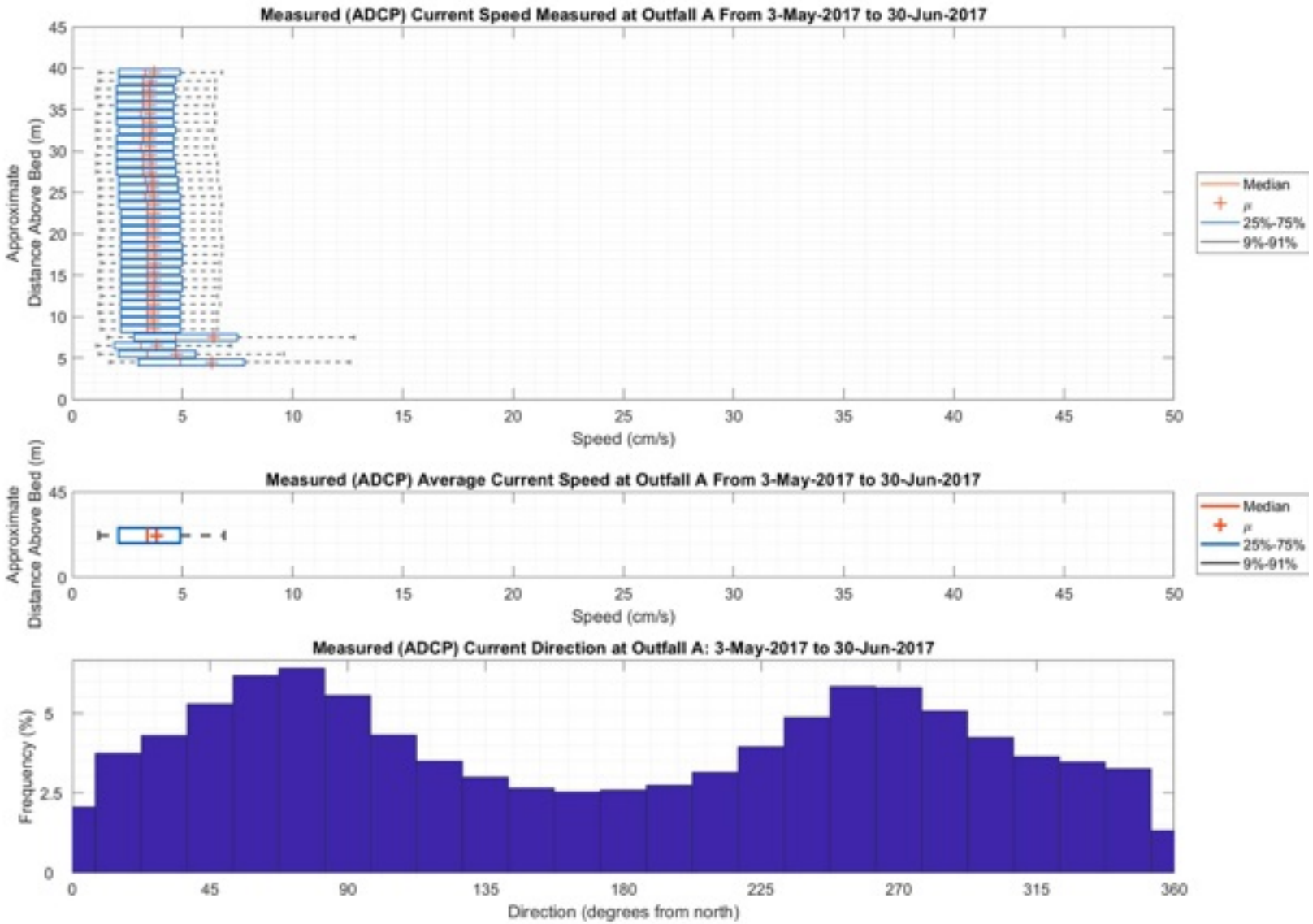

NOTES

IHA ADCP Outfall A Downward Looking Deployment 4
Dates: 03 May 2017 - 30 Jun 2017

STATUS
ISSUED FOR REVIEW

CLIENT

WAFI-GOLPU JOINT VENTURE

TETRA TECH

Wafi-Golpu DSTP Project

Density Current, Plume Dispersion, and Hydrodynamic Modelling

PROJECT NO.	DWN	CKD	APVD	REV
704-TRN.WTRM03037	CY	AH	JAS	JAS

OFFICE: Tetra Tech - VANC
DATE: March, 2018

Figure B-18

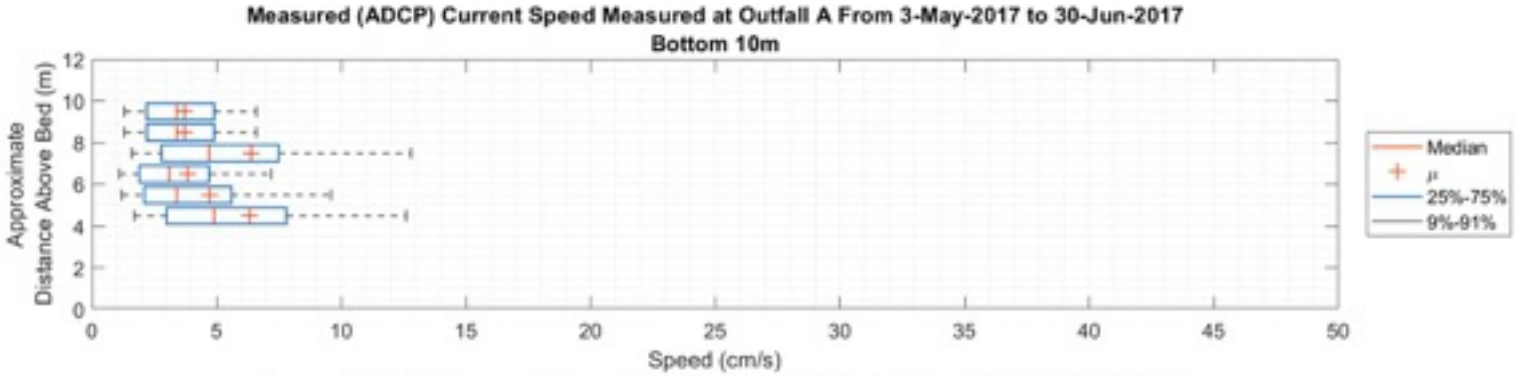

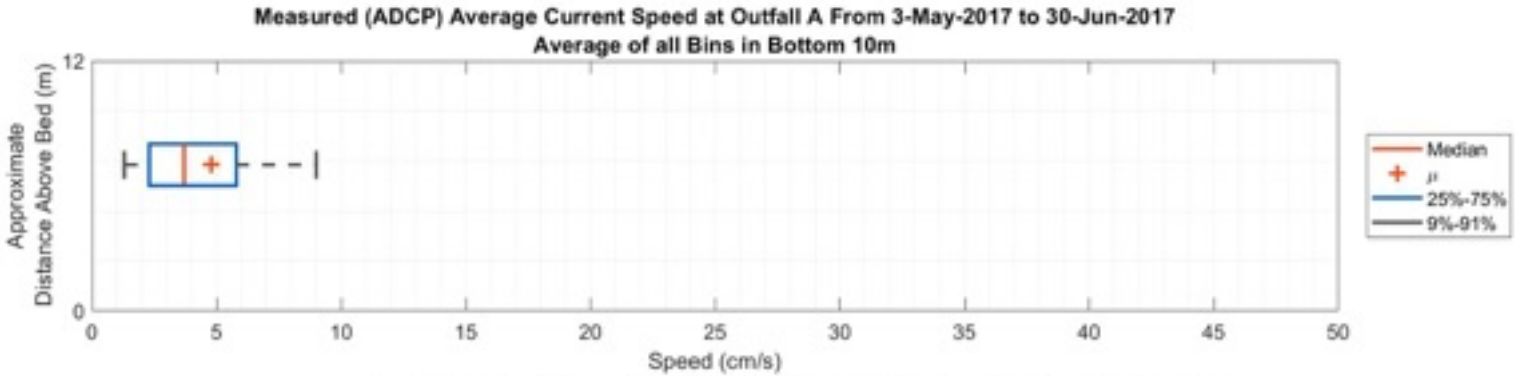

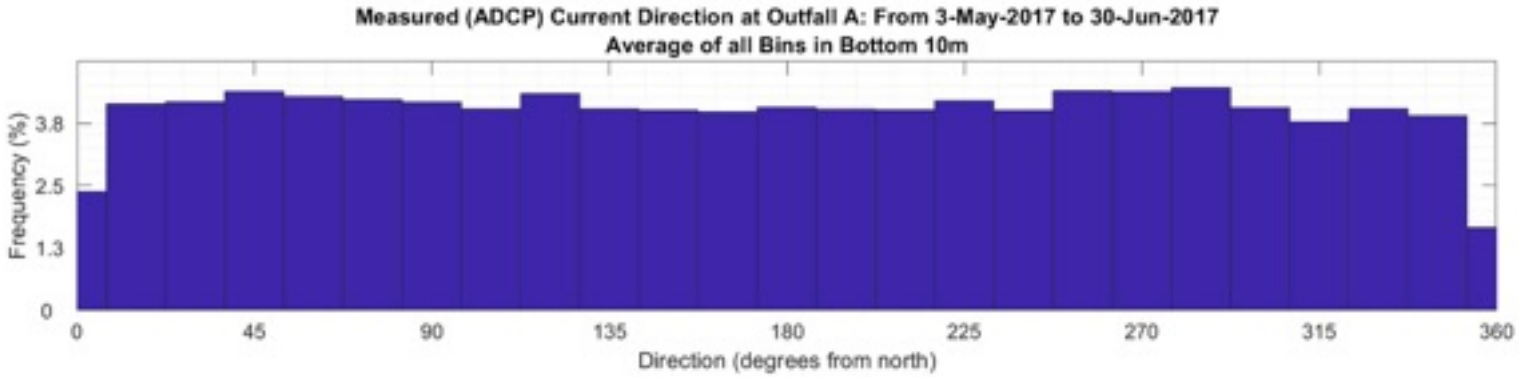

NOTES

IHA ADCP Outfall A Downward Looking Deployment 4 (Bottom 10m)
Dates: 03 May 2017 - 30 Jun 2017

STATUS
ISSUED FOR REVIEW

CLIENT

WAFI-GOLPU JOINT VENTURE

TETRA TECH

Wafi-Golpu DSTP Project

Density Current, Plume Dispersion, and Hydrodynamic Modelling

PROJECT NO.	DWN	CKD	APVD	REV
704-TRN.WTRM03037	CY	AH	JAS	JAS

OFFICE: Tetra Tech - VANC
DATE: March, 2018

Figure B-19

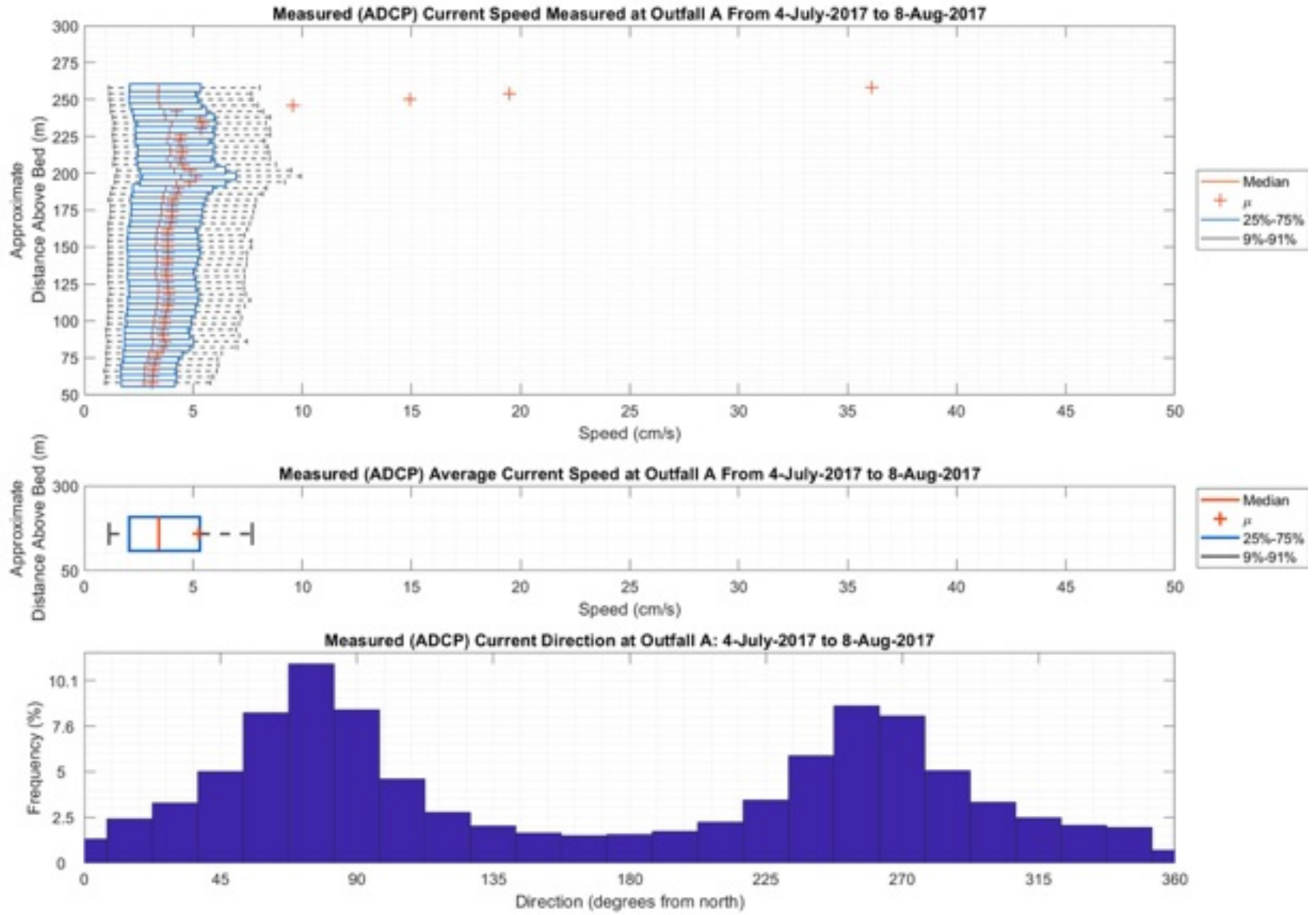

NOTES

IHA ADCP Outfall A Upward Looking Deployment 5
Dates: 04 Jul 2017 - 08 Aug 2017

CLIENT

WAFI-GOLPU JOINT VENTURE

TETRA TECH

STATUS
ISSUED FOR REVIEW

Wafi-Golpu DSTP Project

Density Current, Plume Dispersion, and Hydrodynamic Modelling

PROJECT NO.	DWN	CKD	APVD	REV
704-TRN.WTRM03037	CY	AH	JAS	JAS

OFFICE: Tetra Tech - VANC
DATE: March, 2018

Figure B-20

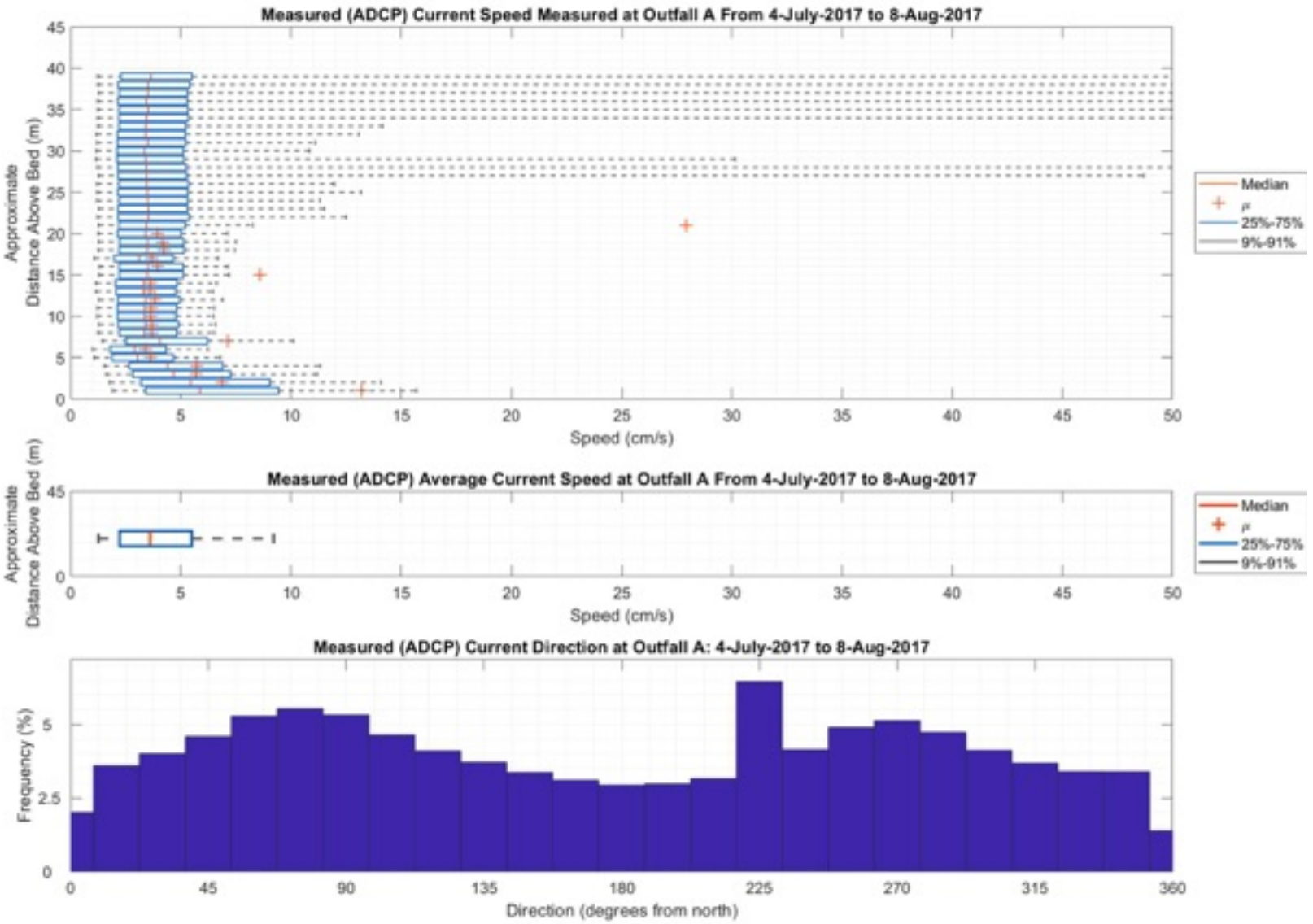

NOTES

IHA ADCP Outfall A Downward Looking Deployment 5
Dates: 04 Jul 2017 - 08 Aug 2017

STATUS
ISSUED FOR REVIEW

CLIENT

WAFI-GOLPU JOINT VENTURE

TETRA TECH

Wafi-Golpu DSTP Project

Density Current, Plume Dispersion, and Hydrodynamic Modelling

PROJECT NO.	DWN	CKD	APVD	REV
704-TRN.WTRM03037	CY	AH	JAS	JAS

OFFICE: Tetra Tech - VANC
DATE: March, 2018

Figure B-21

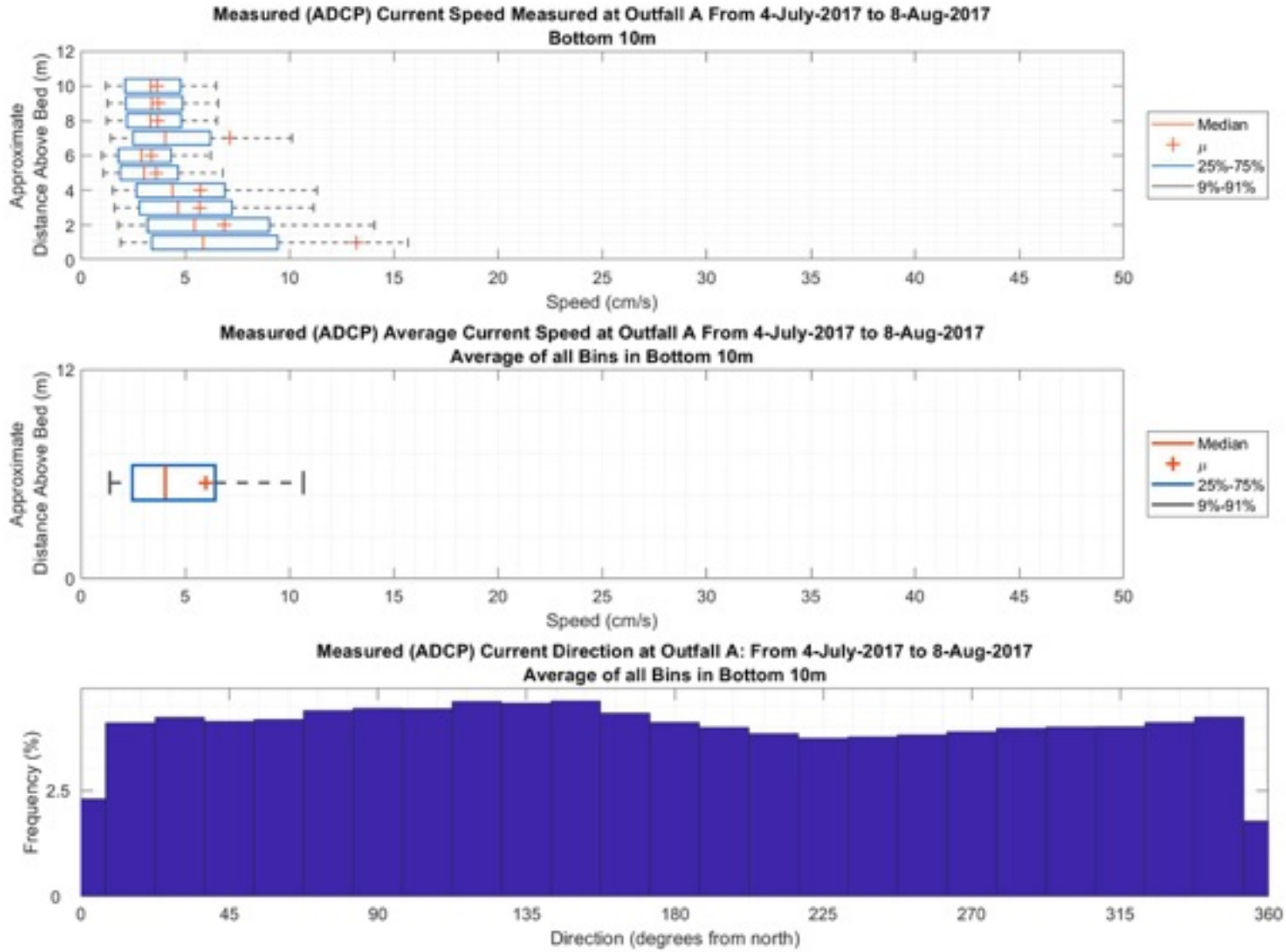

NOTES

IHA ADCP Outfall A Downward Looking Deployment 5 (Bottom 10m)
Dates: 04 Jul 2017 - 08 Aug 2017

STATUS
ISSUED FOR REVIEW

CLIENT

WAFI-GOLPU JOINT VENTURE

TETRA TECH

Wafi-Golpu DSTP Project

Density Current, Plume Dispersion, and Hydrodynamic Modelling

PROJECT NO.	DWN	CKD	APVD	REV
704-TRN.WTRM03037	CY	AH	JAS	JAS

OFFICE: Tetra Tech - VANC
DATE: March, 2018

Figure B-22

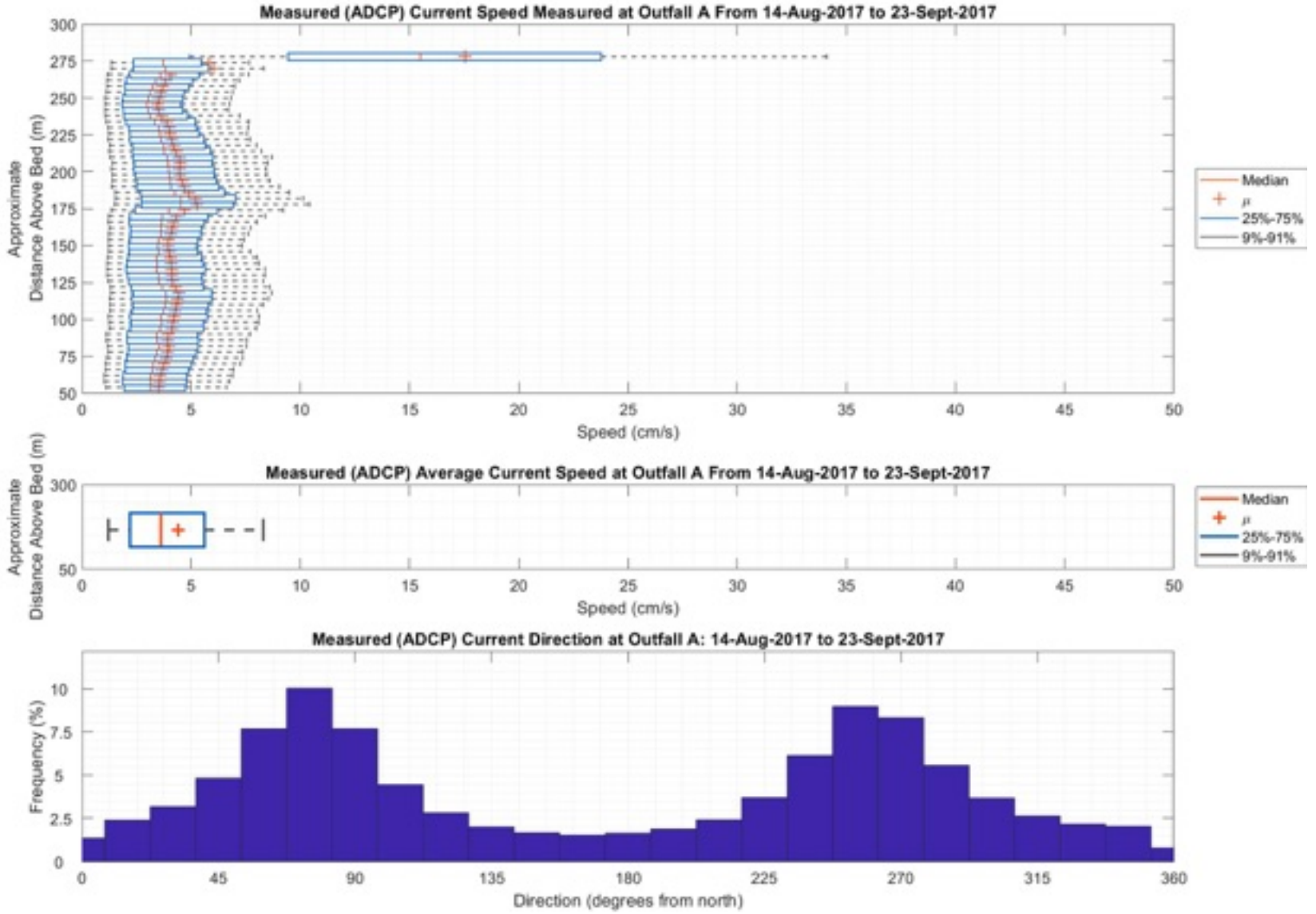

NOTES

IHA ADCP Outfall A Upward Looking Deployment 6
Dates: 14 Aug 2017 - 23 Sep 2017

STATUS
ISSUED FOR REVIEW

CLIENT

WAFI-GOLPU JOINT VENTURE

TETRA TECH

Wafi-Golpu DSTP Project

Density Current, Plume Dispersion, and Hydrodynamic Modelling

PROJECT NO.	DWN	CKD	APVD	REV
704-TRN.WTRM03037	CY	AH	JAS	JAS

OFFICE: Tetra Tech - VANC
DATE: March, 2018

Figure B-23

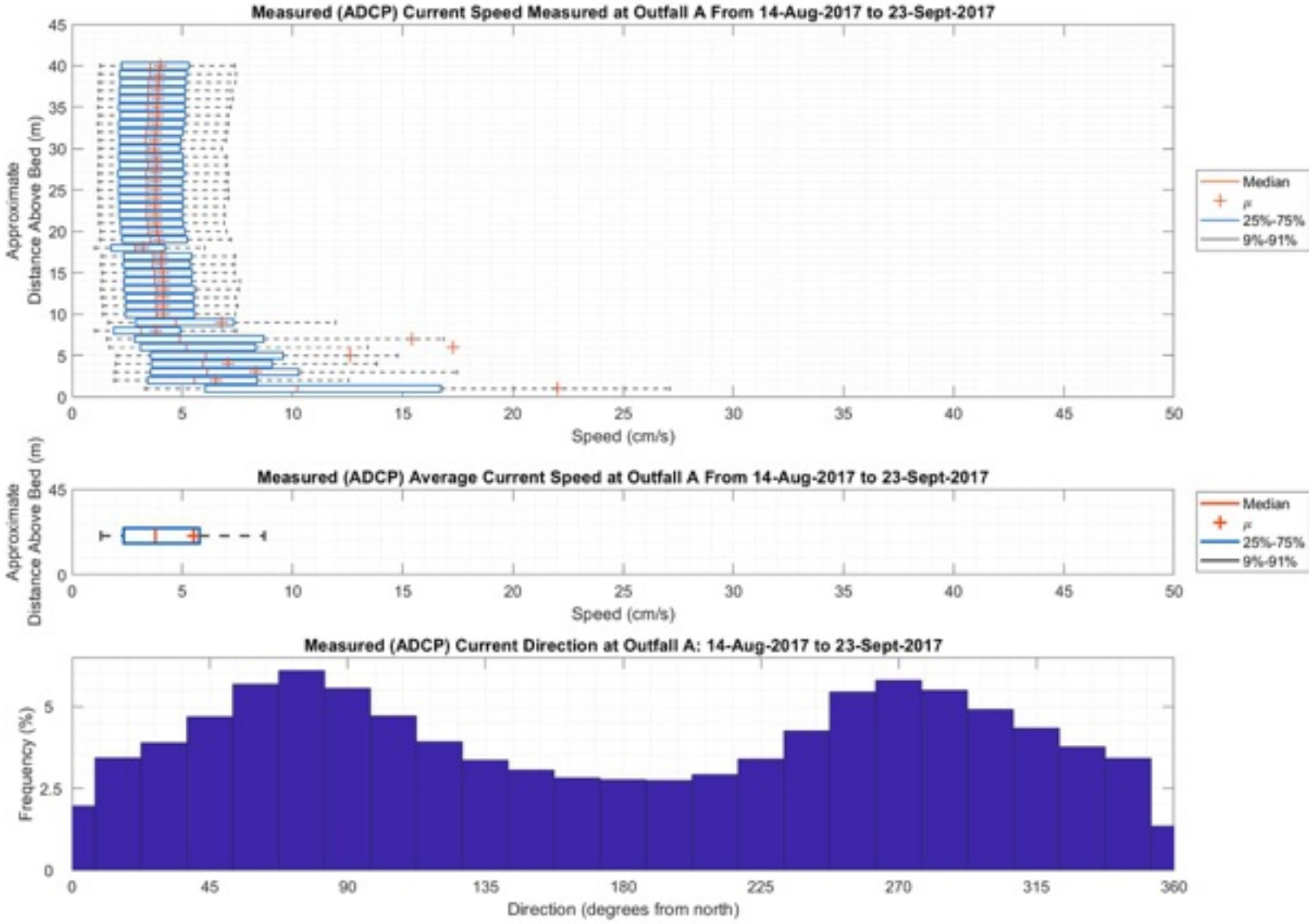

NOTES

IHA ADCP Outfall A Downward Looking Deployment 6
Dates: 14 Aug 2017 - 23 Sep 2017

STATUS
ISSUED FOR REVIEW

CLIENT

WAFI-GOLPU JOINT VENTURE

TETRA TECH

Wafi-Golpu DSTP Project

Density Current, Plume Dispersion, and Hydrodynamic Modelling

PROJECT NO.	DWN	CKD	APVD	REV
704-TRN.WTRM03037	CY	AH	JAS	JAS

OFFICE	DATE
Tetra Tech - VANC	March, 2018

Figure B-24

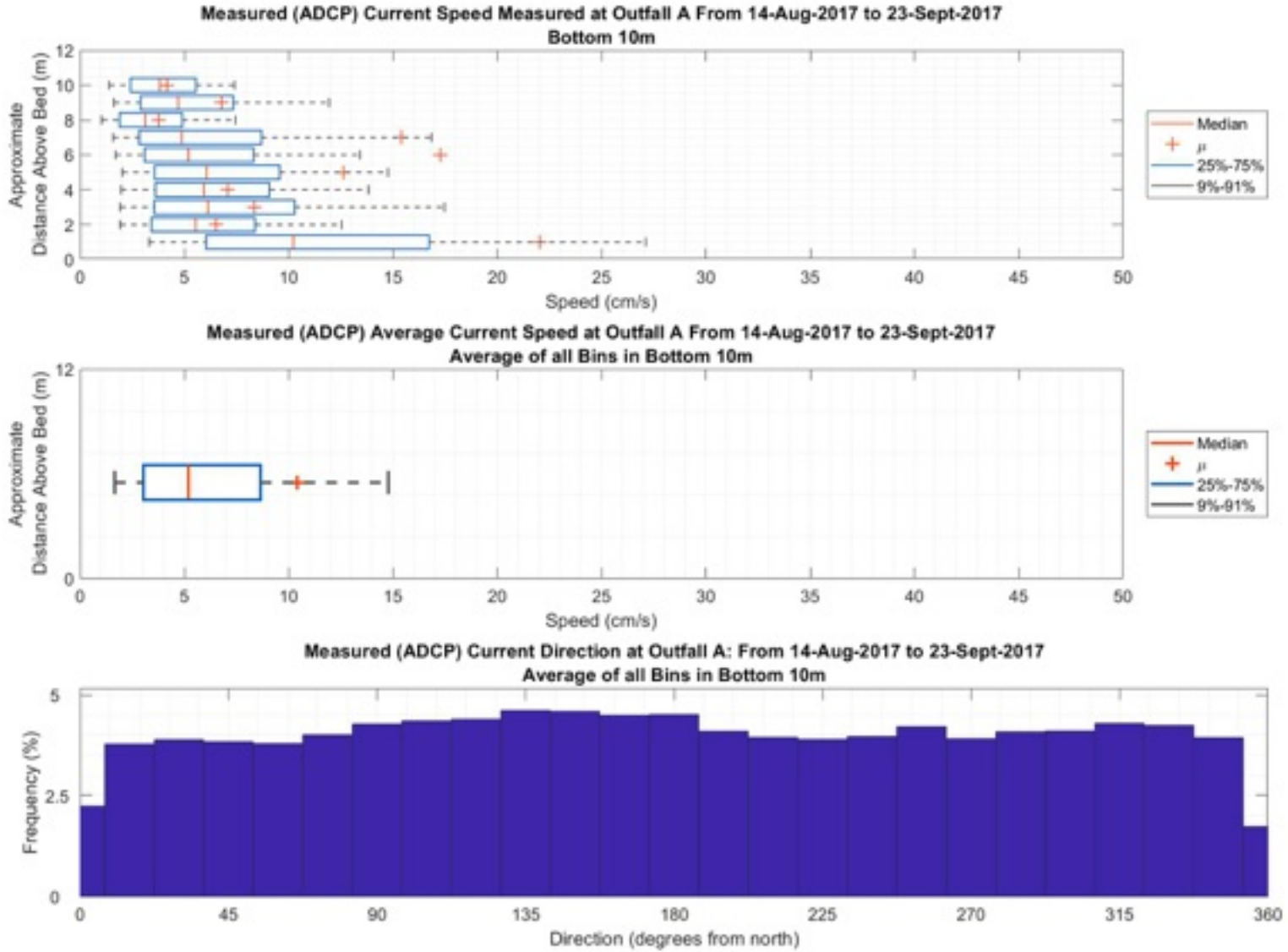

NOTES

IHA ADCP Outfall A Downward Looking Deployment 6 (Bottom 10m)
Dates: 14 Aug 2017 - 23 Sep 2017

STATUS
ISSUED FOR REVIEW

CLIENT

WAFI-GOLPU JOINT VENTURE

TETRA TECH

Wafi-Golpu DSTP Project

Density Current, Plume Dispersion, and Hydrodynamic Modelling

PROJECT NO.	DWN	CKD	APVD	REV
704-TRN.WTRM03037	CY	AH	JAS	JAS

OFFICE: Tetra Tech - VANC
DATE: March, 2018

Figure B-25

APPENDIX C

TETRA TECH'S LIMITATIONS ON THE USE OF THIS DOCUMENT

GENERAL CONDITIONS

HYDROTECHNICAL

This report incorporates and is subject to these "General Conditions".

1.1 USE OF REPORT AND OWNERSHIP

This report pertains to a specific site, a specific development, and a specific scope of work. The report may include plans, drawings, profiles and other supporting documents that collectively constitute the report (the "Report").

The Report is intended for the sole use of TETRA TECH's Client (the "Client") as specifically identified in the TETRA TECH Services Agreement or other Contract entered into with the Client (either of which is termed the "Services Agreement" herein). TETRA TECH does not accept any responsibility for the accuracy of any of the data, analyses, recommendations or other contents of the Report when it is used or relied upon by any party other than the Client, unless authorized in writing by TETRA TECH.

Any unauthorized use of the Report is at the sole risk of the user. TETRA TECH accepts no responsibility whatsoever for any loss or damage where such loss or damage is alleged to be or, is in fact, caused by the unauthorized use of the Report.

Where TETRA TECH has expressly authorized the use of the Report by a third party (an "Authorized Party"), consideration for such authorization is the Authorized Party's acceptance of these General Conditions as well as any limitations on liability contained in the Services Agreement with the Client (all of which is collectively termed the "Limitations on Liability"). The Authorized Party should carefully review both these General Conditions and the Services Agreement prior to making any use of the Report. Any use made of the Report by an Authorized Party constitutes the Authorized Party's express acceptance of, and agreement to, the Limitations on Liability.

The Report and any other form or type of data or documents generated by TETRA TECH during the performance of the work are TETRA TECH's professional work product and shall remain the copyright property of TETRA TECH.

The Report is subject to copyright and shall not be reproduced either wholly or in part without the prior, written permission of TETRA TECH. Additional copies of the Report, if required, may be obtained upon request.

1.2 ALTERNATIVE REPORT FORMAT

Where TETRA TECH submits both electronic file and hard copy versions of the Report or any drawings or other project-related documents and deliverables (collectively termed TETRA TECH's "Instruments of Professional Service"), only the signed and/or sealed versions shall be considered final. The original signed and/or sealed version archived by TETRA TECH shall be deemed to be the original. TETRA TECH will archive the original signed and/or sealed version for a maximum period of 10 years.

Both electronic file and hard copy versions of TETRA TECH's Instruments of Professional Service shall not, under any circumstances, be altered by any party except TETRA TECH.

TETRA TECH's Instruments of Professional Service will be used only and exactly as submitted by TETRA TECH.

Electronic files submitted by TETRA TECH have been prepared and submitted using specific software and hardware systems. TETRA TECH makes no representation about the compatibility of these files with the Client's current or future software and hardware systems.

1.3 STANDARD OF CARE

Services performed by TETRA TECH for the Report have been conducted in accordance with the Services Agreement, in a manner consistent with the level of skill ordinarily exercised by members of the profession currently practicing under similar conditions in the jurisdiction in which the services are provided. Professional judgment has been applied in developing the conclusions and/or recommendations provided in this Report. No warranty or guarantee, express or implied, is made concerning the test results, comments, recommendations, or any other portion of the Report.

If any error or omission is detected by the Client or an Authorized Party, the error or omission must be immediately brought to the attention of TETRA TECH.

1.4 ENVIRONMENTAL AND REGULATORY ISSUES

Unless expressly agreed to in the Services Agreement, TETRA TECH was not retained to investigate, address or consider, and has not investigated, addressed or considered any environmental or regulatory issues associated with the project.

1.5 DISCLOSURE OF INFORMATION BY CLIENT

The Client acknowledges that it has fully cooperated with TETRA TECH with respect to the provision of all available information on the past, present, and proposed conditions on the site, including historical information respecting the use of the site. The Client further acknowledges that in order for TETRA TECH to properly provide the services contracted for in the Services Agreement, TETRA TECH has relied upon the Client with respect to both the full disclosure and accuracy of any such information.

1.6 INFORMATION PROVIDED TO TETRA TECH BY OTHERS

During the performance of the work and the preparation of this Report, TETRA TECH may have relied on information provided by persons other than the Client.

While TETRA TECH endeavours to verify the accuracy of such information, TETRA TECH accepts no responsibility for the accuracy or the reliability of such information even where inaccurate or unreliable information impacts any recommendations, design or other deliverables and causes the Client or an Authorized Party loss or damage.

1.7 GENERAL LIMITATIONS OF REPORT

This Report is based solely on the conditions present and the data available to TETRA TECH at the time the Report was prepared.

The Client, and any Authorized Party, acknowledges that the Report is based on limited data and that the conclusions, opinions, and recommendations contained in the Report are the result of the application of professional judgment to such limited data.

The Report is not applicable to any other sites, nor should it be relied upon for types of development other than those to which it refers. Any variation from the site conditions present at or the development proposed as of the date of the Report requires a supplementary investigation and assessment.

It is incumbent upon the Client and any Authorized Party, to be knowledgeable of the level of risk that has been incorporated into the project design, in consideration of the level of the hydrotechnical information that was reasonably acquired to facilitate completion of the design.

The Client acknowledges that TETRA TECH is neither qualified to, nor is it making, any recommendations with respect to the purchase, sale, investment or development of the property, the decisions on which are the sole responsibility of the Client.

1.8 JOB SITE SAFETY

TETRA TECH is only responsible for the activities of its employees on the job site and was not and will not be responsible for the supervision of any other persons whatsoever. The presence of TETRA TECH personnel on site shall not be construed in any way to relieve the Client or any other persons on site from their responsibility for job site safety.